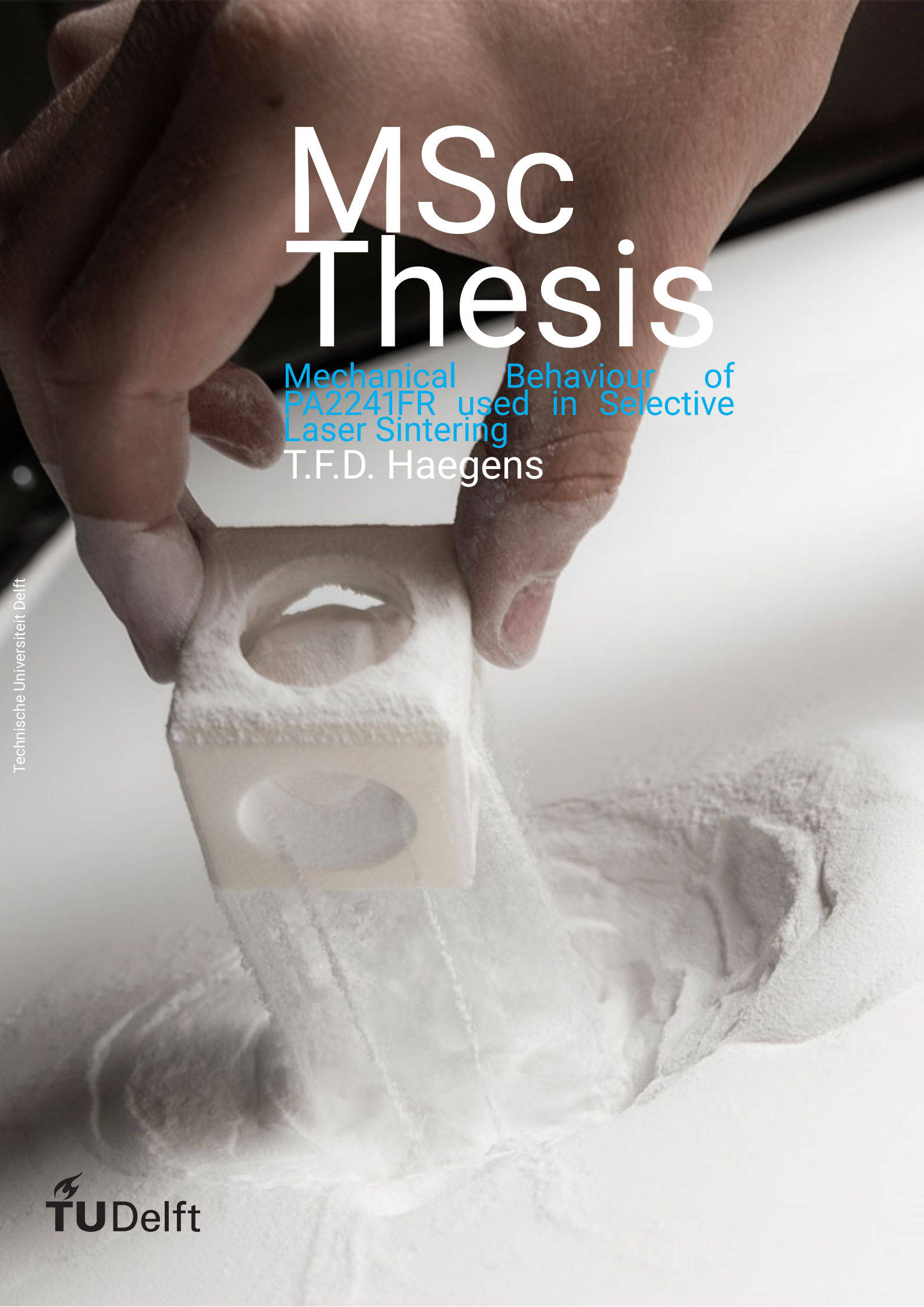

MSc Thesis

Mechanical Behaviour of PA2241FR used in Selective Laser Sintering

T.F.D. Haegens

Technische Universiteit Delft

TU Delft

MSc Thesis Report

Mechanical Behaviour of PA2241FR used in Selective Laser Sintering

by

T.F.D. Haegens

MSc Thesis Report
at the Delft University of Technology,
to be handed in by 4th of December 2020

Supervisor:	Dr. C.D. Rans
Project duration:	March, 2020 – December, 2020
With special thanks to:	Dr. Ir. Toon Roels Dr. Ir. Giovanni Vleminckx
Version:	3.2
Cover image courtesy of	http://www.weirather.com/en/products/weirather-laser-sintering-3232/
This thesis is confidential	and cannot be made public until 31th of January 2023.
An electronic version of	this thesis is available at http://repository.tudelft.nl/

TU Delft

Preface

The final phase in the graduation project at the Aerospace Engineering Faculty at Delft University of Technology is the completion of the MSc Thesis report. Over the duration of several months, I have been submerged into the world of additive manufacturing, in particular Selective Laser Sintering of a variant of polyamide-12. This project was realised in cooperation with Materialise NV, based in Leuven, Belgium.

Additive manufacturing is a relatively new and interesting manufacturing process that has gained my interest during the duration of my studies and internship. This manufacturing process has lots of untapped potential in all engineering disciplines, but especially in the aerospace sector. This drive made me perform my literature study and MSc Thesis in the field of additive manufacturing.

I would like to express my gratitude to those who provided me with the support needed to complete this research project. I wish to thank Dr. Ir. Toon Roels and Dr. Ir. Giovanni Vleminckx from Materialise for the opportunity and support. To Dr. Calvin Rans, I wish to express my special gratitude for guiding me through the graduation project. I also wish to thank Dr. Johan Bijleveld, Dr. Marlies Nijemeisland, Ir. Durga Mainali Sharma, and Dr. S.J. Eustace for their help and support. Finally, I wish to thank the pharmacy of the Imelda Hospital for the use of their testing facilities during the COVID-19 situation.

Tobias Haegens
Delft, 4th of December 2020

List of Symbols

b	Width	$[m]$
c_X	Centroid in X-direction	$[m]$
c_Z	Centroid in Z-direction	$[m]$
d	Depth	$[m]$
d	Distance between parallel lattice planes	$[m]$
d_{hkl}	Spacing of crystal planes	$[m]$
E_T	Tensile Modulus	$[Pa]$
h	Height	$[m]$
m	Mass	$[g]$
$m_{calculated}$	Calculated Mass	$[g]$
MD_X	Mass distribution in X-direction	$[m^5]$
MD_Z	Mass distribution in Z-direction	$[m^5]$
$MD_{X,\,i}$	Mass distribution in X-direction for part i	$[m^5]$
$MD_{Z,\,i}$	Mass distribution in Z-direction for part i	$[m^5]$
n	Order of the ring in Bragg's Law	[-]
P	Power	$[W]$
R^2	Coefficient of Determination	$[-]$
R_{HS}	Ratio Heat Shield	$[-]$
$R_{Local\,Volume}$	Ratio Local Printed Volume	$[-]$
$R_{W.A.S/V}$	Weighted Average Ratio of Surface to Volume	$[-]$
S_{part}	Surface Area of Part	$[m^2]$
T	Temperature	$[^\circ]$
T_{cc}	Cold Crystallisation Temperature	$[^\circ]$
T_m	Melting Temperature	$[^\circ]$
v	Speed	$[\frac{m}{s}]$
V	Volume	$[m^3]$
V_{local}	Local Volume	$[m^3]$
V_i	Volume of Part i	$[m^3]$
V_{part}	Volume of a Part	$[m^3]$
V_{parts}	Volume of Parts	$[m^3]$
X_c	Degree of Crystallinity	$[\%]$
$X_{coord,\,i}$	X-coordinate of Part i	$[m]$
$Z_{coord,\,i}$	Z-coordinate of Part i	$[m]$
$X_{D.o.C.}$	Degree of Crystallinity	$[\%]$
$X_{porosity}$	Degree of Porosity	[-]
ΔH	Melting Enthalpy	$[\frac{J}{g}]$
ΔH_m	Melting Enthalpy	$[\frac{J}{g}]$
ΔH_m^0	Melting Enthalpy 100% Crystalline	$[\frac{J}{g}]$
ε	Elongation at Break	$[\%]$
ε_B	Elongation at Break	$[\%]$
ε_M	Maximum Elongation	$[\%]$
θ	Angle between incident beam and lattice plane	$[^\circ]$
λ	Wavelength	$[m]$
ρ	Density	$[\frac{g}{cm^3}]$
σ_B	Tensile Stress at Break	$[Pa]$
σ_M	Maximum Tensile Stress	$[Pa]$
$\sigma_{M,HeatShielded}$	Maximum Tensile Stress Heat Shielded	$[Pa]$
$\sigma_{M,averagenormal}$	Maximum Tensile Stress Not Heat Shielded	$[Pa]$
σ_Y	Yield Strength	$[Pa]$

List of Acronyms

CCD	Charge-Coupled Device
CAM	Computer-Aided Manufacturing
CAD	Computer-Aided Design
D.o.C.	Degree of Crystallinity
DSC	Differential Scanning Calorimetry
FAR	Federal Aviation Regulation
FEM	Finite Element Modelling
FR	Fire Retardant
JAR	Joint Aviation Requirements
M.D.	Mass Distribution
NMR	Nuclear Magnetic Resonance
RoHS	Restriction of Hazardous Substances
SLS	Selective Laser Sintering
STL	Standard Tessellation Language
XRC	X-Ray Crystallography
XRD	X-Ray Diffraction

List of Figures

List of Tables

Executive Overview

During the manufacturing of aerospace components, Materialise NV experiences a variation in mechanical properties. These components are made of PA2241FR using a process called Selective Laser Sintering. The investigated material is PA2241FR. This is a variation of PA12, a polyamide polymer that is also called Nylon. To comply with FAR25 regulations, this white powder contains a flame retardant additive. As a downside, this additive has a negative effect on the mechanical properties of the material.

In order to address this issue in the process variation, a better understanding is needed of semi-crystalline polymers. The secondary bonds are investigated, more specifically how these bonds affect the behaviour of semi-crystalline polymers and PA12 specifically. A more detailed investigation focused on the selective laser sintering process. First a clear overview of the process is provided. After that the recycling of used powder is investigated. Used powder has aged on an elevated temperature for a long time, as a result post-condensation occurs. This results in a material that is harder to melt. This also results in orange peel, see Figure 2.8, but also in higher porosity, which all result in decreased mechanical properties. The effect of the cooling rate on the crystallisation is also discussed. The slower the cooling rate, the higher the crystallinity of the part. A higher crystallinity results in improved mechanical properties. The lower the density of the material, the higher porosity, the lower the mechanical properties. The next part focuses on the effect of flame retardant additives on the mechanical properties. The additive has been proven to have a negative effect. Next, a couple of other defects are discussed briefly. They are not investigated thoroughly, but may explain possible outliers. These defects and parameters are the dimensional accuracy/deviations, unfused powder and fatigue life.

The literature study identifies several knowledge gaps that results in the following research questions:

1. *How does the crystallinity correlate with strength and stiffness of Selective Laser Sintered PA2241FR?*
2. *How does the amount of FR-additive correlate with strength and stiffness of Selective Laser Sintered PA2241FR?*
3. *What is the influence of the geometrical properties of a printed batch on the strength of Selective Laser Sintered PA2241FR?*

Tensile specimens used by Materialise NV are used to evaluate the porosity, crystallinity and the flame retardant content. The specimens are ground to a fine powder and later analysed using differential scanning calorimetry and nuclear magnetic resonance spectroscopy to determine the degree of crystallinity and the flame retardant content, respectively. The porosity is measured by determining the volume and mass of a sample and comparing it to a maximum value. Combining the above, the research questions can be answered.

A three dimensional model is established in which the effect on the tensile strength in function of the degree of crystallinity and the porosity is plotted. Two models are made, since the tensile strength is different in the printing direction. Both these models are shown to be statistically significant and have a decent correlation coefficient. The model for the vertical orientation has a better fit, which can be explained by the fact the effect of the porosity is more pronounced in the vertical orientation.
Additional factors are proposed which may result in a better model. The crystal size of the samples is determined to be an additional factor that may have a significant impact. The range in which these models can be considered to be valid is also limited. This is the case since the available data and the obtained results have a limited range. More extreme data can be used to establish a stronger model. The current range of the model is in accordance with the processing parameters used by Materialise NV.

Additionally, it is determined that the degree of crystallinity has no apparent effect on the tensile modulus of the material. It is speculated that there is a different parameter which has a much stronger effect on the tensile modulus than the degree of crystallinity has. A possible explanation for this is a variation in the flame retardant content.

Unfortunately, no results on the flame retardant additive could be obtained using NMR spectroscopy, since PA2241FR could not be dissolved in a solvent that can be used for solution NMR spectroscopy.
The analyse of the effect of the degree of crystallinity and porosity on the mechanical properties indicates that there is an important factor which is not yet identified. The presence of the flame retardant additive is a strong

candidate. This is supported by the fact that the addition of the additive in the powdered PA12, causes for an increase in stiffness of more than 15%. This significant increase can also be expected to have a large impact on the mechanical properties and especially the stiffness. Literature does support the effect of the flame retardant additive on the material.

When attempting to answer the final research question, it was discovered that none of the proposed hypotheses could be rejected. The proximity of a part to a tensile bars does not influence its tensile strength. A nesting strategy with a higher number of parts can thus be considered to not influence the tensile strength.
The effect of the printed volume is also shown to be insignificant. The limited range in which the build volume varies may explain this. The mass distribution parameters are all shown to be insignificant.
Unexpectedly, the surface area to volume ratio is also proven to be insignificant. The larger surface area of a part, the more heat it will radiate. This is expected to result in a lower degree of crystallinity. The fact that this phenomenon is not observed, indicates that the presence of an other factor that has a more pronounced effect on the mechanical properties.

A lower cooling rate, will result in improved mechanical properties. Literature support this hypothesis. [8, 19] Possible reasons for the lack of any significant trend is that the proposed parameters are an oversimplification of the actual situation. A set of more complex parameters may be able to predict more reliable results.
The close proximity of the witness specimens to the boundary of the build volume, can also have an impact. The walls of the build chamber houses several heaters to keep the build volume at a constant temperature. Their presence may have a more pronounced effect on the other parameters. Printing sacrificial parts throughout the build volume is expected to result in more useful data.

Contents

Chapter 1
Introduction

Additive manufacturing is a fairly new manufacturing technique. In most forms, it is able to construct complex shapes layer by layer from a variety of materials. Powder bed technologies use a powder that is melted or sintered to form a part. These materials range from polymers to metal alloys, but also ceramics. One of the most used materials in additive manufacturing in general is a powder form of Nylon, or polyamide 12.

Additive manufacturing is a manufacturing process that is rapidly increasing in popularity. This technique allows for the construction of complex shapes layer per layer. There is a large variety in available materials, ranging from polymers to metals, but also ceramics. There are also many types of additive manufacturing processes. The most common used technique is powder bed additive manufacturing, in which a powder is melted or sintered to form a part. A powdered form of Nylon, more specifically polyamide 12, is the most commonly used material. The Belgian company Materialise NV uses several additive manufacturing processes to produce parts for a wide range of costumers, ranging from interior designers to aerospace manufacturers. A special powder called PA2241FR is used for the manufacturing of aerospace parts using Selective Laser Sintering. These parts need to comply to the European regulations (JAR/FAR 25, App. F, part 1| AITM 2.0002 B Vertical Bunsen Burner Test 12s Ignition Time). [1] for flame retardant properties. Halogenated particles are added to the widely used PA12 to have the desired flame retardant characteristics, hence the suffix FR, which stands for Fire Retardant.

Since this manufacturing process is new and not all aspects and effects are fully understood. Materialise NV experienced variation in the mechanical properties of the parts that they manufacture for aerospace applications. An agreement was reached between Materialise, the Faculty of Aerospace Engineering of Delft University of Technology, and myself to investigate these variations. Other sources, such as [45], also indicated this variation. A coefficient of variance of up to 7% was found. This leaves room for a significant improvement.

There are two types of resources made available for this research by Materialise NV. The first type of available resource are the tensile bars. These tensile bars are printed in every batch by Materialise NV to evaluate the tensile strength of the batch. These tensile bars are sacrificial parts that are being tested using a tensile test. From these tests, the modulus, maximum elongation & stress, and stress & elongation at break are determined. If the obtained values are below a certain value, the batch will require further investigation. If the obtained values are within range, it is assumed the quality of the entire batch will meet the requirements.
When parts are produced using selective laser sintering, they will experience anisotropy. This is due to the layer-by-layer manufacturing process. Because of this, a distinction is made tensile properties in vertical and horizontal direction. The standard position of these tensile bars in the build volume is shown in Figure 1.1.

There are several important remarks that must be made about this figure. As stated earlier, tensile bars are printed in horizontal and vertical direction. For later reference, these tensile bars have a label "UP" for the vertical direction and "EDGE" for the horizontal direction imprinted on them.
In Section 2.3, it was stated that two lasers are responsible for the sintering of the desired parts. Because of this, 2 sets of tensile bars are printed, one set in the field of each laser. If a significant difference occurs between the two sets of tensile bars, the origin of this problem could be traced back to one of the lasers.
Ten tensile bars are printed in each laser field, five in horizontal position and five in vertical direction. Of the 20 tensile bars, only 16 are tested. Of these 16 samples 8 are in horizontal position and 8 are in vertical position. Since there are 4 horizontal and vertical in each laser field.

[1] https://www.materialise.com/en/manufacturing/materials/pa-2241-fr

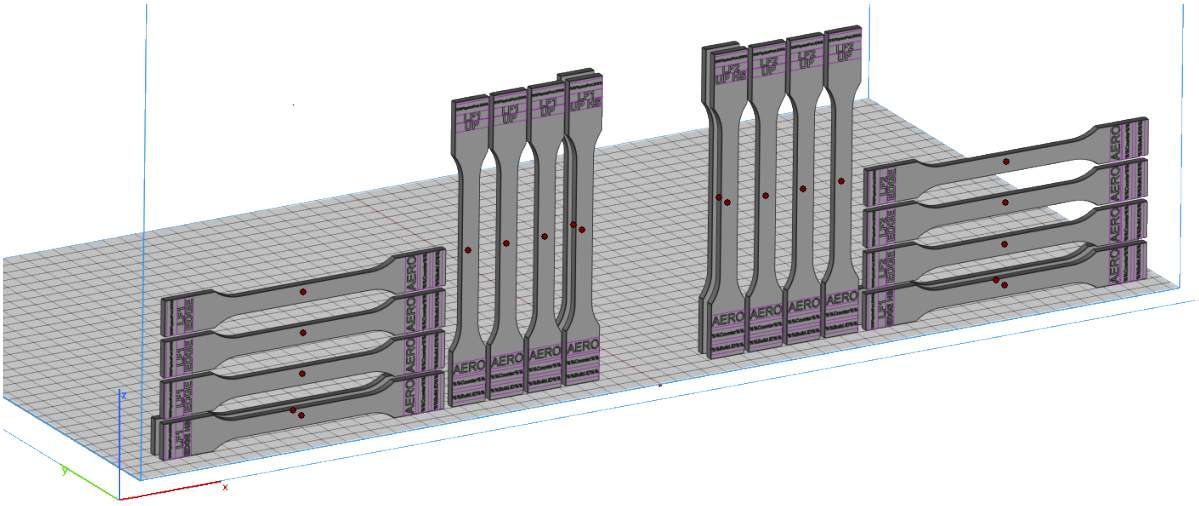

Figure 1.1: Graphical representation of the standard location of the tensile bars

In this research a total of 4 batches are used for the analysis of the mechanical performance of the tensile bars. In Figure 1.1, several tensile bars are shown. When examining this specimen closely, it can be seen that there is information imprinted on each tensile bar. From top to bottom there is:

1. Physical Part ID
2. Laser Field
3. Printing orientation
4. Spare
5. AERO
6. Counter
7. Build ID

The Physical Part ID is a number that is unique for every printed part. The Laser field indicates if it the printed specimen lies in the first or second laser field, or LF1 and LF2, respectively. The printing orientation is also imprinted on the specimen, and it is either EDGE or UP, for horizontal and vertical orientation, respectively. If the imprint *Spare* is present on the specimen, then the specimen will not be tested. The label *AERO* indicates that this specimen is manufactured using PA2241FR and can be considered to be aerospace grade. If the more common PA2200 is used, that is not approved for aerospace applications, the AERO-label is not present. The Build ID is the number of the entire batch. The Counter is a number that is unique for every tensile bar and in combination with the Build ID, it can be used to find the Physical Part ID.

In Table 1.1, an example is given of the data that is given for each tensile bar. From left to right, the following data is presented: the Physical Part ID, Build ID, the Machine number, Technology (always Selective Laser Sintering for this research), Material (always PA2241FR for this research), Build Orientation (EDGE or UP), E_T, σ_Y, σ_M, ε_M, σ_B, ε_B. A list of all available specimens can be found in Appendix B.

Table 1.1: Example of data given for each tensile specimen

Phys ID	**Build ID**	**Machine**	**Tech**	**Material**	**Build Or**	E_T	σ_Y	σ_M	ε_M	σ_B	ε_B
9682338	138448	P770-10	SLS	PA2241FR	EDGE	1780	46.1	46.1	9.3	45.3	10
9682339	138448	P770-10	SLS	PA2241FR	EDGE	1760	-	45.2	8.2	45	8.7
9682340	138448	P770-10	SLS	PA2241FR	EDGE	1770	45.5	45.5	8.8	43	9.6
9682341	138448	P770-10	SLS	PA2241FR	EDGE	1770	-	45.8	8.8	45.4	9.6
9682343	138448	P770-10	SLS	PA2241FR	UP	1790	-	43.4	4.6	42.7	4.6

Figure 1.2: Example of tensile specimens used in this research

A preliminary analysis of the variation of the modulus and the tensile of the data is presented. In Figure 1.3, the distribution of the tensile modulus in EDGE orientation is shown. It can clearly be seen that there is no normal distribution present in the data. It can also be seen that the data has a significant spread.

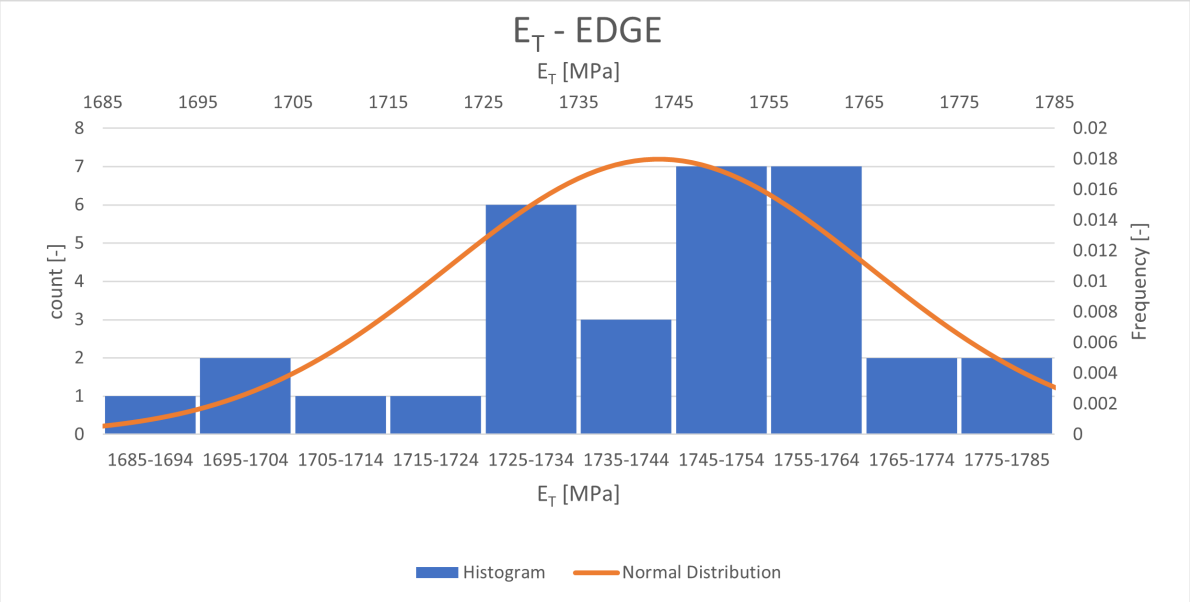

Figure 1.3: Histogram of Tensile Modulus in EDGE orientation

A similar observation can be made for the tensile strength in EDGE orientation. There is also no normal distribution and a significant spread of the data can be observed. The data is presented in Figure 1.4. The spread for both the tensile modulus and the ultimate strength in EDGE orientation allow for improvement of the mechanical process. If the cause of the variation is determined, the manufacturing process could be improved to narrow down this variation.

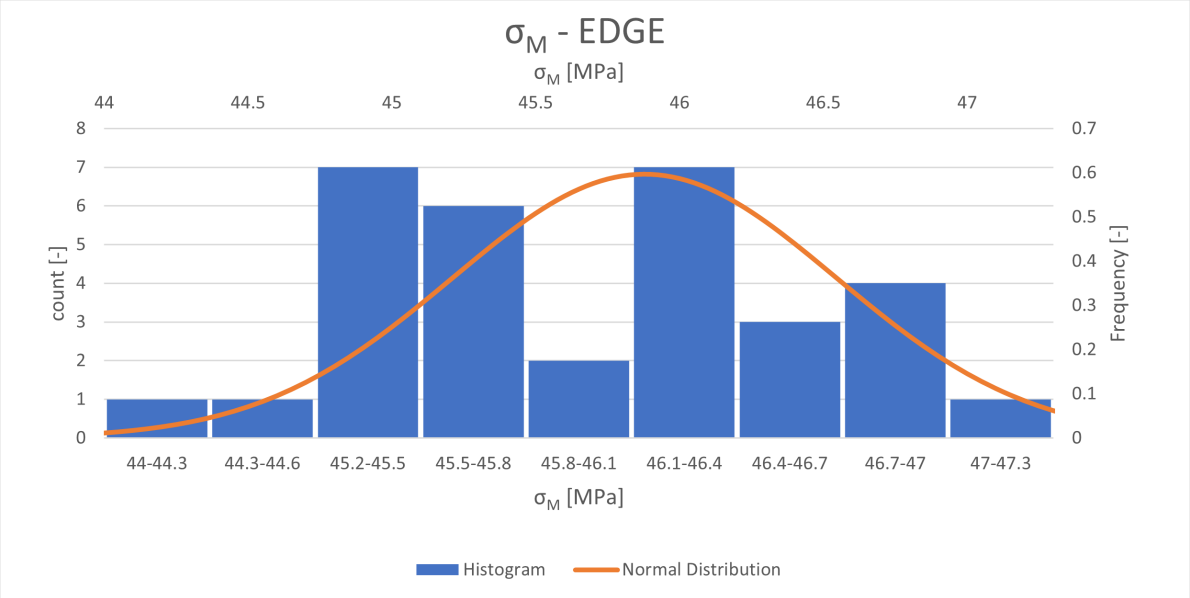

Figure 1.4: Histogram of Ultimate Strength in EDGE orientation

Figure 1.5 presents the distribution of the tensile modulus in the UP orientation. It can again be seen that the spread of the data is very wide and the data is not spread with a normal distribution. The spread seen in Figure 1.6, confirms the wide spread of the ultimate tensile strength in UP orientation. Also for this case, there is no normal distribution. The spread in UP orientation is wider than the spread in the edge orientation.

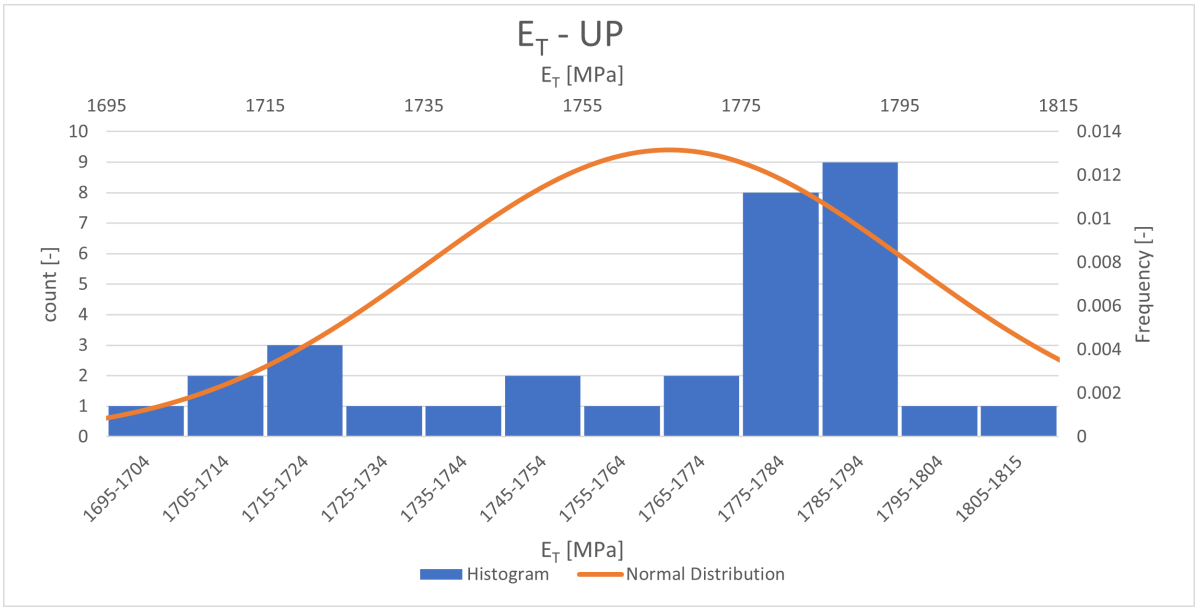

Figure 1.5: Histogram of Tensile Modulus in UP orientation

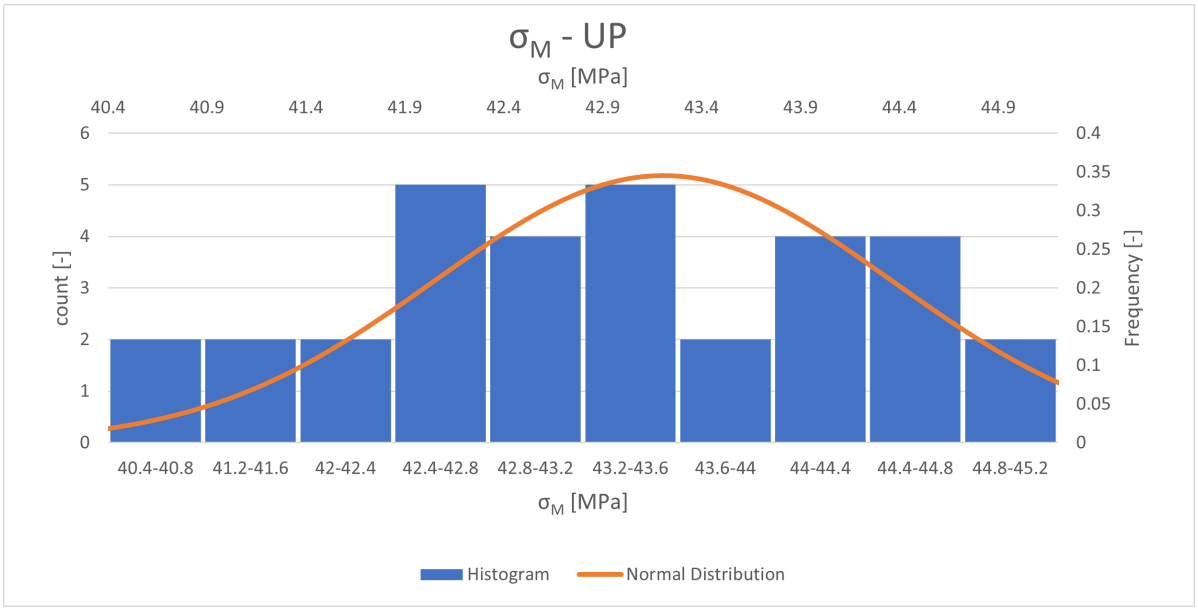

Figure 1.6: Histogram of Ultimate Strength in UP orientation

The second type of resource provided by Materialise NV, is the batch data for several prints and the Computer-Aided Manufacturing software *Materialise Magics*. A more detailed discussion on how the results are obtained will be presented in Section 5.4. An example of batch data is shown in Figure C.4. In the centre of the screen, the build volume is shown in which all the printed parts are nested. All these parts have a unique location, 3 dimensions, volume, surface area, ... In every batch, materialise positions tensile bars as shown earlier. The tensile data for these batches is also available for this research. Materialise NV was so kind to gives us geometrical and tensile data on a total of ten unique batches. All this data can be exported to a more convenient format and processed to gain more insight, which will be discussed in Section 5.4.

The overall goal of this report is to present the results of the performed research on the behaviour of selective laser sintered PA2241FR.
This purpose of this report is twofold. First, the theoretical background to the research problem is presented in Part I. The state-of-the-art in the field of selective laser sintering is presented in Chapter 2. This chapter gives an overview on the behaviour of semi-crystalline polymers and polyamide, but not specifically for additive manufacturing at first. The shift moves later more towards the process of selective laser sintering and how it influences the behaviour of polyamide parts that are manufactured using this process technique. The effect of the flame retardant additive present in aerospace grade polyamide is also discussed. This allows for the identification of a clear knowledge gap. The techniques needed to investigate this gap is presented and discussed in Chapter 4. The final research questions, the scope and the hypotheses are presented in Chapter 3.
The second goal of this report is to present the results of the research and this can be found in Part II. To start of, Chapter 5 discusses the methodology used in this research. The results of the research are presented and discussed in Chapter 6. The findings and its impact are presented in Chapter 7. Finally, the conclusion can be found in Chapter 8.

I

Theoretical Background

Chapter 2
Literature Study

In order to understand the reason for the possible variations that can occur in the mechanical behaviour of a material, it is wise to start at the basis. In this Chapter, first the behaviour of semi-crystalline polymers will be investigated in Section 2.1, followed by an analysis of the behaviour of selective laser sintered polymers in Section 2.2. Finally, in Section 2.3 the machine used for the manufacturing of the aerospace grade parts will be discussed.

2.1 Behaviour of Semi-Crystalline Polymers

In this Section, the behaviour of semi-crystalline polymers will be investigated, starting at the intermolecular forces present in these materials. This is needed to fully understand the behaviour of these materials. The Intermolecular forces are presented in Section 2.1.1. In Section 2.1.2, the behaviour is explained. Finally, Section 2.1.3 will focus on Nylon, or Polyamide in general.

2.1.1 Intermolecular Forces

The primary type of atomic bonds, or intramolecular bonds, consist of ionic bonds, metallic bonds, and covalent bonds. They are significantly stronger compared to the secondary bonds and are responsible for holding together a molecule. The secondary bonds that are experienced by an atom are called intermolecular forces. The secondary type of bonds is much weaker, but still have a significant influence on polymers. The melting temperature points in thermoplastic polymers are determined by the aforementioned secondary bonds. These secondary forces are van der Waals forces, but a classification exists related to the source and intensity. London dispersion force, Dipole-dipole bonds, and hydrogen bonds are presented in the following sections.

London Dispersion Force

The London dispersion force is the weakest of all intermolecular forces. This temporary attractive force is caused by the position of electrons in two adjacent atoms that cause the atoms to form temporary dipoles. This intermolecular force is also called the dipole-induced dipole attraction and is shown in Figure 2.1[1]. On the right hand side of the figure, the electron shift that causes the temporary dipoles is shown. The left shows the atom before the temporary shift. If two adjacent atoms have a similar shift, the London dispersion force will cause the weakest of the secondary bonds. [6]

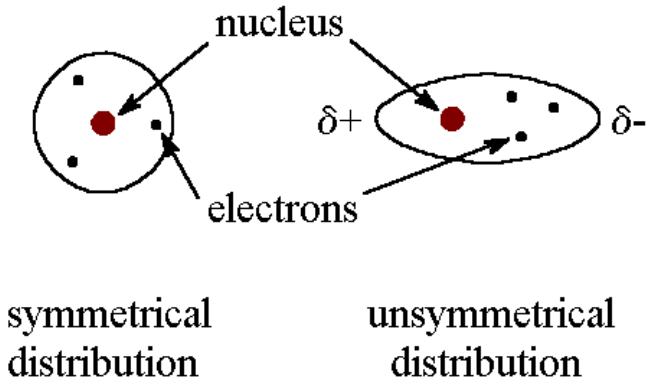

Figure 2.1: Representation of electron shift that cause temporary dipoles

[1] Image is courtesy of Davidson School of Chemical Engineering - Purdue University

Dipole-Dipole Interaction

In Figure 2.2 a clear example of a dipole-dipole interaction is shown. This is the second type of bond and it is an electrostatic interaction between two molecules. A requirement for these molecules is that they must have permanent dipoles. This type of bond is stronger than the London dispersion force mentioned earlier. But it is significantly weaker than the interaction between two ions, since only partial charges are involved. An attraction occurs between polar molecules, when the positive side of one molecule is attracted to the negative side of another molecule. However this interaction can only occur if the molecules are asymmetric. Otherwise the polar sides will cancel each other out. [6]

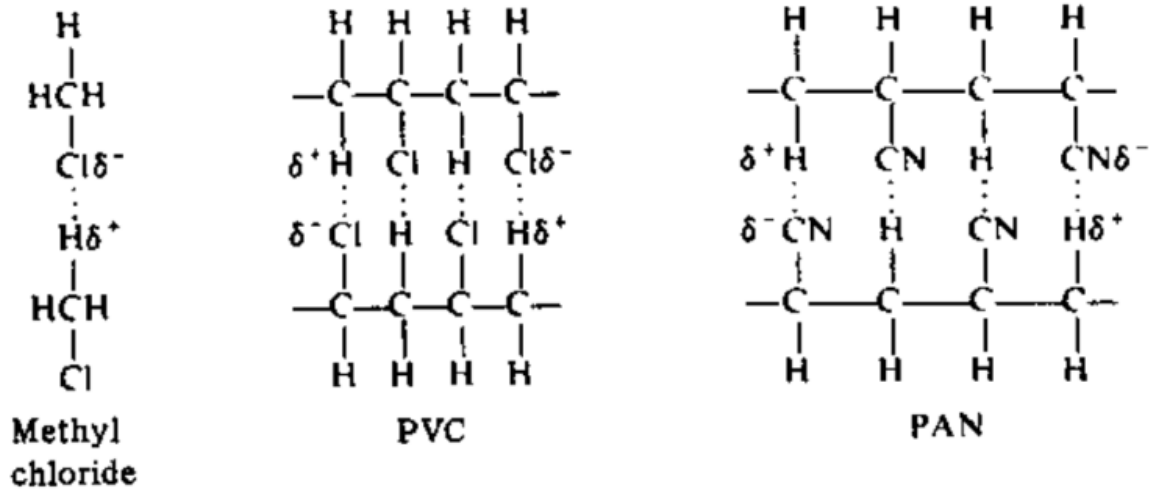

Figure 2.2: Example of typical dipole-dipole interaction between molecules [6]

Hydrogen Bonds

The last secondary bond that is discussed is the strongest of them all. I is shown in Figure 2.3. The hydrogen bond is a very attractive interaction between a hydrogen atom that has bonded to an electronegative atom, such as nitrogen or oxygen atoms, and an electronegative atom. There is some similarity between this type of bond and a covalent bond, since it is directional and stronger than a van der Waals force. [6]

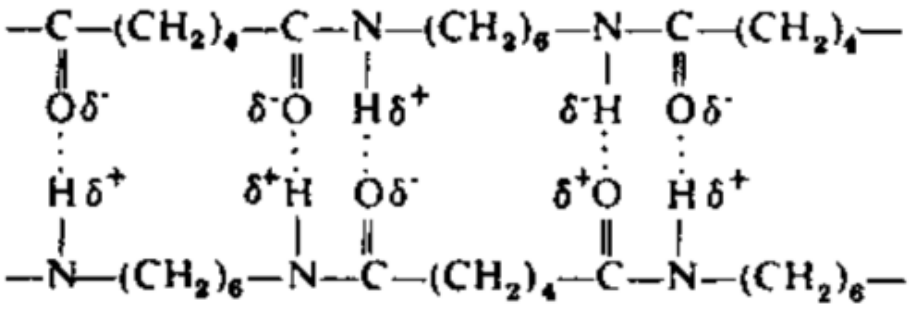

Figure 2.3: Example of typical Hydrogen bonding between Nylon [6]

2.1.2 Behaviour

After the overview of the intermolecular forces, the behaviour of semi-crystalline polymers can be looked into. A semi-crystalline polymer is composed of an amorphous region and a crystalline region. These regions are not ordered and ordered, respectively. This fact influences the chemical & physical properties of the material. [6]

The tensile strength and stiffness of the polymer part is affected by the crystallinity of the part. Ordered molecules are dominant in the crystalline part of the material. This allows for a larger number of secondary bonds compared to the amorphous region of the polymer. These secondary bonds cause the increased stiffness and strength in the crystalline region, since a larger number of intermolecular bonds will need to be broken before the atoms can move independently. This movement can be caused by mechanical forces acting on the polymer, but also due to thermal forces. Because of this the melting temperature of the polymer is higher when the crystallinity of the part is higher.

The flexibility and the elongation at break of the polymer part is determined by the amorphous region. Relatively large polymer molecules that are not fixed into an ordered crystal, can more easily move around. The lack of secondary bonds is the cause for this. The long polymers can rotate, because of this. This allows for a more flexible material, that also breaks at a higher elongation.

Chain entanglement, high intermolecular forces, the presence of reinforcing agents, and cross links affect the flexibility of the amorphous part of a semi-crystalline polymer above the glassy state. These factors also affect the viscosity of the polymer material. It is important to note that a completely amorphous polymer would not have a melting point but only a glass transition temperature. [6]

A rapid cooling rate decreases the amount of crystallinity.[6] This can be explained by the fact that a drop in temperature lowers the mobility of polymers, which causes them to stay in their current position. If the molecules are allowed to move, they can more easily rearrange themselves in an ordered manner, or crystalline part.

	Increased crystallinity	Increased crosslinking	Increased mol. wt.	Increased mol. wt. distribution	Addition of polar backbone units	Addition of backbone stiffening groups
Abrasion resistance	+	+	+	−	+	−
Brittleness	−	M	+	+	+	+
Chemical resistance	+	V	+	−	−	+
Hardness	+	+	+	+	+	+
T_g	+	+	+	−	+	+
Solubility	−	−	−	0	−	−
Tensile strength	+	M	+	−	+	+
Toughness	−	−	+	−	+	−
Yield	+	+	+	+	+	+

[a] +, increase in property; 0, little or no effect; −, decrease in property; M, property passes through a maximum; V, variable results dependent on particular sample and temperature.

Figure 2.4: Relationship between the molecular structure and performance of a polymer [6]

In figure 2.4, the relationship between the molecular structure of a polymer and its mechanical performance is presented. This figure displays several possible approaches on how improve the mechanical performance of a semi-crystalline polymer. The three most obvious candidates are:

1. Increase crystallinity
2. Increase molecular weight
3. Addition of polar backbone units

The first option is definitely achievable since it does not change the molecular structure of the material. The second option is more difficult for application in additive manufacturing. Increasing the molecular weight would results in a more viscous material and this may result in manufacturing issues. The effect of this is explained in Section 2.2.

2.1.3 Nylon

In the Section, the focus will lie on the family of polyamides and how it behaves, since the general behaviour of semi-crystalline polymers has been explained. Another name for polyamide is Nylon. The chemical structure of a polyamide 12 (PA12) molecule is seen in Figure 2.5. The molecular structure of this molecule is an ideal structure for the presence of London dispersion forces, dipole-dipole interactions, and especially hydrogen bonds. A hydrogen bond can occur between the nitrogen atom and the hydrogen atom of another molecule. The presence of this combination of secondary intermolecular forces results in a high melting point and glass transition point, higher than most polymers. These bonds make polyamides a very strong and resistant material. For example, the melting point of nylon-66 is at 265°C. The longer the nylon chain, the higher the processing viscosity of the material. The melt flow should still be high enough for smooth processing. The processing temperature of the material should be high enough to guarantee a good flowing material, but this temperature should not be above the temperature at which the primary bonds would start to break. Polyamides have very interesting mechanical properties but are relatively hard to process.

2.2 Behaviour of SL Sintered polymers

Now that the general behaviour of semi-crystalline polymers is discussed, their behaviour, when applied in additive manufacturing, can be studied in further detail. To start, it is important to fully understand the selective laser sintering process. The additive manufacturing technique that is used to manufacture parts out of PA2241FR is also called SLS in short. In Section 2.2, a brief overview of the process is presented. In Section 2.2 the effect of powder recycling will be explained. The sintering window is an important feature of the additive manufacturing process, and will be explained in Section 2.2.2. At last, the effect of the cooling rate will be discussed in Section 2.2.3.

Selective Laser Sintering Process

Selective laser Sintering is a manufacturing process that uses a laser beam to introduces energy into a layer of polymer powder particles to fuse them together. The most common used material is polyamide 12 (PA12), or a variant of it like the one used for aerospace applications. The structure of this polymer molecule is shown in Figure 2.5 [2]. The material that will be investigated is PA2241FR. This material has PA12 as a basis, however a halogenated additive, chloride or bromide based, is present in a significant concentration. This will be further discussed in Section 2.2.1.

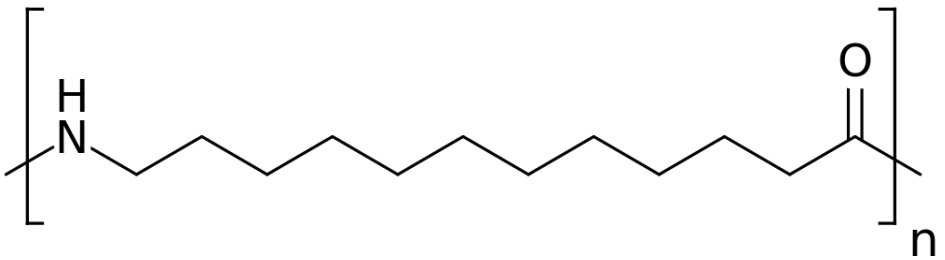

Figure 2.5: Chemical structure of Polyamide 12

A schematic representation of the Selective Laser Sintering Setup is shown in Figure 2.6. An area is coated with a polymer powder layer by layer, this part of the printer is called the build area. One or two lasers beams are reflected using mirrors, and corrective lenses, onto the fresh layer of powder. The heat added by the laser result in the homogeneous melting of the powder at a desired location. Geometric information of the part, as well as several processing parameters, such as the printing speed, laser power, laser track strategy, ..., dictates the

[2] https://en.wikipedia.org/wiki/Nylon_12#/media/File:Nylon-12.svg

movement of the mirrors.
The platform on which the build area is placed, will be lowered by a single layer thickness after the laser is finished with the a layer. The application device then spreads a thin layer of powder onto the build area. The laser and mirror then start the localised melting process for the new layer.

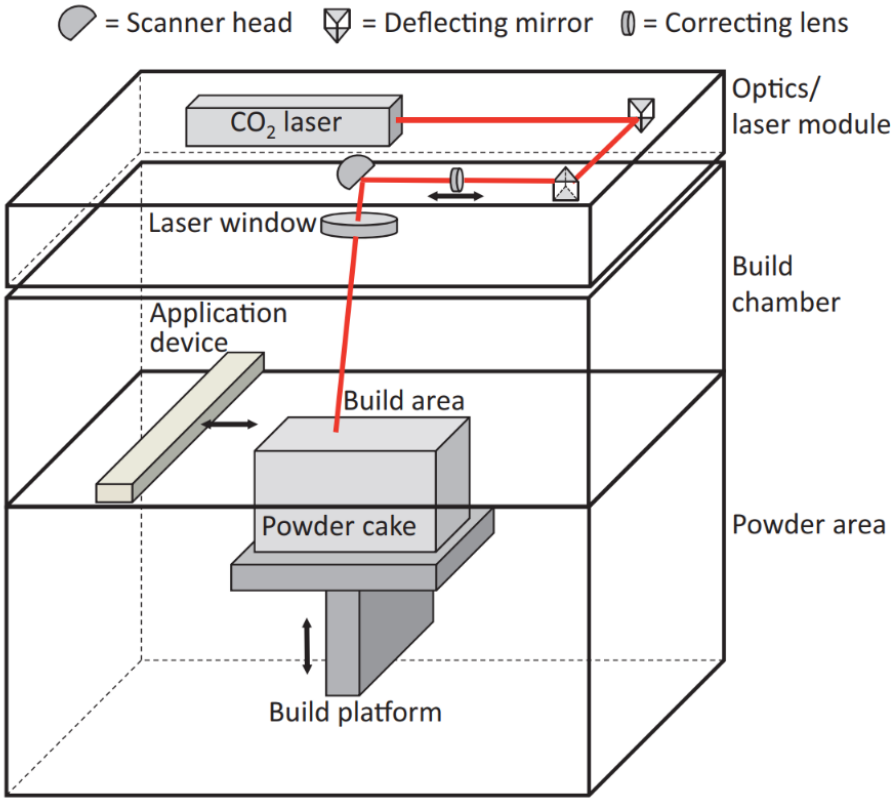

Figure 2.6: Schematic Illustration SLS Setup [41]

A general Selective Laser Sintering machine can be divided into three major modules. The first one is the optics module and is home to one or more lasers that are being used to melt the powder. In this module, there are also several deflecting mirrors, a correcting lens, and a scanner head. Since losses of laser radiation must be avoided at all cost, this module must be dust free and is hermetically sealed off from the rest of the machine. Otherwise the quality of the parts built would experience increasingly negative results.
The second module of the machine is the building area. In this area the application device spreads the preheated powder onto the build area. The importance of the preheating of the powder will further be discussed in Section 2.2.2.
The last module of the machine is called the powder area. When the build platform is lowered, the build volume grows taller as it lowers deeper in the powder module. The large block of powder is still being heated to keep the temperature of this powder cake as constant as possible, for more information see Section 2.2.3. Heaters are installed surrounding the build volume for this sole purpose. [41]

It is important to note that only a minor fraction of the build volume, or powder cake as referred to in Figure 2.6, houses actual parts. The rest of this volume is loose powder that can be removed and recycled.

Reusing of Powder

The reusing or recycling of polymer powder is a trade-off between cost and quality. Only a small percentage of the build volume is filled with actual printed components, the rest of the powder is removed to expose the printed parts, the excess powder is captured and reused to lower the cost. A mix of used and fresh powder is being used for the following prints. For the types of material and printers that are being used for this research, Materialise NV uses a ratio of 50% fresh and 50% recycled powder. The powder recycling chain is shown in Figure 2.7. [41]

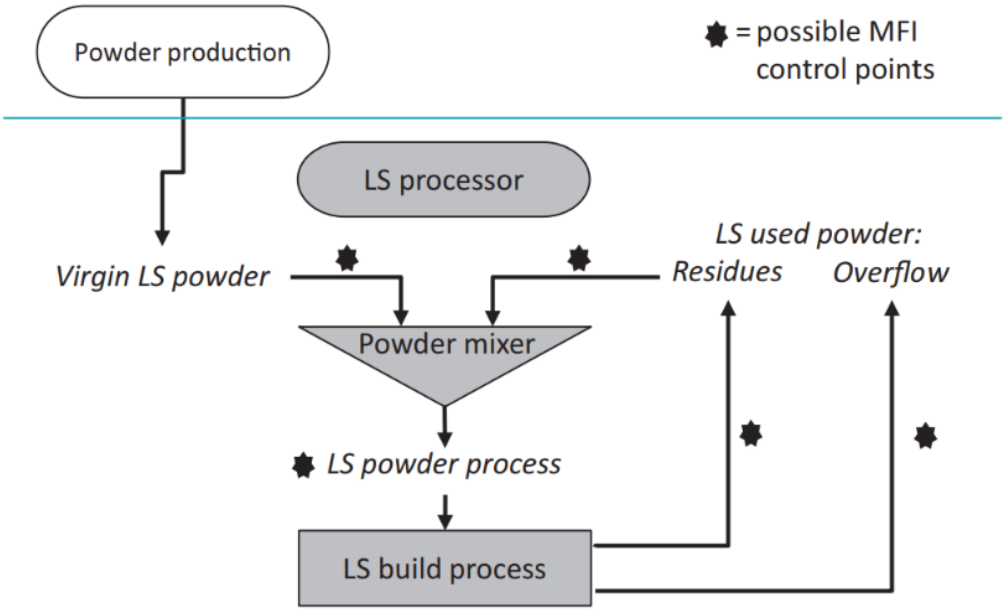

Figure 2.7: Graphical Representation of powder flow in SLS process [41]

Recycling of the powder also has an adverse effect on the print process. When powder is used in the process but is not actually melted, it will still be exposed to an elevated temperature just below the melting temperature of the polymer material for possibly the duration of the entire printing process. This can easily be up to 48 hours. The thermal conditions by the powder during the manufacturing process is presented in Section 2.2.2. This effect on the molecular composition of the material, which is called ageing, results in a higher melt viscosity. If the amount of recycled powder that is used is too high, the part will experience a phenomenon that is called orange peel, see Figure 2.8. This undesirably phenomenon is due to the post-condensation that occurs at these conditions. Post-condensation increases the length of the chains present in the polymer molecules. The increased molecular weight results in an increased melt viscosity and lowered the flowability of the material. This results in rough and uneven surfaces. [49] As a result, a mix with a ratio of 50/50 is used by Materialise NV.

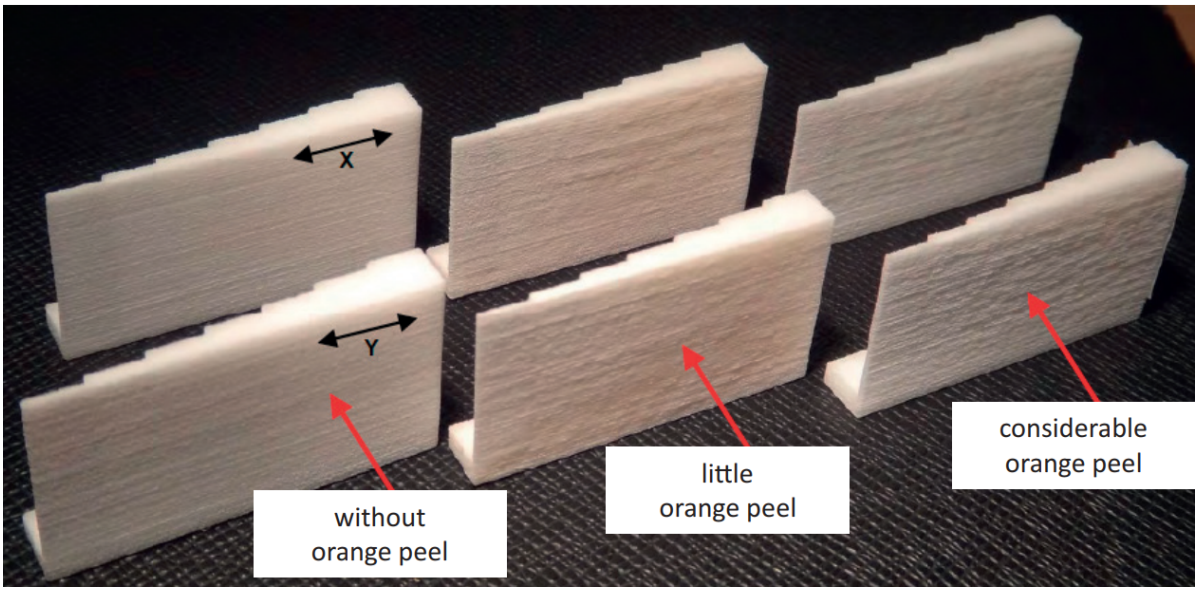

Figure 2.8: Different Severities of Orange Peel [41]

Research has shown that the long exposure of the powder to the high temperature increases the viscosity and the molecular weight of the material. [10] This research also finds that the crystallinity of the powder drastically decreases after melting by the laser beam. The type of crystal structures that are present in the

material changes from α- to γ-form. The larger the amount of aged powder is used in a single build, the lower the degree of crystallinity. By use of differential scanning calorimetry it can also be confirmed that the fresh powder melts at lower temperatures compared to the aged powder. This is due to the increased molecular weight caused by the post-condensation of the material. These microstructural differences in the material affect the tensile and shear properties of the material. Mixed powder behaves as a combination of the recycled and virgin powder. The aged and the mixed powder have shown much better densification due to a more homogeneous crystallisation. Using more virgin powder on the other hand results in an increased tensile strength. Also, this research recommends using a 50–50 virgin-aged mixture of powders, since this will provide a high tensile strength and high ductility. This is also the case for Materialise NV. This is caused primarily due to the good coalescence behaviour and an intermediate microstructure.[10] Experimental results proved PA12 powder that is reused, characterised by a higher melt viscosity, has a higher entanglement due to the longer molecule chains caused by the post-condensation. This causes an increased resistance to flow and this results in parts with a poor surface finish, such as orange peel. [49]

2.2.1 Flame Retardant

Polyamides are widely used in Selective Laser Sintering applications, because of the low cost and the mechanical properties. However, this material is flammable and cannot be used as-is for aerospace applications. Because of this, there is a clear need for an additive that allows the material to meet the JAR/FAR 25 regulations of flame retardancy. Several types of flame retardants are presented in [27]. Most of the used flame retardants are based upon a chemical reaction. These reactions can based upon several elements. The most common used flame retardant is halogen based. Because of environmental concerns, phosphorous-based compounds are also used. Other options are based upon metal hydroxides, boron, nitrogen, and nanofillers.

PA2241FR is a flame retardant variation of PA2200 produced by EOS. This material uses halogenated flame retardant additives, on a basis of Chloride or Bromide. The exact content is not know and is a company secret from EOS. However, it is known that this additive accounts for at least 25% of the powder mixture.

Further research into this additive results in a better understanding of the process. In [24], several types of smoke suppressants for polymers are elaborated upon. [24] makes a distinction between fillers and additive compounds. The latter are non-polymeric compounding substances that consist of less than 20% of the polymer mass. Fillers are also non-polymeric compounding materials, but their concentration is between 20% and 40% of the polymer mass. Since our flame retardant additive is estimated to have a concentration of at least 25%, it can safely be assumed that the additive can be considered to be a filler.

The filler can be considered to be inert or active. Halogenated flame retardants are active fillers, since they rely on endothermic processes to inhibit the propagation of fire. [24] Halogenated compounds can theoretically consist out of every type of halogen. However, fluorine and iodine base compounds are studied to be significantly less effective. [23]

A more in depth discussion of the chemical reactions that causes the flame retardant effect is discussed in [25]. The halogenated additive effect is caused by the interference in the combustion train of the polymers. [16, 25] Pyrolysis of the polymer produces species that are able to react with atmospheric oxygen, which results the $H_2 - O_2$ scheme. This allows for the propagation of the fuel combustion by the branching reactions seen in Equations 2.1 and 2.2. [16, 25]

$$H^* + O_2 = OH^* + O^* \tag{2.1}$$

$$O^* + H_2 = OH^* + H^* \tag{2.2}$$

In Equation 2.3, the main exothermic reaction is shown. This reaction provides the majority of the energy that is needed to maintain the flame.[16, 25]

$$OH^* + CO = CO_2 + H^* \tag{2.3}$$

In order to slow down or even stop the combustion, it is essential that the reactions shown in Equations 2.1 and 2.2 are hindered. Luckily, the halogen derivatives, in PA2241FR this is chlorine and/or bromide, have an inhibiting effect that operates in the aforementioned mechanism. This effect occurs by releasing the halogen atom or a

hydrogen halide. The latter is the case of the flame-retardant molecule does not contain a hydrogen atom. These reactions are shown in Equations 2.4 and 2.5, where M^* is the residue left behind by the flame-retardant molecule.

$$MX = M^* + X^* \tag{2.4}$$

$$MX = HX + M^* \tag{2.5}$$

$$RH + X^* = HX + R^* \tag{2.6}$$

Equation 2.6 shows the reaction of the hydrogen atom with the fuel/polymer which results in the production of hydrogen halide. It is the hydrogen halide that is believed to be responsible for the actual inhibiting of the flame generation, since it will affect the chain branching, see Equations 2.7 and 2.8.

$$H^* + HX = H_2 + X^* \tag{2.7}$$

$$OH^* + HX = H_2O + X^* \tag{2.8}$$

Equation 2.8 was found to be half as fast as Equation 2.7. The reaction speed together with the magnitude of the ratio $\frac{H_2}{OH}$ in the flame front indicate that the main reaction that acts as the inhibitor is 2.7. [25] states that the competition between the reactions in Equations 2.1 and 2.7 causes the flame retardant effect. This is the case since in Equation 2.1 two free radicals are produced for each hydrogen atom that is consumed. On the other hand, the recombination of the halogen radical, shown in Equation 2.7, results in the relatively stable halogen molecule. [16]

[25] throws some light on the synergism between bromide and chloride in pyrolysis experiments. When both elements are present, a higher effectivity of the additive is observed. One of the reasons for this might be that the radicals Br^* and Cl^* do not only recombine to Br_2 and Cl_2, but also to $BrCl$. The latter is polar and as a result is more reactive compared to Br_2 and Cl_2. $BrCl$ reacts with the H^* radicals to produce both HBr and another Cl^* radical. As a result the inhibiting effect is more efficient. However, [25] indicates that a lot is still unknown about the chemical process that caused the flame retardant effect.

[5] states that usually a metal oxide is added in conjunction with the organic brominated or chlorinated compounds. This metal oxide is typically antimony trioxide, denoted by AO, and this is supported by [25]. Antimony trioxide does in itself enhance the fire retardant properties, however, it does strongly enhance the effectiveness of the halogenated additive. This is called the synergistic effect. [5] also indicates that, when possible, the halogenated structures are introduced into the polymer chain of the material by use of co-polymerisation.

The addition of the flame retardant does however have a significant impact on the mechanical performance of the printed parts. The process characteristics of the laser sintering process are significantly disrupted. The effect this additive has can be seen in Table 2.1 [3]. Both [24] and [16] confirm that the physical properties of polymers are adversely affected by the presence of fillers. More specifically, the impact strength is lowered as well as an effect on the tensile strength. This table presents the mechanical properties of both PA2200 and PA2241FR. Both materials are produced by EOS, and their only difference is the presence of the flame retardant additive.

Table 2.1: Mechanical properties of PA2200 and PA2241FR from EOS

Material Properties	PA2200	PA2241FR	Units
Density	0.95	1	$\frac{g}{cm^3}$
Tensile Strength	48	49	MPa
Tensile Modulus	1650	1900	MPa
Elongation at Break	20	15	%

It can be seen that the density of the flame retardant variant of the material is higher compared to the basic material. The tensile strength is also higher for PA2241FR. However these differences are minimal.
However, the elongation at break is significantly less for the polyamide with flame retardant. This is the price that is paid in order to meet the FAR25 regulations.

[3] https://www.materialise.com/system/files/resources/materialise_datasheets_def_file_PA-AF.PDF

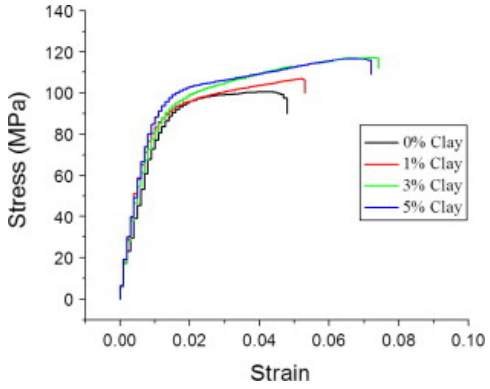

Figure 2.9: Effect of nano-fillers on Stress-strain curve [22]

In [26], the effect that a nano-filler has on the mechanical properties of a material is investigated. The nano-filler improves both the ultimate strength and the modulus of the material up to a certain concentration. If the amount of additive is increased even further, the filler has an adverse effect. This research did not focus on polyamide and the effect of the halogenated additive, however it is possible a similar effect is present for PA12 and the halogenated additive. The tipping point for the improvement of the modulus in this case is at $\pm 7\%$ filler for the ultimate strength it is $\pm 5\%$. A similar effect could explain the significant increase in Young's Modulus and only a minor improvement on the tensile strength. The findings of this research are confirmed by similar studies. [22, 44] The effect can clearly be seen in Figures 2.9 and 2.10. It is interesting to see that the ultimate strength in all three mentioned cases experiences its tipping point at a lower concentration than the tensile modulus does. This could also be the case for PA 2241 FR and the halogenated additive.

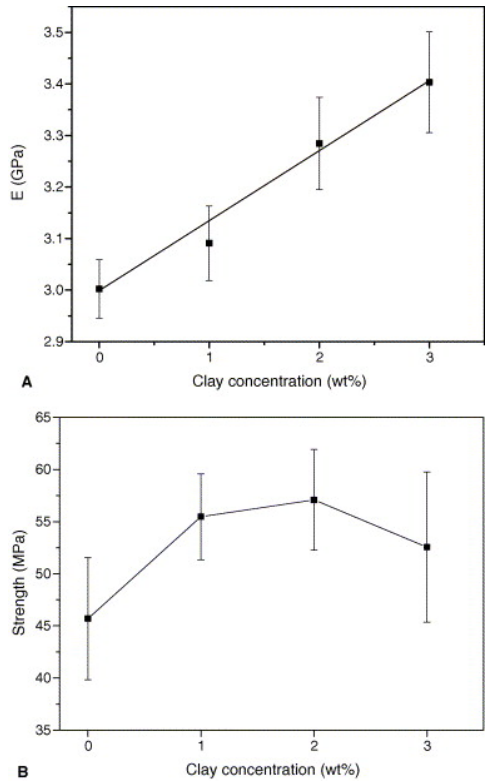

Figure 2.10: Effect of nano-fillers on (A) tensile modulus and (B) tensile strength [44]

2.2.2 Sintering Window

The additive manufacturing process is a thermal process and in this Section the thermal conditions will be investigated further. The sintering window is the range between the melting and the crystallisation range in the laser sintering process. This range must be wide enough in order to be a suitable a polymer powder is for the laser sintering process. The powder that is used experiences four thermal stages. It is important for these conditions to be correct for a successful process. Literature supports the fact that it is crucial to have a thorough understanding of the exact sintering window of the used material, since this will influence the success of the build and the dimensional accuracy. [42] These four thermal conditions can be seen in Figures 2.11, 2.12, 2.13, & 2.14. For each of these thermal conditions a DSC curve is shown with a clearly identified region that is called the sintering window. The DSC technique is explained in Section 4.1.

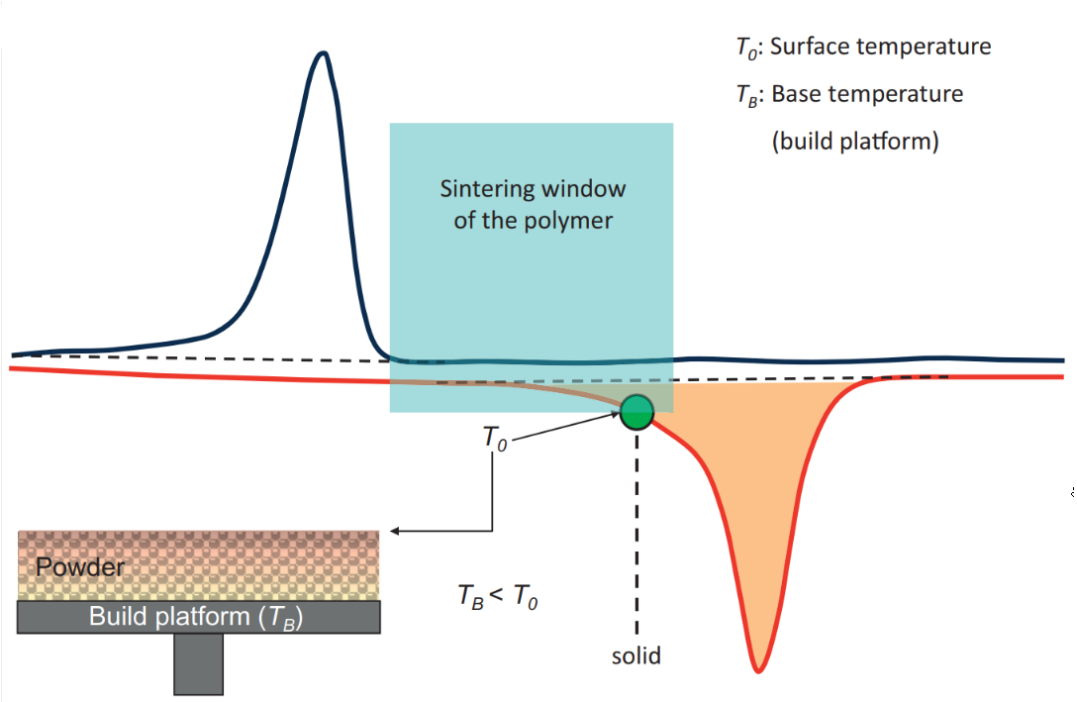

Figure 2.11: Initial condition before the first sintered layer [41]

In Figure 2.11, thermal equilibrium, denoted as T_0, is experienced by the uppermost powder layer. This layer of powder has a temperature just below the melting point of this material. Using a radiant heating system, that uses infrared light, the powder is heated from above. The radiant heating system controls T_0. The build platform is lowered by a single layer thickness and the next phase starts.

In Figure 2.12, fresh and colder powder is applied on top of the build area. The powder that was already present undergoes a drop in temperature. If this thermal shock is too big, crystallisation can be induced. This is undesired, as it will result in the warping of the part in the layers below. Due to the latter, it is every important for the surfaces heating unit to increase the temperature in the build cavity back to the required value T_0. It is also important that this happens very homogeneously,

Figure 2.13 shows the third phase, the actual laser sintering phase. The actual sintering of the material is performed by a laser beam. This beam instantly melts the applied powder particles in its predetermined path. The molten particles should flow completely and homogeneously together with the surrounding particles that are molten for complete coalescence. The laser causes the temperature of the powder (in its path) to increase very rapidly above the polymers melting point. Immediately after the passing of the laser, the temperate decreases rapidly back to the equilibrium temperature T_0, but this decrease is uncontrolled. This is however not really a problem, since the equilibrium temperature is approached from above. As a result, the powder will not be cooled

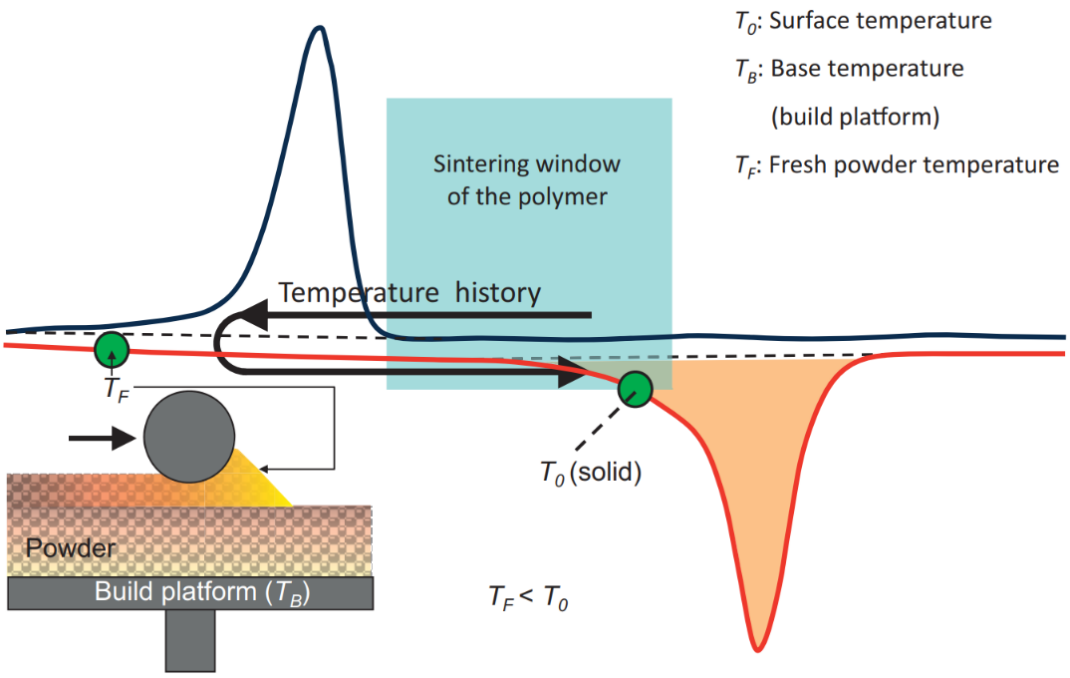

Figure 2.12: Condition after application of a fresh and cold layer of powder [41]

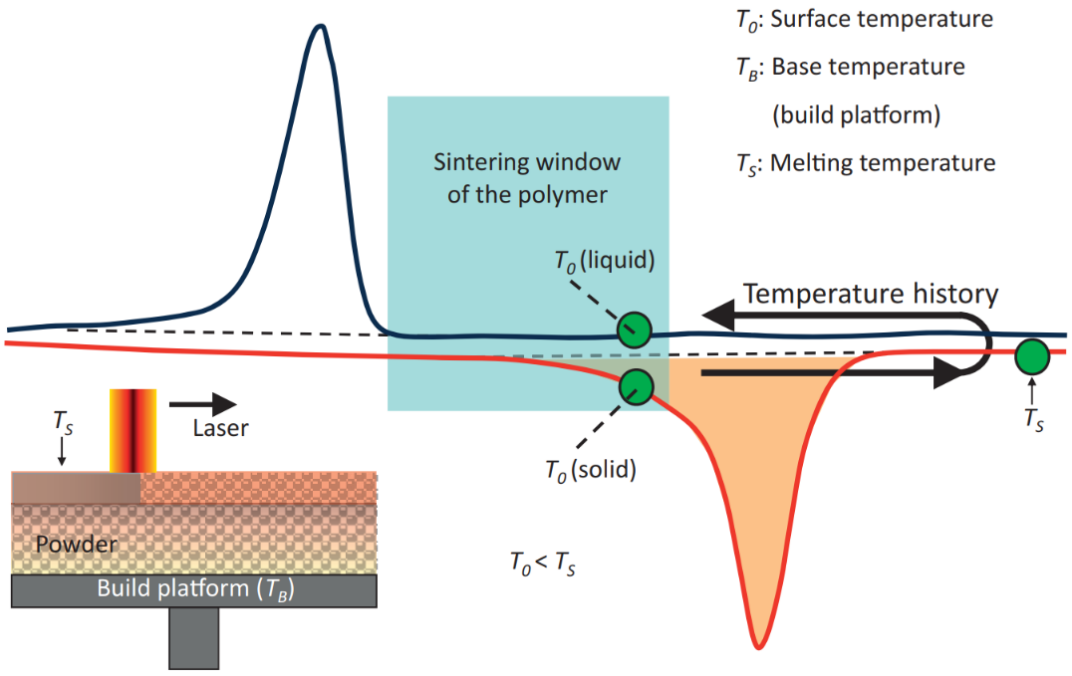

Figure 2.13: Condition during sintering of a layer with a laser beam [41]

down past the crystallisation point. Both the melted powder and untouched powder thus remain at the equilibrium temperature above the crystallisation temperature. In other words, the material will not yet start to crystallise.

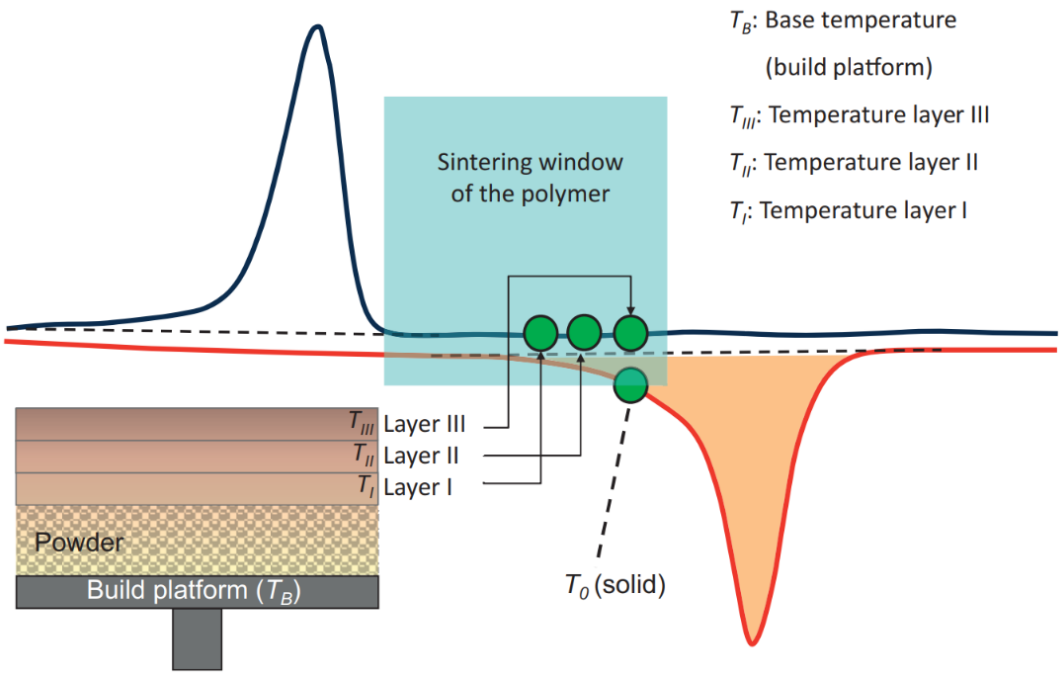

Figure 2.14: Condition after the application of multiple layers [41]

The final phase of the printing is shown in Figure 2.14. This phase starts after a layer is sintered. The cycle is repeated when a new layer of polymer powder is added. Each layer experiences a short-term cooling, and a short and intense heating (on the laser track). When the layers that are already printed are steadily moving down, they experience a slow cooling process. This process is hard to be controlled. In Figure 2.15, it can be seen that heaters are present to keep the temperature of the build cavity constant and above the crystallisation temperature. Preferably for all layers, but especially for the uppermost layers. Otherwise the undesirable curling effect will occur due to fast crystallisation.

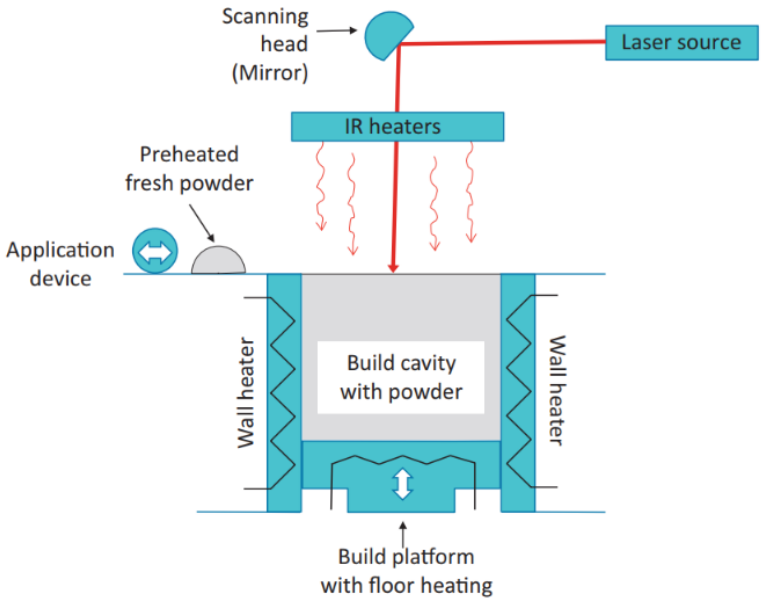

Figure 2.15: Heaters present in an SLS machine [41]

2.2.3 Cooling Rate

When the actual process is finished the build cavity is still at the processing temperature, or T_0, that is above the crystallisation temperature. The built parts are hidden in the build volume of mostly unsintered powder. It is important to have a slow and controlled cool down of the powder cake. In a perfect scenario, the entire powder cake remains in the machine in the enclosed environment of inert gas. This is needed to prevent oxidation of the polymer material. Especially with (variants of) polyamide, oxidation results in a significant yellowing of the surface. This may be a cause for a successful sintered part to still be discarded.

If the parts would be removed prematurely from the powder cake, when the temperature is still too high, uncontrolled rapid crystallisation would occur. This will lead to undesirable distortion or warping/curling of the parts. To mitigate these effects, it is advised for a build job to cool down as long as the build time, or even longer. Often this time can increase by a factor 1.5 or even more. The parts should not be removed if the temperature of the part is still above $50°C$. [41]

The cooling rate has an effect on the degree of crystallinity of the printed parts. The exact relationship between the two, however, has not yet been determined. Research was performed in which a model was created to determine the degree of crystallinity of parts manufactured using Selective Laser Sintering. [50] This research emphasized the importance of a thorough understanding of the crystallisation behaviour of the sintered material. The crystallisation has a highly significant influence on both the mechanical and thermal properties. Both isothermal and non-isothermal crystallisation is modelled, using crystallisation kinetics. The Avrami model was used to determine the degree of crystallinity of the material for isothermal crystallisation between 160 and $168°C$. Ozawa, Jeziory, and Nakamura equations were used for modelling the non-isothermal crystallisation between 0.2 and 20 $\frac{K}{min}$. This research also used PA12 supplied by EOS (PA2200). The same material that is also used by Materialise NV. For Aerospace Applications a variant of this material is used with halogenated additives, as mentioned earlier. The research concludes that a higher isothermal holding temperature requires a longer crystallisation process. When the cooling rate is lower, the crystallisation time is also longer. For isothermal and non-isothermal, the deviation between the measured crystallisation and the crystallisation model is only 5% and 10% respectively. [50] also indicates that it would be possible to model the crystallisation behaviour with respect to the location in the build volume. But it would require that both the temperature profile and the crystallisation kinetics are known. However this is not possible even with the current state of the art technologies, since the temperature of a part during and after exposure to the laser, and during cool down cannot be measured precisely.

According to [7], a decrease in degree of crystallinity for polyamide results in a lower Young Modulus and Ultimate Tensile Strength. The focus of this research lies on the influences on the impact of the energy density of the laser on the porosity and crystallinity. No clear trend was identified between the degree of crystallinity and the mechanical properties.

Other research, see [9], indicates the importance of the cooling rate on the crystallisation of polyamide 12. However, a clear need for additional research is identified to better understand the effect of cooling rates on the mechanical properties of parts manufactured using Selective Laser Sintering. Being able to reproduce a constant degree of crystallinity is indicated by other literature to be an important priority. [40]
The research by [17] focuses on obtaining a more homogeneous temperature field during the Selective Laser Sintering process, as this is very important to have parts with uniform mechanical qualities as was established earlier to be important. [18] showed that the mechanical properties of the part increased when the energy density is improved. [3, 18] confirmed that the material is anisotropic. A higher energy input level will result in a more isotropic material but have a bad result on the dimensional accuracy of the printed parts. [1] focuses on the effect of the printing orientation on the mechanical properties of the parts. The result showed that the horizontal orientation represents the mechanical properties of the material for the application in aerospace.

Literature indicates that it still remains unknown if sacrificial parts, that are used to test the quality of the entire build, are representative for the quality of all printed parts. [41]

2.2.4 Porosity

The porosity of a part is the volume fraction of this part that is not made out of the material but is empty. Open and closed pores can be present. Unfortunately, porosity has a bad effect on the mechanical properties of PA12. [49] The higher the porosity, the lower the tensile strength and stiffness of the tested material. According to [35, 36], the Energy density distribution affects the porosity. If a region experiences a lack of energy, it can be associated with a higher porosity. These findings are confirmed by [2]. The relationship between the energy density and porosity on the mechanical properties is also established. A clear relationship between the fracture location and the porosity was found by [34].
However, other research was unable to find a relationship between the porosity and the variation in the mechanical properties. [21] This is possibly because of the low and relatively constant porosity in the samples. As a result the influence is insignificant.

The results from [37] suggest that generated structures will have a different mechanical behaviour depending on their orientation, position in the build volume, and size. Clear trends can be seen in Figures 2.16 and 2.17. Up to 3 mm diameter the porosity and the pore count increase rapidly. If the diameter is more than 3 mm, these factors remain fairly constant.

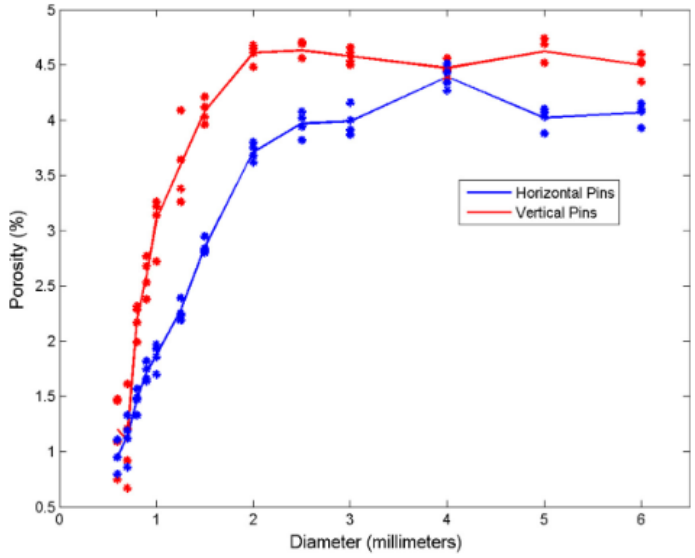

Figure 2.16: Porosity content in two orientations for different diameters of SLS printed pins [37]

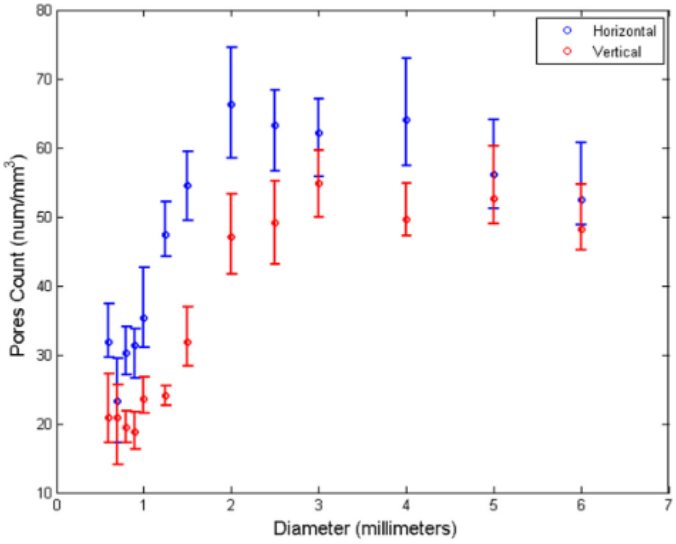

Fig. 3. Average pores counts per volume of pins printed in both orientations.

Figure 2.17: Pore count in two orientations for different diameters of SLS printed pins [37]

A rapid and accurate measurement technique to establish the porosity is hard to find. For accurate results, most research uses X-ray Computed Tomography, since it is a non-destructive measurement technique that allows for the determination of the porosity and thus also the density of parts. The main advantage of the CT scanning is the accuracy, which is significantly higher than any alternative. This technique also provides information on the volume and the form factors of the pores, but also on the exact number of pores. The main disadvantage of this very accurate technique is the fact that it is very expensive and time consuming. [41] An example of a typical cross-section from a X-ray CT-scan of PA12 can be seen in Figure 2.18. According to [41], the average porosity for PA 12 parts is $4\% \pm 1\%$. The incomplete coalescence of the polyamide melt is the cause of the significant residual porosity. This results in brittle behaviour during tensile tests.
In this research [38], the influence of the scanning parameters on the porosity measurements are elaborated upon. However, the repeatability of the measurements is shown to be high, and barely any difference is present during the reconstruction of the tests.

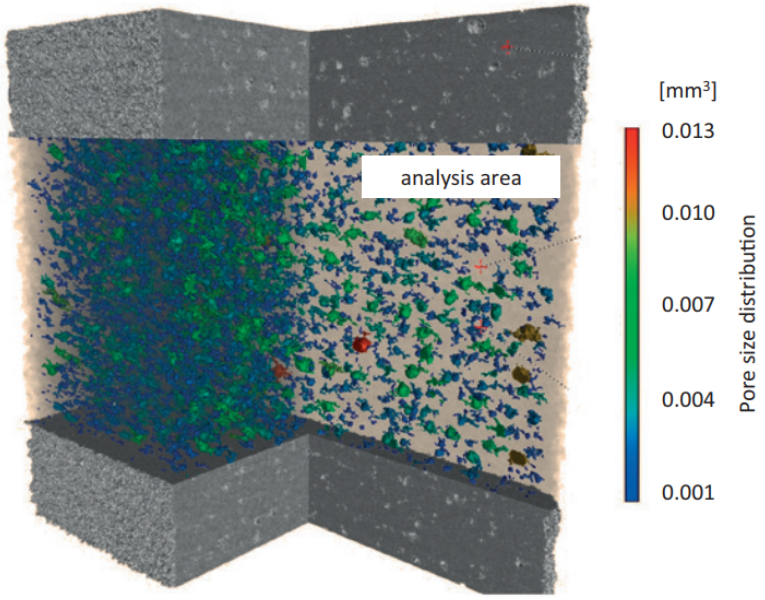

Figure 2.18: Example of pore distribution in PA12 using CT scanning [41]

[43] found that the pore density (number of pores per volume) is a much better indicator for mechanical performance compared to the porosity (volume of pores per volume). Along the build direction this is especially true. The anisotropy in this direction is also confirmed by other research [12] and advised to further look in to this effect. The pore morphology is strongly anisotropic in this direction. The process temperature has a significant impact on pore density. The porosity needs to be controllable for a reproducible selective laser sintering process. This anisotropy caused by the porosity, has an adverse effect on the fatigue life of the material. Although, this effect is less significant due to a relatively high variation on the fatigue life overall. [32]

2.3 EOS P 770

The last section of this chapter will conclude with a discussion of the machine used for the manufacturing of the aerospace grade parts. This machine is called the EOS P 770 from the German Company EOS and is shown in Figure 2.19.

Figure 2.19: EOS P 770

This machine uses Selective Laser Sintering to form parts out of many types of polymers: Alumide, PA 1101, PA 1102 black, PA 2200, PA 2201, PA 3200 GF, PrimeCast 101, PrimePart FR (PA 2241 FR),PrimePart PLUS (PA 2221). All of these materials are types of polyamides.The PrimePart FR is used in this study and complies with the aerospace regulations.

This EOS P 770 has one of the largest build volumes for this class of machines. The build volume is 700 mm wide, by 380 mm deep, with a maximum height of 580 mm. This allows for the manufacturing of parts up to one meter in length. The melting of the powder is achieved by using two 70 W CO_2 lasers. Each of these lasers can operate in a region a bit larger as half of the build volume. As a result there is a small region where both laser have an overlap. This is indicated by the centre region in red in Figure 2.20. No parts can be printed in the red regions at the corners. Compared to its predecessors, this system has improved the laser accuracy. This results in no visible effects occurring in the region where both lasers overlap. Depending on the material and layer thickness, this system is able to build 32 mm/h in height. The maximum scan speed is $10\frac{m}{s}$ for each individual laser. The layer thickness varies from 0.06 mm to 0.18 mm depending on the used material.

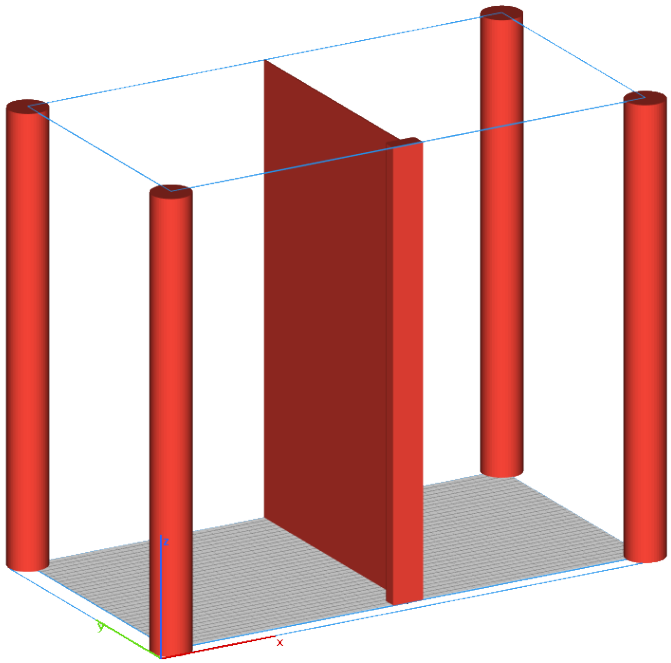

Figure 2.20: Graphical representation of the build volume, with special areas highlighted in red.

The entire machine is 2.25 m wide, 1.55 m deep and 2.1 m tall. It speaks for itself that the build volume is less than the total machine volume. This is necessary to allow for all needed subsystems, but also to allow for insulation of the build volume. This allows for a more gradual cool down, which has an desirable effect on the mechanical properties of the part. [13]

Chapter 3
Research Definition

From the literature study that is presented earlier, several gaps in knowledge can be identified. This results in a set of research questions that will need to be answered. These research questions and objectives are presented in Section 3.1. Three research questions are identified and will now be elaborated upon. The scope of these research questions is explained in the corresponding Section 3.2. Finally, the hypothesis for the aforementioned research questions are stated.

3.1 Research Questions

In this section the three proposed research questions are expanded upon. After the statement of each research question, a brief explanation is given for its relevance.

3.1.1 Research Question 1

The first research question:

How does the crystallinity correlate with strength and stiffness of Selective Laser Sintered PA2241FR?

This research question arises from the fact that crystallinity and porosity are the two most important factors influencing the mechanical properties of semi-crystalline polymers. A lot of research has already been performed on porosity of Selective Laser Sintered polyamide, see Section 2.2.4, leaving the crystallinity of these polymers open for further investigation.

3.1.2 Research Question 2

The second research question:

How does the amount of FR-additive correlate with strength and stiffness of Selective Laser Sintered PA2241FR?

PA2241FR distinguishes itself from other polyamide powders due to its halogenated additive that increases the fire retardancy of the material. It is known that PA2241FR has worse mechanical properties compared to PA2200, see Section 2.2.1. However, it is not known how the additive is dispersed in the material. A variation in the content of this additive, may cause a variation in the mechanical properties of this material. It is thus crucial to identify if the mixture is not constant and if it is a possible cause of variation of the mechanical properties.

3.1.3 Research Question 3

The third and final research question:

What is the influence of the geometrical properties of a printed batch on the strength of Selective Laser Sintered PA2241FR?

As identified earlier in the literature study, the cooling rate during manufacturing is an important factor for the degree of crystallinity of semi-crystalline polymers. Since the build chamber will not cool down uniformly, it is possible that the mechanical properties of the material may also vary depending on geometrical properties of the printed parts. To answer this research question, a possible correlation between the geometrical properties and the mechanical properties will be investigated. Since the sintered parts experience a higher temperature than the unsintered powder, they can be considered as a local heat source. The rest of these parameters will be explained in Section 5.4.

3.2 Scope

Since the above research questions are too broad to be considered in a single Master of Science thesis, the scope of these questions needs to be more narrow. Since the available resources are limited, it was decided that the results of this thesis will only serve as an identification of any found trends. It is not within the scope of this thesis to form a detailed model of the effect of all investigated parameters.

For the first research question, the statistical relevance of an increase in degree of crystallinity on both the maximum stress and tensile modulus will be investigated. A differentiation is made between the tensile specimens in horizontal and vertical direction, as printing orientation has a significant effect on the mechanical properties.[1] However the porosity of a sample is known to have a significant effect on the mechanical properties of these samples. Because of this, their porosity is also determined. If a trend with a (high) correlation can be found, it will also be presented.

For the second research question, the statistical relevance of an increase in flame retardant additive on both the maximum stress and tensile modulus will be investigated. Again, a differentiation is made between the tensile specimens in horizontal and vertical direction.

For the third and final research question, the statistical relevance of several build parameters will be investigated. These build parameters are the following:

1. Ratio of surface area over volume
2. Total printed volume
3. Local printed volume
4. Proximity of a part
5. Volume Distribution in Z-direction
6. Volume Distribution in X-direction

3.3 Hypotheses

In this thesis, several hypotheses are tested. The goal of this thesis is to test these hypotheses using experimental data. These hypothesis are stated in the form of falsifiable statements, or null hypotheses. If these statements can be rejected, the alternative hypotheses can be accepted. The final hypotheses for all research questions are presented below.

1. Effect of crystallinity on mechanical properties:
   (a) H_0: The maximum stress is unaffected by the degree of crystallinity.
      - H_1: The maximum stress is affected by the degree of crystallinity.

   (b) H_0: The tensile modulus is unaffected by the degree of crystallinity.
      - H_1: The tensile modulus is affected by the degree of crystallinity.

   (c) H_0: The maximum stress is unaffected by the porosity.
      - H_1: The maximum stress is affected by the porosity.
2. Effect of amount of FR-additive on mechanical properties:
   (a) H_0: The maximum stress is unaffected by the amount of flame retardant additive.
      - H_1: The maximum stress is affected by the amount of flame retardant additive.

   (b) H_0: The tensile modulus is unaffected by the amount of flame retardant additive.
      - H_1:The tensile modulus is affected by the amount of flame retardant additive.
3. Effect of build characteristics on mechanical properties:
   (a) H_0: The maximum stress is unaffected by the weighted aspect ratio of surface area over volume.
      - H_1: The maximum stress is affected by the weighted aspect ratio of surface area over volume.

   (b) H_0: The maximum stress is unaffected by the total printed volume.
      - H_1: The maximum stress is affected by the total printed volume.

   (c) H_0: The maximum stress is unaffected by the local printed volume.
      - H_1: The maximum stress is affected by the local printed volume.

   (d) H_0: The maximum stress is unaffected by the proximity of a part.

[1] `https://erpro-group.com/wp-content/uploads/2019/06/PA-2241.pdf`

- H_1: The maximum stress is affected by the proximity of a part.

(e) H_0: The maximum stress in Z-direction is unaffected by the mass distribution in Z-direction.
- H_1: The maximum stress in Z-direction is affected by the mass distribution in Z-direction.

(f) H_0: The maximum stress is unaffected by the mass distribution in Z-direction.
- H_1: The maximum stress is affected by the mass distribution in Z-direction.

(g) H_0: The maximum stress in X-direction is unaffected by the mass distribution in X-direction.
- H_1: The maximum stress in X-direction is affected by the mass distribution in X-direction.

(h) H_0: The maximum stress is unaffected by the mass distribution in X-direction.
- H_1: The maximum stress is affected by the mass distribution in X-direction.

Chapter 4
Tests Methodology

The state-of-the-art of the possible test methodologies are presented in this chapter. In order to determine the degree of crystallinity of the material two types of tests are useful. The first test that will be discussed will be Differential Scanning Calorimetry or DSC in short. The second test that can be used is X-Ray Diffraction or XRD in short. It is can also be used to determine the degree of crystallinity of the material. The last test that can be used is Nuclear Magnetic Resonance Spectroscopy or NMR. The flame-retardant content can be evaluated using this test.

4.1 Differential Scanning Calorimetry (DSC)

Differential Scanning Calorimetry or DSC is an instrumental thermal analysis technique. A sample is heated at a fixed rate, the difference in the amount of heat absorbed by the sample and a standard is measured by the power that is needed to increase the temperature. This thermal analysis method is very important in polymer science, more precisely for the investigation of processes that involve a change of heat capacity. These are called second order transformations. But also, the first order transformations, that are defined as a change in enthalpy. DSC will have many uses but for the scope of this research, it will be used to investigate the melting and crystallisation characteristics of PA2241FR. A schematic representation of a typical DSC setup is shown in Figure 4.1. There are two possible types of systems. In the first system, displayed on the right, the sample and a reference sample are kept at the same temperature, but the amount of added energy is different for each sample. In the second system, the amount of added energy is kept constant for both the reference and the test sample. The temperature of these two specimens will be different, if a phase change occurred. [6, 41, 48]

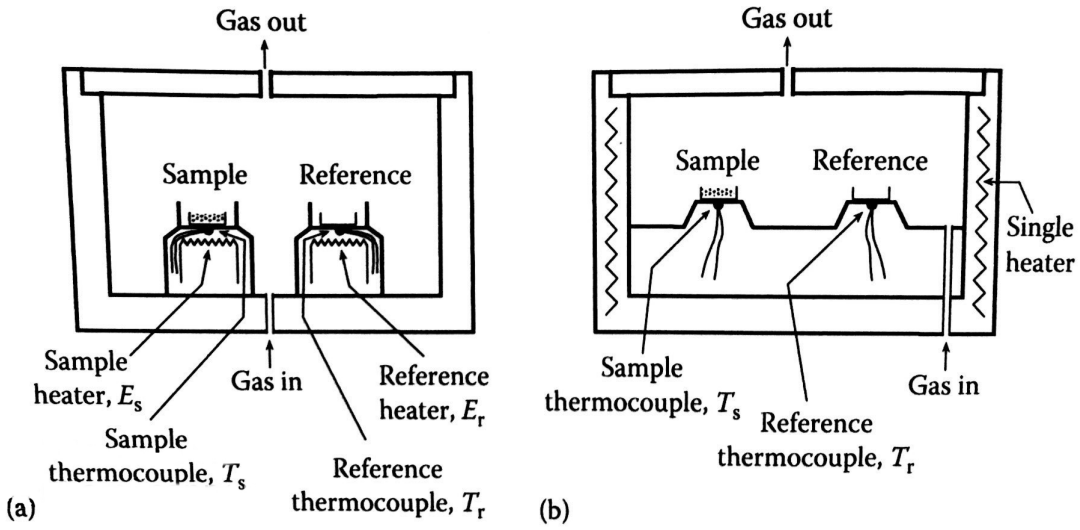

Figure 4.1: Schematic Illustration DSC Setup [48]

These phase changes are represented by the peaks in Figure 4.2. T_m denotes the melting temperature and is represented by an endothermic peak, meaning heat must be added before the material can melt. T_{cc} represents the cold crystallisation temperature, this phase changes is an exothermic reaction.

It is important to note that the exact location of these curves depends on the heating and cooling rate that is used in the experiment. It is of crucial importance, that these rates are kept constant for all tests. It is important to note

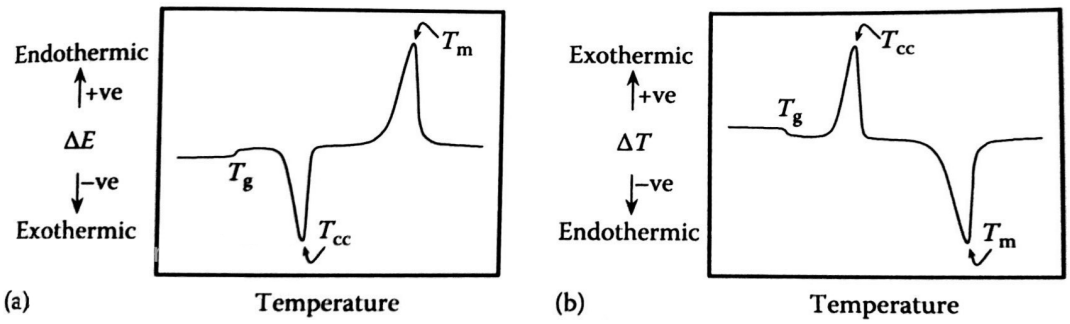

Figure 4.2: Schematic representation of the peaks experienced during heating or cooling of a sample [48]

that for laser sintering processes, differential scanning calorimetry is an essential analytical instrument. The use of this instrument is crucial for the determination of the sintering window, as can bee seen in Section 2.2.2. This technique is very useful to evaluate how suitable a polymer powder is for the laser sintering process. In Figure 4.3, an actual DSC curve can be seen of PA2200.

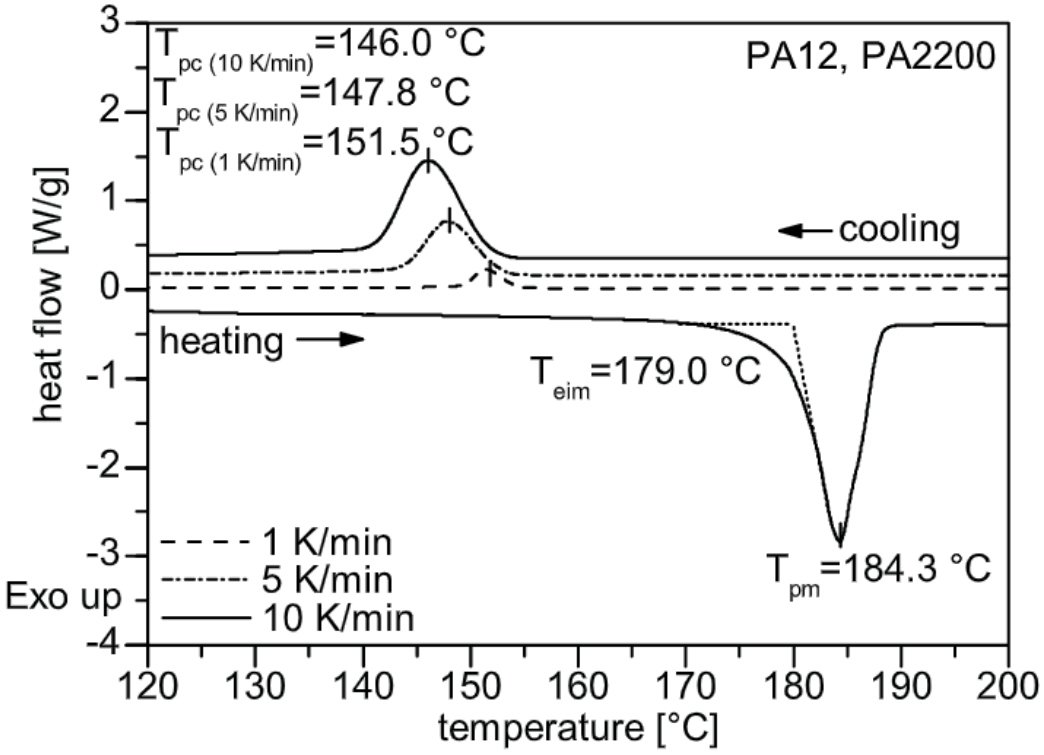

Figure 4.3: Actual Differential scanning Calorimetry Curve of PA2200 [12]

4.2 X-Ray Diffraction (XRD)

X-Ray Diffraction or XRD is a technique that is used to analyse both the relative position of the atoms on the molecular repeat units and the arrangement of these segments in the unit cell. For the determination of the crystal structure of a semi-crystalline polymer. This method is less precise than when it is used for determining the crystal structure of a single crystal. Modern DSC machines use two-dimensional CCD cameras that are capable of capturing the diffraction patterns digitally.

X-Ray Diffraction or XRD is a technique that finds its primary use in the structural identification of all solids, but are especially useful for the determination of the structure of a semi-crystalline polymer. The sample must either be a single crystal or the finely grounded powder.

This technique is based on constructive interference of monochromatic X-rays and a crystalline sample of material. A concentrated monochromatic beam of X-rays are being generated by a cathode ray tube, and are directed towards the sample. Constructive interference will occur due to interaction of the incident rays and the sample only when the local conditions are correct for Bragg's Law.

$$n\lambda = 2d \sin\theta \tag{4.1}$$

Where n is the order of reflection λ is the wavelength, d is the distance between parallel lattice planes, and θ is the angle between the incident beam and a lattice plane. This angle is also defined as the Bragg angle.

A typical XRD setup can be seen in Figure 4.4. In the left of the figure, a graphical representation is shown of the diffraction of X-rays by the crystal lattice. The right half of the figure shows the X-ray diffraction of a polycrystalline polymer sample. [48]

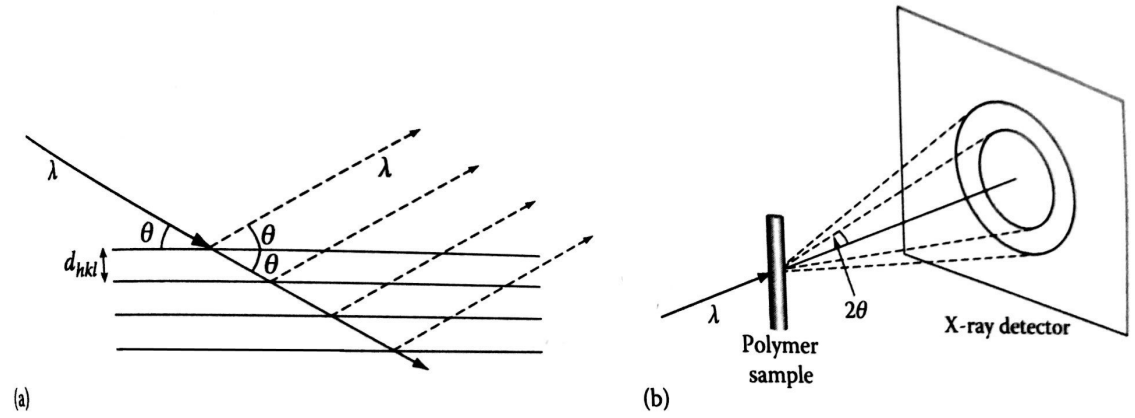

Figure 4.4: Schematic Illustration X-Ray Diffraction technique [48]

The distance between the concentric circles can be related to the spacing of the crystal planes, noted as d_{hkl}, through the scattering geometry that can be seen in the left part of the figure and through Bragg's law.

In Figure 4.5 an example of X-ray diffraction pattern of Nylon-6 and Nylon-6,6 can be found. These patterns are obtained from polypropylene samples. A clear distinction can be made between these results. Each pattern indicates a different situation.

The grey background in these figures caused by the amorph part or phase of the semi-crystalline polymer. The disorganised polymer molecules cause a diffuse background in the test. The circles on the other hand indicate a presence of small randomly-oriented crystallites.

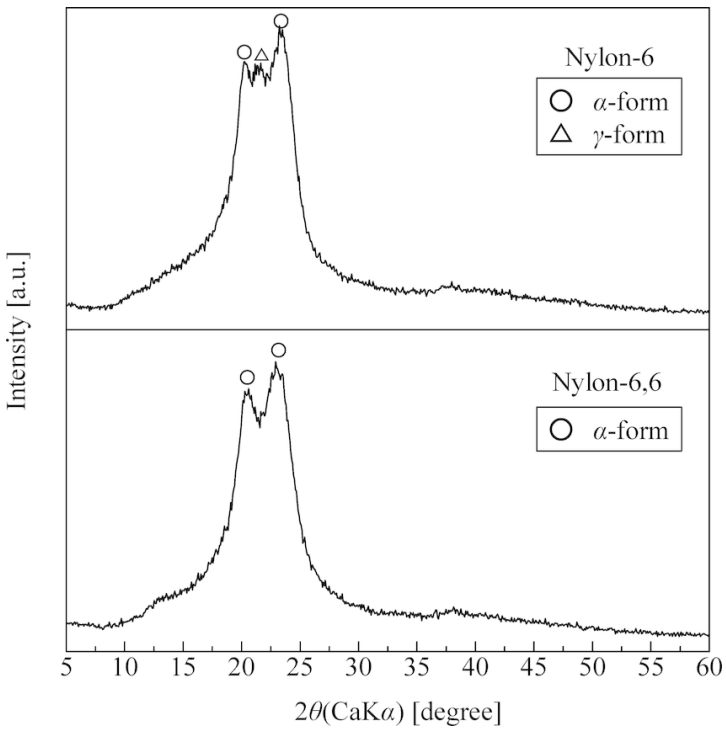

Figure 4.5: Example of X-ray diffraction pattern of Nylon-6 and Nylon-6,6 [47]

4.3 Nuclear Magnetic Resonance Spectroscopy (NMR)

Nuclear Magnetic Resonance spectroscopy, or abbreviated as NMR, is an analytical chemistry technique used for determining the content of a sample, the chemical structure, and other purposes. It will be used to quantitatively analyse the PA2241FR mixture containing the halogenated additive.

The principle behind this spectroscopy technique is that all atomic nuclei have an electric charge and most have a spin. Applying an external magnetic field allows energy transfer that raises the atom from base energy to a higher energy level. This is often a single energy gap, see Figure 4.6. [1]

This energy transfer is characterised by a wavelength that is classified as a radio frequency. The same energy and frequency are emitted, when the spin returns to its original base level. This radio frequency is received, measured, and analysed thoroughly in order to generate the desired NMR spectrum for the desired nucleus. This technique is the simplest for nuclei with $I \ \frac{1}{2}$, for example $^{1}H, ^{13}C, \& ^{19}F$. This is because their nuclei magnetic moments align either parallel with or parallel against the magnetic field. The energy difference between these two states is then used to identify the bond of the atom.

The effective magnetic field that acts at the nucleus influences the exact resonant frequency of the energy transition. The electron shielding affects the aforementioned magnetic field. The electron shielding is determined by the chemical environment. Due to this, it is possible to obtain information about the chemical environment of the nucleus from the resonant frequency. In layman's terms, the more electronegative a nucleus is, the higher the resonant frequency is. Tetramethylsilane, or TMS, is often adopted as the proton reference frequency. This reference is needed since the exact resonant frequency shift of each nucleus depends on the used magnetic field. An example of a ^{1}H-NMR spectra of nylon can be seen in Figure 4.7. From this curve, the flame retardant content of the sample can be determined.

[1] Image is courtesy of Institute of Chemistry - The Hebrew University of Jerusalem

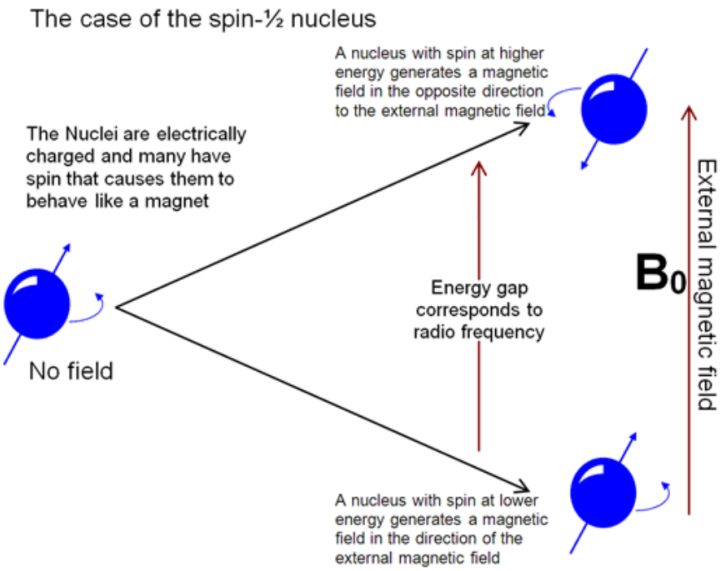

Figure 4.6: Behaviour of atom in external magnetic field

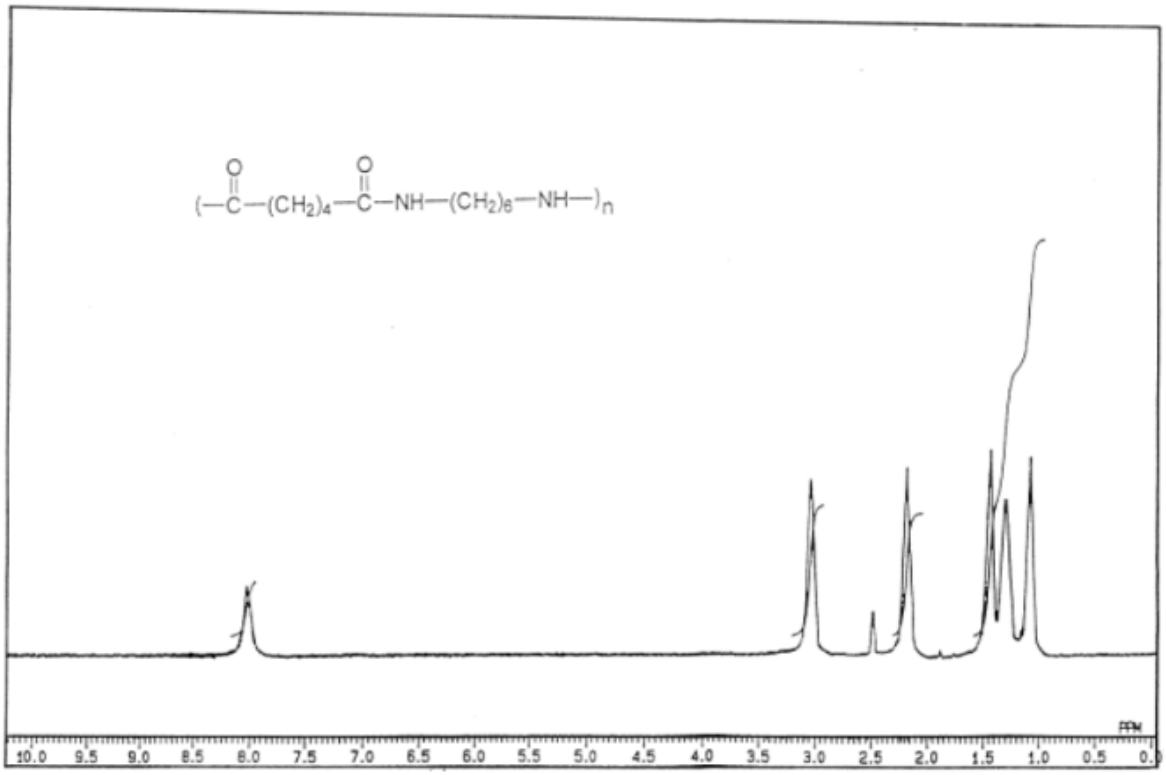

Figure 4.7: ^{1}H-NMR spectra of nylon [11]

II

Performed Research

Chapter 5
Methodology

Now that the theoretical background has been presented and the scope of the research has been defined, the methodology used in this research can be presented. A detailed overview of the steps that are taken are presented. More information on the used equipment can be found in Appendix C. These steps can be followed to recreate the results.

5.1 Preparing Samples

Before the material can be investigated, the specimens are ground down to a fine powder using the cryogenic grinder mentioned in Section C.4. The samples for the porosity measurements must also be prepared. First, the specimens that are going to be used in this research are selected.

5.1.1 Choosing Samples

A list of all available specimens can be found in Appendix B. Eventually it was chosen to test 40 specimens, 20 specimens in horizontal direction and 20 specimens in vertical direction. These samples are not chosen randomly, the ten specimens with the highest and lowest maximum stress are chosen for both printing orientations. The data from these specimens can be seen in Table 5.1 for the horizontal orientation. For the vertical orientation, this data can be found in Table 5.2. It can readily be seen that there is a difference in tensile strength in both orientations.

Table 5.1: Used specimens with EDGE orientation

Phys Part ID	**Orientation**	**Build ID**	**Counter**	E_T **[MPa]**	σ_M **[MPa]**
9613545	EDGE	137470	13	1730	45.2
9613547	EDGE	137470	15	1750	45.4
9613554	EDGE	137470	22	1740	46.2
9671766	EDGE	138297	12	1760	45.4
9671769	EDGE	138297	15	1750	45.3
9671777	EDGE	138297	23	1760	46.6
9671778	EDGE	138297	24	1760	46.8
9682340	EDGE	138448	14	1770	45.5
9682348	EDGE	138448	22	1780	47.2
9682349	EDGE	138448	23	1750	46.6
9682691	EDGE	138456	10	1750	45.5
9682694	EDGE	138456	13	1730	45.2
9682703	EDGE	138456	22	1710	46.2
9682704	EDGE	138456	23	1730	46.8

Unfortunately, some samples were ruined during the testing, as a result only 18 samples in vertical orientation and 14 in horizontal orientation could be investigated. The samples that are shown here are the samples that were tested successfully and from which the data can be used reliably in this research. There was one additional sample that overheated during the grinding due to a shortage of liquid nitrogen in the grinding chamber. This sample did melt during the grinding and crystallised while still in the cryogenic grinder. This sample was later tested using DSC in order to determine the crystallinity. It is known that this error affected the degree of crystallinity of the specimen, making it useless for this research itself. However, the results from this specimen served as a quick check if any other specimens overheated.

Table 5.2: Used specimens with UP orientation

Phys Part ID	Orientation	Build ID	Counter	E_T [MPa]	σ_M [MPa]
9613559	UP	137470	27	1780	45
9613549	UP	137470	17	1810	44.7
9613551	UP	137470	19	1770	44.5
9613552	UP	137470	20	1780	44.8
9613560	UP	137470	28	1750	44.4
9613562	UP	137470	30	1750	42.7
9671772	UP	138297	18	1790	44.1
9671773	UP	138297	19	1790	42.6
9671774	UP	138297	20	1800	44.3
9671783	UP	138297	29	1790	42.5
9682345	UP	138448	19	1780	43.1
9682354	UP	138448	28	1790	44.1
9682355	UP	138448	29	1780	44.3
9682696	UP	138456	15	1730	42
9682697	UP	138456	16	1720	40.5
9682698	UP	138456	17	1700	40.6
9682699	UP	138456	18	1710	41.4
9682708	UP	138456	27	1720	42.7

Table 5.3: Specimen that overheated

Phys Part ID	Orientation	HS?	Build ID	Counter	E_T [MPa]	σ_M [MPa]
9682706	UP	HS	138456	25	1740	42.3

5.1.2 Grinding Samples

Now that it is known which specimens are going to be tested, the actual preparation of these specimens can begin. The specimens are ground down into a fine powder using the cryogenic grinder mentioned in Section C.4. As the tensile bars are broken into two large parts, see Figure 1.2, it was chosen to grind the top part into a powder, while the bottom part will be used for the determination of the porosity of the samples. However, the top part is still too large to fit into the funnel of the machine. A specimen must first be bathed in liquid nitrogen, since this will make the sample really brittle, which facilitates the breaking of the specimen into smaller pieces using a hammer.

The mesh used in the cryogenic grinder is a sieve shells with 0.08 mm trapezoidal perforation made of stainless steel 316L. The final powder will thus have a grain diameter smaller than 0.08 mm. This perforation size was chosen since it was available, a larger perforation size would also be acceptable.[1]

Before starting the grinding process, the machine is examined to see if no dust is present in the grinding chamber or in the funnel on top of the grinding chambers. If this is the case, the machine is cleaned. The machine is powered on, then the following procedure is repeated for each sample:

1. Pour liquid nitrogen into the funnel
2. Start the machine (grinding knifes will start to rotate)
3. Add several small pieces of the sample
4. Add liquid nitrogen
5. Add rest of the small pieces of the sample
6. Add liquid nitrogen
7. Wait until the power required by the engine drops to a minimum
8. Turn the machine off
9. Remove powder for the machine and put into a designated specimen zip lock bag
10. Clean the machine

[1] `https://www.fritsch-international.com/sample-preparation/milling/ball-mills/details/product/pulverisette-14-premium-line/accessories/`

It is important to note that the machine needs to be cleaned entirely after every sample in order to eliminate the chance of contamination of the powder by previously grounded samples. Also important to note is that a sudden peak in the required power will most likely result in an increase in temperature of the powder. It is very important to add sufficient liquid nitrogen immediately to minimise the risk of melting of the powder.

5.2 Methodology for the Analysis of the Degree of Crystallinity & Porosity

In this section, the methodology used to analyse the degree of crystallinity and porosity is presented. The following sections elaborate on the steps that occurred in order to analyse the effect of the degree of crystallinity and the porosity respectively.

5.2.1 Degree of Crystallinity

The degree of crystallinity is analysed using Differential Scanning Calorimetry. A more elaborate discussion on the results can be found below, but first a summarised version of the methodology is presented.

1. Deposit between 5 and 10 mg of the sample in a pan.
2. Determine the mass of the sample.
3. Close the sample with a top lid using the designated press.
4. Put the sample in the sample area of the DSC machine.
5. Repeat for all samples
6. Run DSC scans using determined process, see Table 5.4.

The Differential Scanning Calorimetry machine heats and cools the sample as explained earlier in Section 4.1. More details on the exact machine can be found in Section C.1. For this machine to operate correctly, it needs a small quantity of the material, between 5 and 10 mg. This is needed since the amount of heat that is needed to increase the temperature is proportional the mass of the sample. A small quantity of the powder of each sample is put into a small separate pan and its mass is determined accurately using a scale. This pan is sealed hermetically using a designated tool. The samples are then put into the sample area. It is important to note that the pans may not be touched by hand, as the oils present on the skin will contaminate the pan and this will result in inaccurate results.

For this material it was chosen to let it operate between $25.00°C$ and $250.00°C$, since the melting temperature is at $185°C$, according to the data sheet of the manufacturer of the powder, see [14]. A standard cooling and heating rate of $10\frac{°C}{s}$ was chosen. The procedure used by the TA Instruments DSC is shown in Table 5.4. First the sample will be held at $25.00°C$ for 1 minute. This is added as an extra buffer between the heating and cooling steeps of the test. Secondly, the material will be heated to a temperature of $250.00°C$, where it waits one minute, before cooling down again to $25.00°C$. Again it will wait a minute. This process is repeated once more. This allows for a visual distinction between the first heating run and the second heating run. If the two runs are the same, the same pan has been tested earlier. This happened during the testing since the machine can run out of coolant (liquid nitrogen), and it will repeat the last test. The material will grab the next pan autonomously when it is finished with the previous one.

As mentioned earlier, the machine needs liquid nitrogen to function. A large number of automated tests, require a large amount of liquid nitrogen. During the testing some problems were experienced and the machine did ran out of coolant. Because of this, some tests needed to be repeated to obtain useful results. The DSC data that is obtained from these tests gives the normalised heat flow Q [W/g] at a given temperature T [$°C$].

Now that the physical test have been carried out, the raw obtained data needs to be processed. This needs to be done using the same software that runs the DSC machine. This software is called *TRIOS*. An example of a processed curve is shown in Figure 5.1. The area in the peak of the first heating cycle needs to be determined, since this peak characterises the degree of crystallinity before melting. A baseline needs to be determined first.

Table 5.4: Procedure Differential Scanning Calorimetry

Step	Discription
1	Initial Temperature 25.00°C
2	Isothermal 1.0 min
3	Ramp 10.00$\frac{°}{s}$ to 250.00°C
4	Isothermal 1.0 min
5	Ramp 10.00$\frac{°}{s}$ to 25.00°C
6	Isothermal 1.0 min
7	Ramp 10.00$\frac{°}{s}$ to 250.00°C
8	Isothermal 1.0 min
9	Ramp 10.00$\frac{°}{s}$ to 25.00°C
10	Isothermal 1.0 min

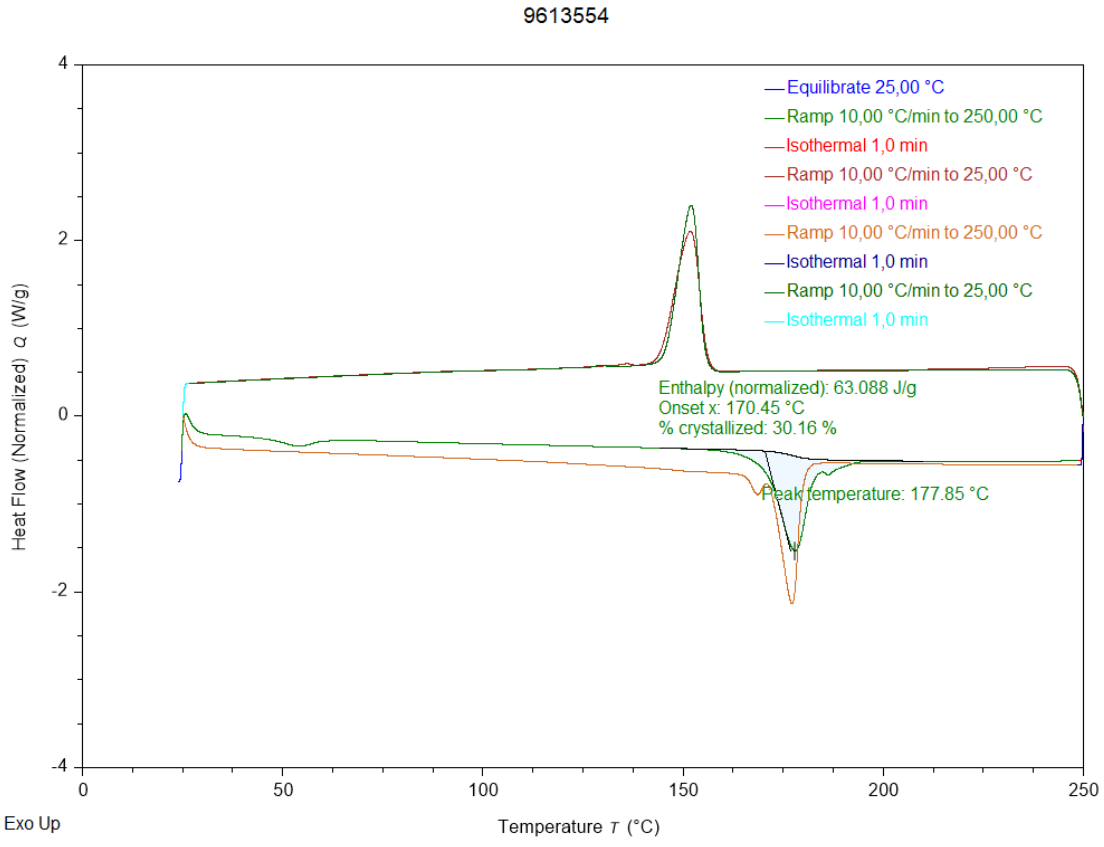

Figure 5.1: Graphical representation of DSC data of specimen 9603554

This line needs to be tangent to the region before and after the curve. If this line is drawn properly, the software gives the normalised enthalpy in J/g. Using this result and the melting enthalpy for a 100% crystalline sample of PA12, the degree of crystallinity can be calculated, see Equation 5.1. [39]

$$X_c = \frac{\Delta H_m}{\Delta H_m^0} \tag{5.1}$$

Where ΔH_m is the measured melting enthalpy of the PA2241FR and ΔH_m^0 is the melting enthalpy for a 100% crystalline sample of PA12, it assumed to be equal to 209.2 J/g . [8, 39] This calculation can be done manually, but TRIOS is also able to do this automatically. This can be seen in Figure 5.1. It also shows the melting temperature of the sample.

5.2.2 Porosity Samples

As mentioned earlier, the bottom part of the tensile specimen will be used to determine the porosity of the sample. The porosity is determined by following the steps present below, a more elaborate discussion on these steps will follow after.

1. Cut the sample as large as possible.
2. Make sure the sample is a straight beam.
3. Determine the volume using caliper.
4. Determine the mass using scale.
5. Calculate the density.
6. Compare calculated density to theoretical density.

An example of the used samples can be seen in Figure 5.2. Three of the four tested specimens have two red cutting lines drawn. The part between these lines is a beam, and this facilitates the determination of the volume of these specimens.
On these red lines, the samples are cut with a sharp cutter knife. This knife is pressed down into the material until it is completely trough the tensile bar. It is important not the make a sawing motion since this will add heat that might locally deform the specimen and influence the degree of porosity.
Note that if the bottom part is too small, it cannot be used. An example of this can be seen in sample 28 in Figure 5.2. In order to increase the accuracy as much as possible and to limit the effect of the cutting planes, the porosity samples are cut as large as possible. Any possible error regarding dimension or weight will be less significant.

After the samples are cut, they are measured using a caliper. This allows for the determination of the volume of the beam shaped parts. A theoretical maximum mass of each specimen can be determined simply by multiplying the volume with the maximum density.
Finding the maximum density of PA2241FR is not obvious. From the datasheet of the material used by Materialise NV, the density is stated as $1.00 \pm 0.03 \frac{g}{cm^3}$. [29] The maximum density is definitely higher, since some specimens have a density of $1.02 \frac{g}{cm^3}$. Since not much is known about PA2241FR, it was chosen to look at the density of PA12. Also at the density of the material using injection moulding since it usually much more dense. Polyram PlusTek RD120 Nylon 12, Injection Molding is stated to have a density of $1.03 \frac{g}{cm^3}$ [2]. Since this is also the most extreme value given by Materialise, it is chosen to use a value of $1.03 \frac{g}{cm^3}$ as the maximum density this material can have.

The mass of each specimen is determined using the scale presented earlier, see Section C.5. This value can be compared to the maximum mass of the specimen. The ratio presented in Equation 5.2 gives an indication of the porosity of the sample.

$$porosity = \frac{m_{measured}}{m_{calculated}} \tag{5.2}$$

This will give a result between 0 and 1. The closer this value is to 1 the lower the porosity. Since this means the beam is more dense. The closer this is to 0, the higher the porosity, since the material is less dense. The density of the specimen can easily be determined by multiplying the calculated porosity by the maximum density.

[2] `http://www.matweb.com/search/datasheet.aspx?matguid=d0f08048761a4941ad9bfc853b7a0004&ckck=1`

Figure 5.2: Example of tensile specimens cut for the use as an estimation of the porosity

5.3 Methodology for Analysis of Flame Retardant Content

In this section, the proposed methodology is presented for investigating the effect of the Flame Retardant additive that is present in PA2241FR. This will be investigated using Nuclear Magnetic Resonance Spectroscopy. This technique is already explained in Section C.2. Since NMR Spectroscopy is an expensive testing method, only a limited number of points can be tested. Because of this, it is advised to choose the data points that are outliers when investigating the crystallinity and porosity. Since the degree of crystallinity and the porosity cannot explain their extreme values, it is more efficient to limit the NMR test to these values. As mentioned earlier, both solution and solid-state Nuclear Magnetic Resonance Spectroscopy is considered, and the proposed methodology for each of these techniques is discussed now.

5.3.1 Solution Nuclear Magnetic Resonance Spectroscopy

Since solution Nuclear Magnetic Resonance Spectroscopy is associated with the lowest cost, this technique is preferred and will be presented first. A more detailed explanation is given in Section C.2.1. The type of NMR test that needs to be run is explained, followed by a discussion on the solvent.

The halogenated additive, chloride or bromide will replace a hydrogen atom that is bonded on the backbone of the polymer. The carbon atom present will experience a different spin. This will cause a new peak in the obtained spectra. If a larger number of hydrogen atoms are replaced by chloride or bromide, the higher the peak will become. The area under this curve is proportional to the amount of additive that is present in the sample. Since the change in spin will be experienced by a carbon atom, it advised to investigate the polyamide with ^{13}C NMR spectroscopy [4, 15].

Now that it is known what type of tests are needed for the analysis of the sample. The used solvent can be discussed. In [28], it is stated that PA12 will dissolve in $DMSO-d6$, DMF, $DMAc$, dimethyl sulfoxide, NMP, Py and in H_2SO_4 at room temperature. It however is insoluble in chloroform, tetrahydrofuran, methylene chloride, cyclohexane, acetone and water. It is partially soluble in in methanol and ethanol and precipitated in MeOH/water. Note that this is the case at room temperature and for PA12, not PA2241FR.

The spectra obtained from the NMR spectroscopy, can be analysed to obtain data on the FR-additive. The area under each of the peaks corresponds to amount of bonds of a certain type. The area of the peak that correspond to the flame retardant additive can be compared to the peak of other tested samples.

5.3.2 Solid-state Nuclear Magnetic Resonance Spectroscopy

The methodology for solid-state Nuclear Magnetic Resonance Spectroscopy will be discussed. ^{13}C NMR spectroscopy will also be used for solid-state NMR, the reasoning behind this is still the same as for solution NMR. This is also confirmed to be a correct approach by [15].

As mentioned in Section 5.3.2, standard solid-state NMR tests only give qualitative results on the composition of a material, but no quantitative results. The techniques presented by [33] and [20], can be used to obtain quantitative spectra.

A method is presented by [20], that yields quantitative solid-state magic-angle spinning ^{13}C NMR spectra of organic materials, such as polyamide, with good signal-to-noise ratios. However, this method thus requires multiple scans for a single sample. For economic reasons, the number of samples that could be tested using NMR was already limited. Since multiple scans are needed for a single specimen, this method is cannot be considered to be economically viable for this research. The same holds for the approach used by [33]. The monetary benefit of these tests, does not outweigh the cost.

5.4 Methodology for Analysis of Geometrical Parameters

The methodology for the analysis of the geometrical parameters is presented here. This data is obtained from Materialise Magics, a more elaborate discussion of this software is found in Section C.3. The geometrical parameters are compared to the mechanical properties of that build. But first, the methodology for obtaining the data from Materialise Magics is presented. It can be summarised into the following steps, a more elaborate discussion follows after.

1. Make a template in order to export data.
2. Export build data for each build.
3. Calculated needed geometrical parameters for each build.
4. Bundle data for all prints with the corresponding mechanical data.
5. Find possible trend.
6. Perform an analysis of variance.

Before the data is exported from Materialise Magics, a template is needed. This template allows you to select which data is exported for the selection of parts in the print volume. There is a wide variety of parameters that can be chosen from. Only the values that can be used in this research are exported. The final data contained the following information of every part:

1. Part (or STL) name
2. Volume [mm^3]
3. Surface [mm^2]
4. Centre X-coordinate [*mm*]
5. Centre Y-coordinate [*mm*]
6. Centre Z-coordinate [*mm*]
7. Dimension in X-direction [*mm*]
8. Dimension in Y-direction [*mm*]
9. Dimension in Z-direction [*mm*]
10. Minimum X-coordinate [*mm*]
11. Minimum Y-coordinate [*mm*]
12. Minimum Z-coordinate [*mm*]

For all ten batches, this data was exported for every part in the batch. The number of parts in a single batch/build varies approximately between 100 and 700 parts. This because some builds have a large number of relatively small parts, while other builds have a small number of relatively bigger parts. Now that it is known how the data is obtained, the focus can shift more towards the processing of this data. As mentioned earlier several parameters will need to be calculated in order the obtain useful results.

The effect of these parameters will be analysed using ANOVA, or analysis of variance. This is a method used to analyse the differences among group means in a group of individuals. The analysis of variance was performed using the ANOVA Excel function. The output of the analyse of variance is the probability value, or p-value. This parameter aids in the interpretation of the results. In order for the relationship between the data to be significant, the probability value needs to be less than 0.05. If this is the case, the null hypothesis must be rejected. The alternative hypothesis can be considered to be valid.

5.4.1 Proximity of a Part

In the available batches, several tensile bars are proximate to a different printed part. The distance between the tensile bar and the other printed part is 0.5 cm in all cases. The dimensions of the parts in the vicinity of the tensile bars have similar dimensions in all batches. The other tensile bars did not have a printed part in its vicinity for at least several centimetres. The effect of the proximity of these tensile bars to the other printed part is investigated in this section. It is possible for the printed part to act as an additional heat source. A region of the build volume that is hotter will radiate heat to its surroundings since the temperature of the build volume will become uniform if sufficient time is given. The printed part will reduce the cooling rate. The reduced cooling rate will result in increased mechanical properties. [50]

To test this, the maximum stress of the tensile specimen close to an other part is compared to the maximum stress of those that are not close to a part. For a given laser field and orientation, the average maximum stress of the normal specimens is compared to the maximum stress of the specimen with a close neighbour, see equation 5.3. Where R_{HS} is the aforementioned ratio.

$$R_{HS} = \frac{\sigma_{M,\,proximate}}{\sigma_{M,\,averagenormal}} \tag{5.3}$$

5.4.2 Total Printed Volume

The next parameter that is discussed is the total printed volume. The more volume is printed, the more heat is added to the system by the two lasers. If more volume is printed, the total heat of the system is higher. Subsequently, it is expected that it requires more time to cool down. As mentioned earlier, a slower cooling rate will result in a higher degree of crystallinity.

$$R_{TotalVolume} = \frac{\sum V_{parts}}{V_{printer}} \tag{5.4}$$

The total printed volume in a single build is determined by a summation of the volume of all printed parts in that build. The total printable volume is given by the printer dimension. The build volume has the following dimensions 700 x 380 x 580 mm, resulting in a volume of 154 280 000 mm^3. The ratio of these two is given in Equation 5.4. This ratio is compared to the average maximum stress, σ_M, of all tensile specimens in that build to see if the printed volume has an effect on the mechanical strength of a build.

5.4.3 Local Printed Volume

The next parameter that is discussed is the local printed volume. This parameter is similar to the total printed volume, except that only a partial region of the build volume is considered. The more volume that is printed, the higher the total heat of the system, which is excepted to result in better mechanical properties. However, it is expected that the finished build will not cool down uniformly, the presence of a higher amount of printed parts may only have a local effect on the cooling rate and thus the degree of crystallinity and mechanical strength.

$$R_{LocalVolume} = \frac{\sum V_{parts}}{V_{Local}} \tag{5.5}$$

The local printed volume in a single build is determined by a summation of the volume of all printed parts in that build. The local printable volume is chosen to be only a small part of the total volume. The build volume has the following dimensions: 700 x 380 x 580 mm. The final chosen region has the following dimensions for the vertical tensile specimens: 200 x 190 x 580 mm. This results in a volume of 22 040 000 mm^3. The final chosen region for the horizontal tensile specimens: 120 x 190 x 580 mm. This results in a volume of 13 224 000 mm^3. The height of these region was chosen to be approximately 20 mm higher as the maximum Z location of the specimens in the specified orientation. Since the tensile specimens are positioned over the entire length of the build volume, the width remained 580 mm. Only half the depth of the machine was chosen, meaning a region with a depth of 190 mm. The ratio of these two is given in Equation 5.5. Due to constraints of the software, the parts are considered to be point volumes. The volume of the part is only considered in this analysis, if the centroid is positioned within the provided range. This ratio is compared to the average maximum stress, σ_m, of the tensile specimens in the specified orientation in that build to see if the printed volume has an effect on the mechanical strength of a build.

5.4.4 Ratio of Surface and Volume

As stated above, the larger the printed volume the more heat is added. However, the larger the surface area of the printed part, the more heat it can dissipate through the surface. The ratio between the volume and the surface might be an interesting parameter to investigate. A large part with a large surface area will lose its additional heat more rapidly compared to a large part with only a small surface area. An example of these specimens are a

large plate and sphere. If these two have the same volume, the plate will dissipate its heat more easily. If only the ratio between the volume and surface area are compared, a large and a small sphere would have the same ratio. Because of this, it was chosen to determine the weighted average of this ratio. This ratio is given in Equation 5.6.

$$R_{W.A.S/V} = \frac{\sum (V_{part} \cdot \frac{S_{part}}{V_{part}})}{\sum V_{part}} \tag{5.6}$$

Where $R_{W.A.S/V}$ is the weighted average of the Surface area to volume ratio of all parts in the build. It is expressed in $\frac{1}{m}$. The surface area to volume of a part was weighted with volume of that part. The sum of this weighted value was divided by the total volume in order to normalise it again. This value is compared to the average maximum stress, σ_m, of all tensile specimens in that build to see if it has a significant effect.

5.4.5 Mass Distribution in Z-direction

The last two parameters will both investigate the mass distribution of the parts in the build. First, the mass distribution in Z-direction will be investigated. In Section 5.4.6, the mass distribution will be discussed in X-direction. It was chosen to analyse the mass distribution in Z-direction, because again the proximity of mass closer to the tensile specimens are expected to have a beneficial effect. A higher mass distribution would mean the parts are spread out over the build volume. If the mass distribution is low, the parts would all be together relatively close to the centre of the build. If this is the case, they are expected to have no impact on the tensile specimens. It is important to note that mass and volume distribution are proportional since the density of these parts is assumed to be constant. To facilitate the calculations, the volume is considered instead of the mass.

$$c_Z = \frac{\sum (Z_{coord,\,i} \cdot V_i)}{\sum V_i} \tag{5.7}$$

$$MD_{Z,\,i} = (Z_{coord,\,i} - c_Z)^2 \cdot V_i \tag{5.8}$$

$$MD_Z = \sum MD_{Z,\,i} \tag{5.9}$$

In equation 5.7, the calculations needed to determine the centroid in Z-direction is shown. The centroid is later needed in Equation 5.8, here a term is calculated that is an indication of the volume distribution of a single part. The difference between the centroid in Z-direction of the part, noted by $Z_{coord,\,i}$, and the overall centroid is squared to get rid of the sign, and increases the impact of parts that are positioned more outwards. This square is then multiplied by the Volume of that part. In Equation 5.9, the result of previous equation is summed together for all parts. This final value is the volume or mass distribution of the entire build. Note that these calculations are similar for the determination of the Steiner Term used in the parallel axis theorem.

5.4.6 Mass Distribution in X-direction

A similar explanation can be given as for the choice to analyse the mass distribution in X-direction, since the proximity of mass closer to the tensile specimens are expected to have a beneficial effect. Especially since the tensile specimens in horizontal orientation are positioned outwards in X-direction. Again a higher mass distribution in this direction would mean the tensile bars are closer to the other printed bars.

$$c_X = \frac{\sum (X_{coord,\,i} \cdot V_i)}{\sum V_i} \tag{5.10}$$

$$MD_{X,\,i} = (X_{coord,\,i} - c_X)^2 \cdot V_i \tag{5.11}$$

$$MD_X = \sum MD_{X,\,i}c \tag{5.12}$$

Similar to the previous section, in equation 5.10, the expression for the centroid in X-direction is shown. Which is used to determine the volume distribution for a single part in Equation 5.8. In Equation 5.9, the total volume distribution in X-direction is shown.

It is also important to note that it was decided not to look at the mass distribution in Y-direction. This is done since the build volume is already significant smaller in this direction compared to the other directions. Any effect on the mass distribution in Y-direction might be insignificant.

Chapter 6
Results

After the discussion of the used methodology, the results can be presented. In this Chapter, the raw results are processed and presented. First, the results for the analysis of the degree of crystallinity are presented, together with the porosity measurements. These are followed by the results of the flame retardant content. Finally, the geometrical data obtained from Materialise Magics is discussed.

6.1 Results of Crystallinity & Porosity

As mentioned in Chapter 5, the degree of crystallinity is obtained using differential scanning calorimetry. All the data obtained from the DSC tests are presented in Appendix B. The baseline that is used for the determination of the degree of crystallinity is also shown. The degree of crystallinity of each sample is presented together with the melting enthalpy of the sample. This information can be bundled together into a table. This data can be found in Table 6.1 for the specimens with a horizontal orientation. For the specimens with a vertical orientation, this data can be found in Table 6.2.

Table 6.1: Degree of crystallinity for specimens with horizontal orientation

Phys Part ID	Or.	HS?	Build ID	Count	E_T [MPa]	σ_M [MPa]	Enthalpy [J/g]	D.o.C. [%]
9613554	EDGE	HS	137470	22	1740	46.2	67.013	32.03
9682704	EDGE	-	138456	23	1730	46.8	81.282	38.85
9671778	EDGE	-	138297	24	1760	46.8	74.365	35.55
9682703	EDGE	-	138456	22	1710	46.2	81.694	39.05
9671777	EDGE	-	138297	23	1760	46.6	71.845	34.34
9671766	EDGE	HS	138297	12	1760	45.4	56.454	26.99
9682348	EDGE	HS	138448	22	1780	47.2	81.545	38.98
9613547	EDGE	-	137470	15	1750	45.4	70.392	33.65
9682340	EDGE	-	138448	14	1770	45.5	76.446	36.54
9682349	EDGE	-	138448	23	1750	46.6	83.721	40.02
9682691	EDGE	HS	138456	10	1750	45.5	75.398	36.04
9682694	EDGE	-	138456	13	1730	45.2	75.503	35.61
9671769	EDGE	-	138297	15	1750	45.3	67.397	32.22
9613545	EDGE	-	137470	13	1730	45.2	72.065	34.45

Unfortunately, the data presented in a table does not give any insight in the results. Because of this, it is chosen to perform an analysis of the variance and determine a linear trend line through these points. First the results for the horizontal orientation will be discussed. In Figure 6.1, the maximum stress is plotted in function of the degree of crystallinity. The R^2-value is 0.2932. When the tensile modulus is plotted in function of the degree of crystallinity, see Figure 6.2, the R^2-value is almost equal to zero.

However, when an analysis of variance is performed on the maximum stress and the degree of crystallinity, the p-value is equal to 0.045524. The p-value for this case is equal to 0.40996.

Now the effect in vertical direction can be investigated. In Figure 6.3, the maximum stress is plotted in function of the degree of crystallinity. The R^2-value is equal to 0.1372. In the plot of the tensile modulus in function of the degree of crystallinity, see Figure 6.4, the R^2-value is equal to 0.0813,

For this data set, an analysis of variance is also performed on the maximum stress and the degree of crystallinity. For the maximum stress and the degree of crystallinity, the p-value is equal to 0.035036. The tensile modulus and the degree of crystallinity are also subjected to an analysis of variance. The p-value for this case is equal to 0.16819.

Table 6.2: Degree of crystallinity for specimens with vertical orientation

Phys Part ID	Or.	HS?	Build ID	Count	E_T [MPa]	σ_M [MPa]	Enthalpy [J/g]	D.o.C. [%]
9613559	UP	HS	137470	27	1780	45	85.884	41.05
9682696	UP	HS	138456	15	1730	42	49.308	23.57
9682354	UP	-	138448	28	1790	44.1	54.808	26.2
9613551	UP	-	137470	19	1770	44.5	57.632	27.55
9682699	UP	-	138456	18	1710	41.4	56.396	26.96
9613552	UP	-	137470	20	1780	44.8	73.682	35.22
9682355	UP	-	138448	29	1780	44.3	81.44	38.93
9682708	UP	-	138456	27	1720	42.7	70.707	33.8
9682345	UP	-	138448	19	1780	43.1	76.302	36.47
9671783	UP	-	138297	29	1790	42.5	68.772	32.87
9671774	UP	-	138297	20	1800	44.3	70.607	33.75
9671772	UP	-	138297	18	1790	44.1	75.405	36.04
9671773	UP	-	138297	19	1790	42.6	70.681	33.34
9613560	UP	-	137470	28	1750	44.4	69.738	41.86
9613549	UP	HS	137470	17	1810	44.7	84.659	40.47
9613562	UP	-	137470	30	1750	42.7	77.649	37.12
9682706	UP	HS	138456	25	1740	42.3	124.43	59.48
9682697	UP	-	138456	16	1720	40.5	73.691	35.22
9682698	UP	-	138456	17	1700	40.6	70.565	33.73

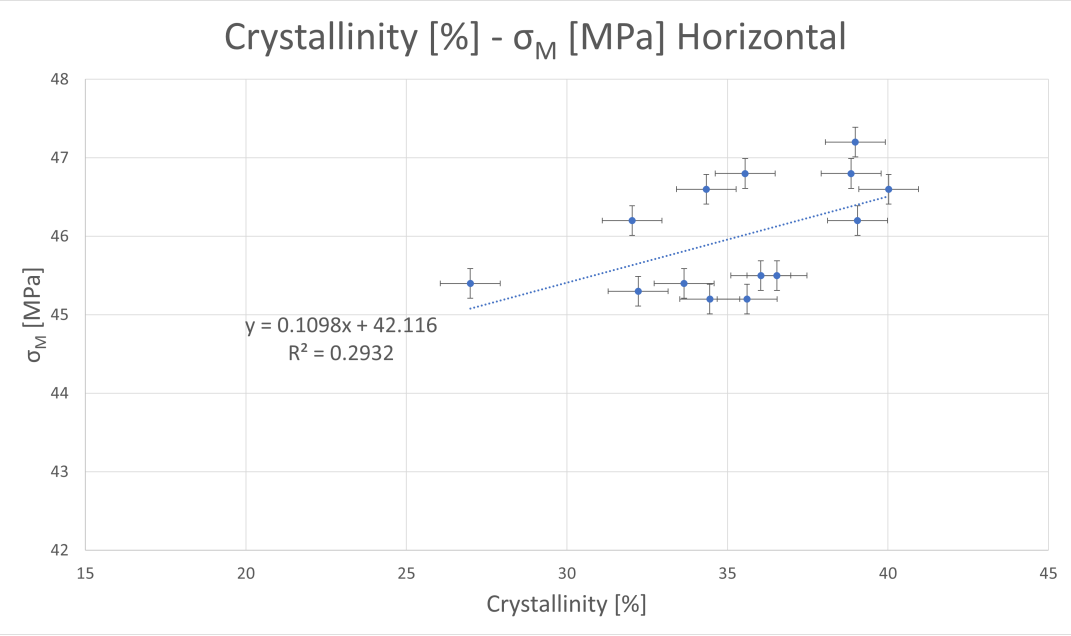

Figure 6.1: Graphical representation of degree of crystallinity vs. σ_M for horizontal direction

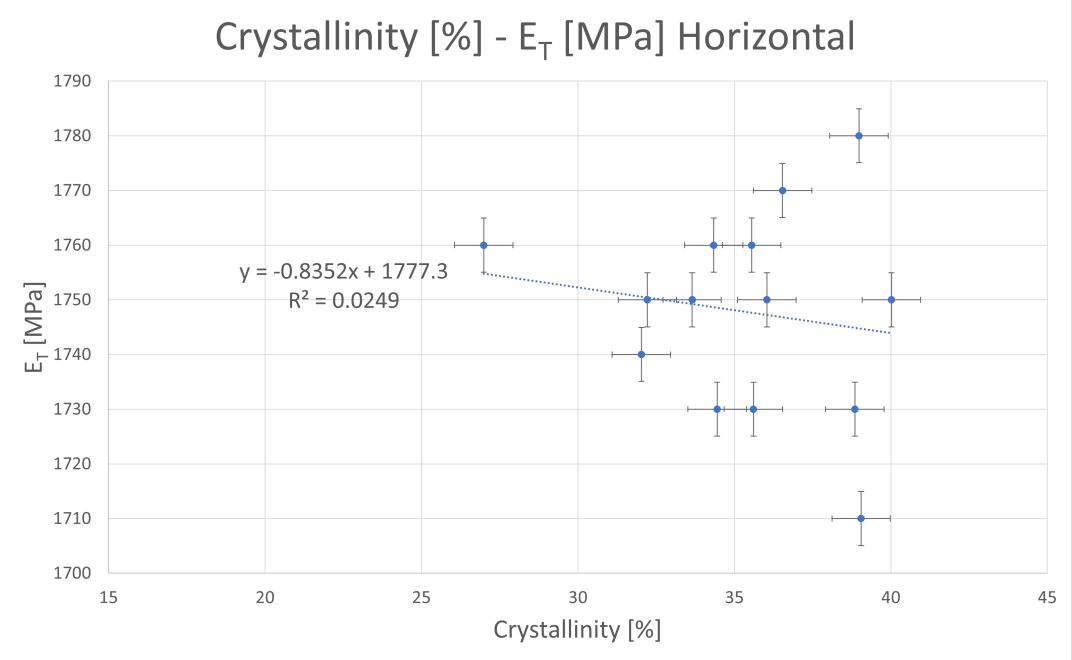

Figure 6.2: Graphical representation of degree of crystallinity vs. E_T for horizontal direction

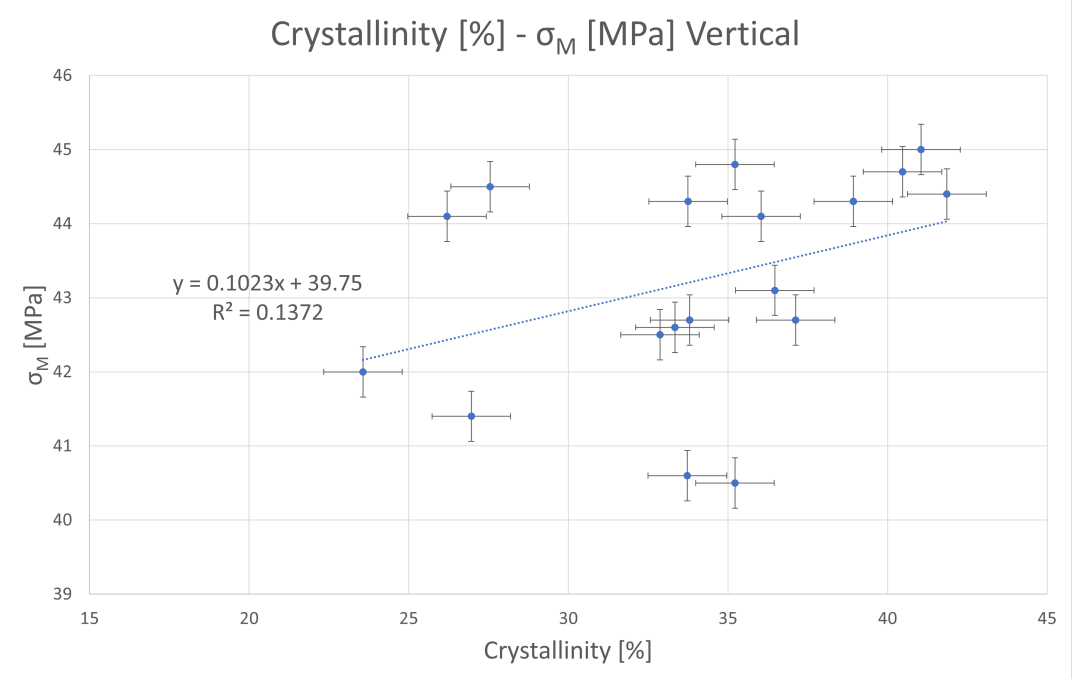

Figure 6.3: Graphical representation of degree of crystallinity vs. σ_M for vertical direction

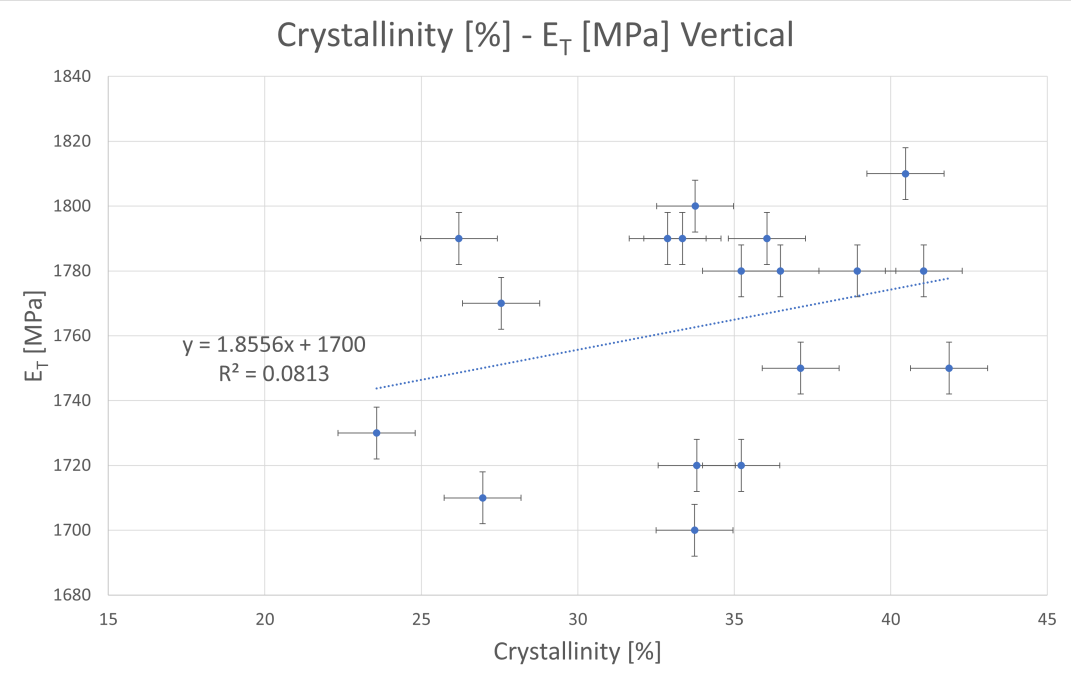

Figure 6.4: Graphical representation of degree of crystallinity vs. E_T for vertical direction

In both cases there is a very low correlation. This may imply that there is another variable that is more significant or that, in combination with the degree of crystallinity, may result in a better model. Because of this the porosity of the tensile specimens is determined. It is chosen to look at the porosity as literature indicated that it is responsible for variation in Selective Laser Sintered PA12, see Chapter 2.

In Table 6.3, the data used to obtain the porosity is shown for the specimens in horizontal direction. A graphical representation of this data facilitates the interpretation of these results. This can be seen in Figure 6.5.

Table 6.3: Data for the porosity in horizontal direction.

Phys Part ID	**b [m]**	**h [m]**	**d [m]**	**Volume** $[cm^3]$	**Calc Mass [g]**	**Real Mass [g]**	**Porosity [-]**	σ_m **[MPa]**
9682348	3.7	10	17.9	0.6623	0.682169	0.6759	0.991	47.2
9682340	3.8	10	65.3	2.4814	2.555842	2.4782	0.970	45.5
9682349	3.7	10	47.0	1.739	1.79117	1.7471	0.975	46.6
9671778	3.7	10	21.5	0.7955	0.819365	0.803	0.980	46.8
9671777	3.7	9.9	11.6	0.424908	0.43765524	0.4311	0.985	46.6
9671766	3.7	10	57.7	2.1349	2.198947	2.1255	0.967	45.4
9671769	3.7	10	57.4	2.1238	2.187514	2.1477	0.982	45.3
9682704	3.7	9.9	6.9	0.252747	0.26032941	0.2564	0.985	46.8
9682703	3.7	9.9	73.6	2.695968	2.77684704	2.7104	0.976	46.2
9682691	3.8	10	62.2	2.3636	2.434508	2.3626	0.970	45.5
9682694	3.7	10.1	62	2.31694	2.3864482	2.3141	0.970	45.2
9613554	3.8	10	8.0	0.304	0.31312	0.3084	0.985	46.2
9613547	3.8	10	76.7	2.9146	3.002038	2.9555	0.984	45.4
9613545	3.9	10	49.7	1.9383	1.996449	1.9204	0.962	45.2

When performing the analysis of variance on the data presented in Table 6.3, the p-value is determined to be equal to 0.002. The linear approximation shown in Figure 6.5 has a R^2 that is equal to 0.4653.

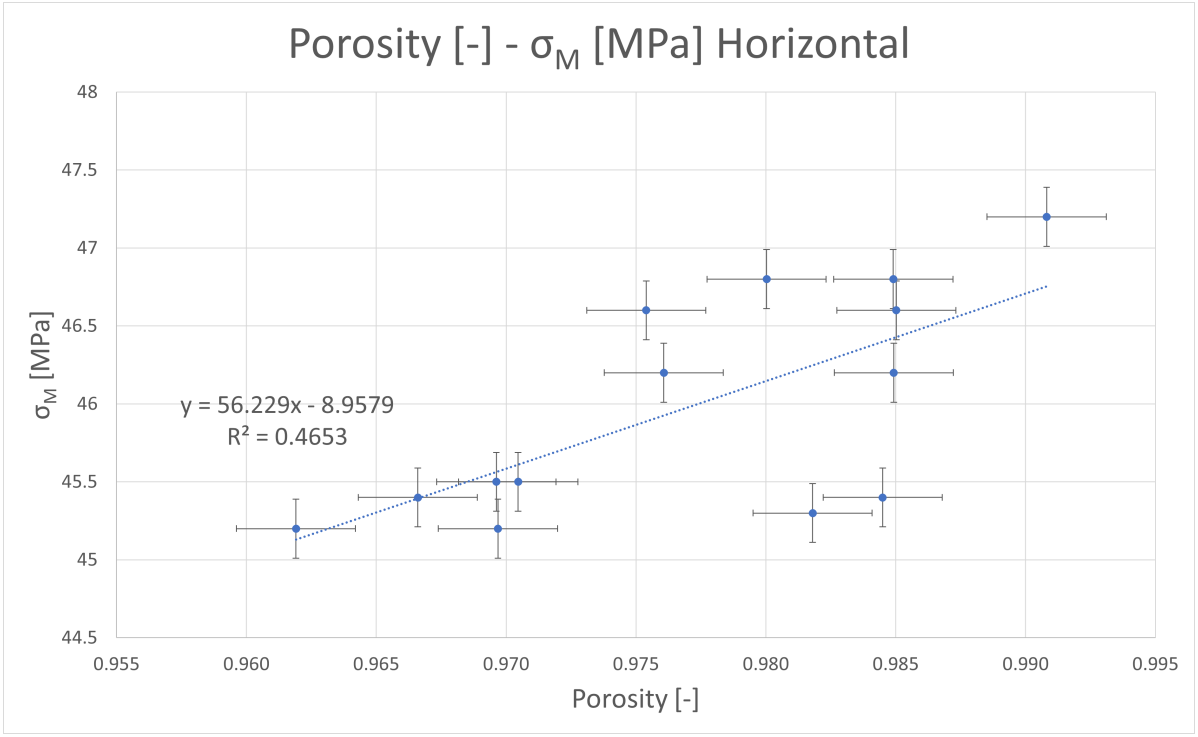

Figure 6.5: Graphical representation of degree of crystallinity vs. the porosity for horizontal direction

In Table 6.4, the data used to calculate the porosity of the specimens in vertical direction is shown. The graphical representation of this data can be seen in Figure 6.6.

Table 6.4: Data for the porosity in vertical direction.

Phys Part ID	**b [m]**	**h [m]**	**d [m]**	**Volume** $[cm^3]$	**Calc Mass [g]**	**Real Mass [g]**	**Porosity [%]**	σ_m **[MPa]**
9682354	3.7	9.7	67.6	2.426164	2.49894892	2.4859	0.995	44.1
9682345	3.6	9.7	9.6	0.335232	0.34528896	0.3407	0.987	43.1
9671783	3.7	9.7	56.8	2.038552	2.09970856	2.0815	0.991	42.5
9671773	3.7	9.7	69.9	2.508711	2.58397233	2.5538	0.988	42.6
9682696	3.7	9.8	7.4	0.268324	0.27637372	0.2713	0.982	42.0
9682698	3.7	9.7	50.6	1.816034	1.87051502	1.8114	0.968	40.6
9682699	3.7	9.7	52.6	1.887814	1.94444842	1.9022	0.978	41.4
9682697	3.7	9.7	38.4	1.378176	1.41952128	1.3780	0.971	40.5
9682708	3.7	9.7	56.6	2.031374	2.09231522	2.0566	0.983	42.7
9613551	3.8	9.8	11.5	0.42826	0.4411078	0.4367	0.990	44.5
9613562	3.8	9.8	48.2	1.794968	1.84881704	1.8290	0.989	42.7
9682355	3.7	9.7	32.5	1.166425	1.20141775	1.1842	0.986	44.3
9671774	3.7	9.7	66.3	2.379507	2.45089221	2.4204	0.988	44.3
9671772	3.7	9.7	47.2	1.694008	1.74482824	1.7278	0.990	44.1
9613559	3.8	9.8	4.9	0.182476	0.18795028	0.1873	0.997	45.0
9613552	3.8	9.8	31.6	1.176784	1.21208752	1.1983	0.989	44.8
9613560	3.8	9.8	69.5	2.58818	2.6658254	2.6203	0.983	44.4
9613549	3.8	9.9	32.4	1.218888	1.25545464	1.2416	0.989	44.7

The analysis of variance for this set of data is also performed. The p-value for this case is equal to 0.0465. The linear trend shown in Figure 6.5 has a R^2 that is equal to 0.6285.

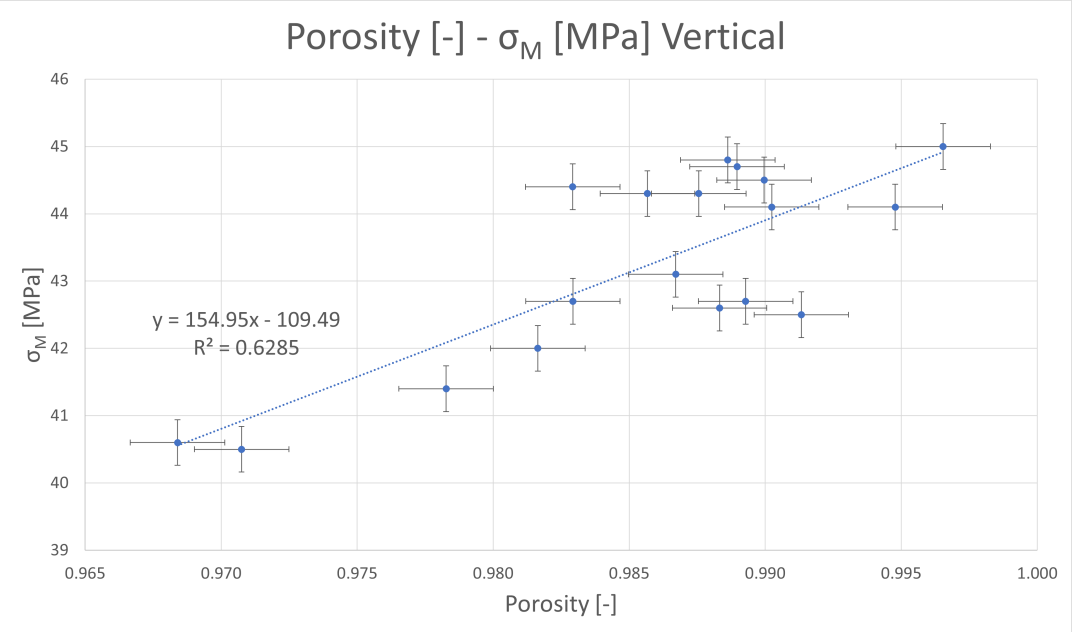

Figure 6.6: Graphical representation of degree of crystallinity vs. the porosity for vertical direction

A 3D model is determined in which the effect of both of these parameters on the maximum stress is combined. In Section 7.1, a 3D model is shown for both orientations. In Figure 7.2, the model is shown for the vertical direction. It has a R^2 that is equal to 0.71480.
Figure 7.1 shows the model for the horizontal direction. It has a R^2 that is equal to 0.52795.

6.2 Results of Flame Retardant Content

It is attempted to solve 5 to 10 mg the samples in $DMSO-d6$ at room temperature, but it does not dissolve. Even at $100°C$ while stirring at 2000 rpm, it does not dissolve.
In the chemistry lab at the Faculty of Aerospace Engineering of the Delft University of Technology, only a few solvents are available:

- H_2SO_4
- DMF
- Dimethyl sulfoxide

Of the solvents above, the sample would only dissolve (slowly) in sulphuric acid with a concentration of 95.0 - 98.0 %. However, this solvent cannot be used in the sensitive solution NMR machine. The powder did partially dissolve in hydrogen-peroxide of 30%. Since the powder could not be dissolved in any available solvent, solution NMR could not be used as a test. As mentioned in Chapter 5, the samples could not be tested using Nuclear Magnetic Resonance Spectroscopy. Solution NMR did not work, since no suitable solvent is found. Solid-state NMR is considered to be too expensive, especially since multiple runs per sample are necessary in order to obtain quantitative results.

6.3 Results of Geometrical Data

In this section, the results obtained from Materialise Magics will be presented. To start off, the results on the effect of the proximity of a part be presented. Again, a distinction is made between the printing orientation. Table 6.5, shows the data for the vertical orientation. The data for the horizontal orientation is shown in Table 6.6. In the first column the number of the set is displayed. As mentioned earlier, a single build prints 2 batches in both

directions. In the second column, the average maximum stress of the three tensile specimens that are not in close proximity to another part is shown. In the third and last column, the maximum stress of the tensile specimen that is in close proximity to another part is shown.

Table 6.5: Maximum stress for specimens in vertical orientation, both with and without the proximity of another part

Set	σ_M, NHS **[MPa]**	σ_M, HS **[MPa]**
1	43.27	43.4
2	43.83	43.2
3	43.67	43.5
4	43.03	41.3
5	40.83	42.0
6	42.9	42.3
7	44.6	44.7
8	43.6	45.0

An analysis of variation is made for both cases, but the results are the same. For the vertical and horizontal cases, the p-values are equal to 0.4646 and 0.2034, respectively.

Table 6.6: Maximum stress for specimens in horizontal orientation, both with and without the proximity of another part

Set	σ_M, NHS **[MPa]**	σ_M, HS **[MPa]**
1	45.5	46.1
2	46.67	47.2
3	45.43	45.4
4	46.6	45.9
5	44.63	45.5
6	46.37	46.2
7	45.43	45.6
8	46.03	46.2

In Table 6.7, the additional calculated data from Materialise Magics is presented. This table contains data that is unrelated to the printing orientation. In Table 6.8, the geometrical data is shown that is related to the printing orientation, in this case the Z-direction. The σ_M that is shown in this table is the average of all samples in this batch that are printed only in the UP orientation. A similar Table, containing the data for the X-orientation, is shown in Table 6.9.

Table 6.7: Average maximum stress, printed volume, and the weighted average ratio of surface area over volume of all available prints

BUILD ID	σ_M **[MPa]**	**printed Volume [%]**	**W.A. Ratio S/V** $[m^{-1}]$
138448	44.85625	3.11630371	0.832648228
138297	44.51875	5.12612121	0.697580966
138456	43.7625	3.1069307	0.688070251
137470	45.03125	2.99195321	0.678365038
143098	41.1875	3.9090912	0.65905865
144129	43.19333333	4.5609397	0.58822148
144178	40.3	3.11111337	0.96381041
145651	42.36666667	2.35155492	0.482648329
145528	41.675	3.07307768	0.968070702
145318	40.71428571	2.08532737	0.901976071

The data from these tables require graphical representations to be fully understood and to facilitate the analysis. As a result, Figures 6.7 to 6.13 are obtained and will be discussed individually.

Table 6.8: Local printed Volume for samples in Z-direction, average maximum stress in Z-direction and mass distribution in Z-direction

BUILD ID	local printed volume[%]	UP σ_M [MPa]	M.D. Z [mm^5]
138448	2.789620662	43.4875	7.33E-05
138297	4.436777868	43.1125	0.000141
138456	4.157074617	41.9375	9.74E-05
137470	1.859795361	44.2875	4.84E-05
145651	7.061458323	41.1875	0.00013
144129	2.729462842	42.21818182	9E-05
143098	3.575002147	40.3	0.000118
144178	4.735170541	41.51428571	2.41E-05
145528	3.804635132	41.675	0.000116
145318	3.950227214	40.71428571	1.51E-05

Table 6.9: Local printed Volume for samples in X-direction, average maximum stress in X-direction and mass distribution in X-direction

BUILD ID	local printed volume[%]	EDGE σ_M [MPa]	M.D. X [mm^5]
138448	3.579436353	46.225	0.000805
138297	5.73537958	45.925	0.000256
138456	2.509430201	45.5875	0.00016
137470	2.048903885	45.775	0.000109
145651	4.280241122	45.35	0.000114
144129	4.378675501	45.875	0.000273

Figure 6.7 shows the maximum stress in function of the total printed volume. The calculated correlation coefficient however is only equal to 0.1176. When performing an analysis of variation, the p-value is calculated to be equal to 0.3321.

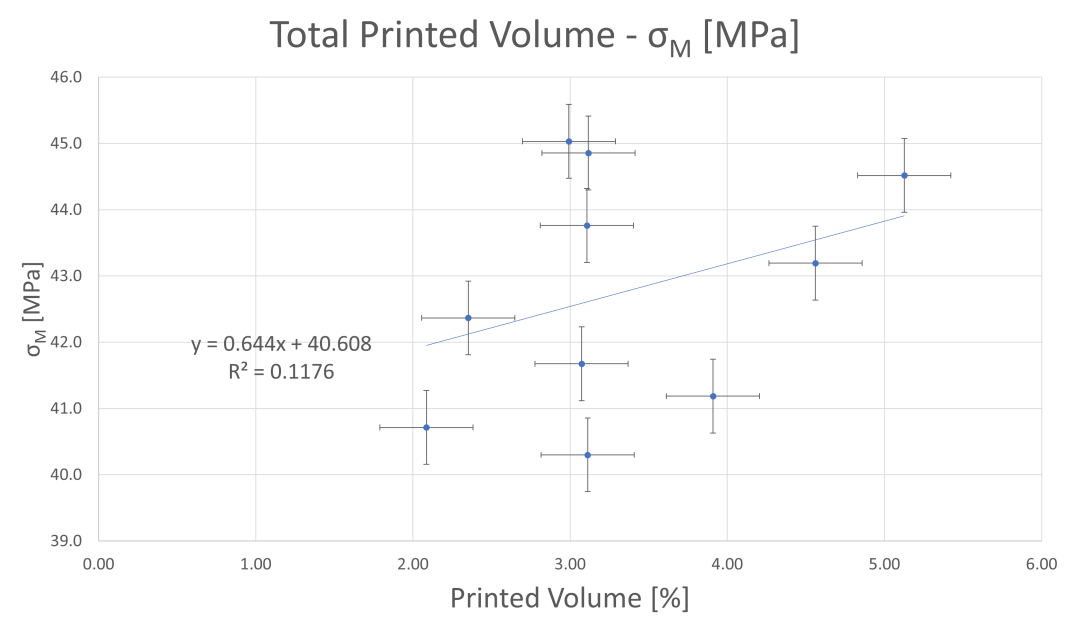

Figure 6.7: Graphical representation of maximum stress in function of total printed volume

In Figure 6.8 the maximum stress in function of the local printed volume for both orientations is shown. The calculated correlation coefficient however is only equal to 0.0207 for the horizontal orientation, for the vertical

orientation it is equal to 0.2795. When performing an analysis of variation, the p-value is calculated to be equal to 0.7856 for the horizontal orientation and 0.1162 for the vertical orientation.

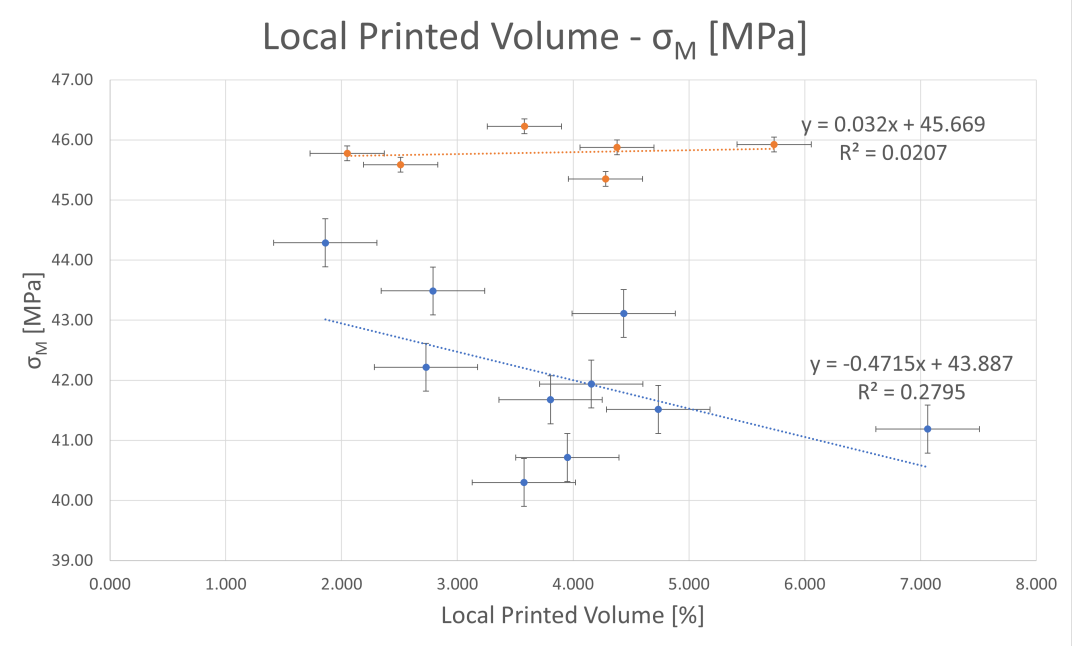

Figure 6.8: Graphical representation of maximum stress in function of local printed volume for both orientations

Figure 6.9 shows the average maximum stress in function of the mass distribution in X-direction. The calculated correlation coefficient is equal to 0.2301. The analysis of variation resulted in a p-value of 0.4105.

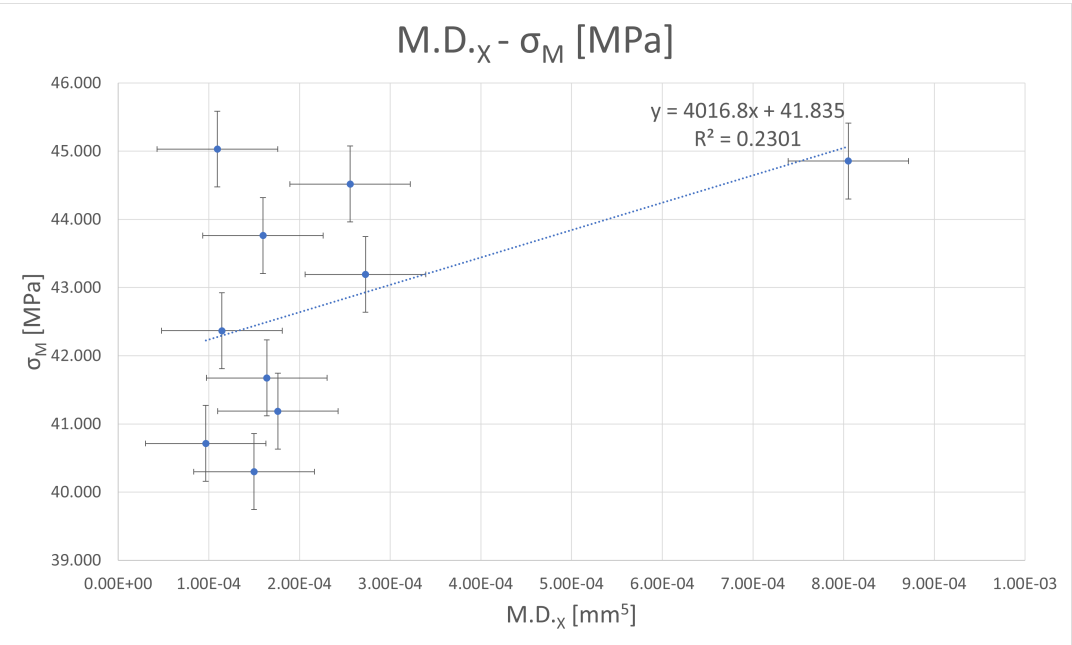

Figure 6.9: Graphical representation of average maximum stress in function of the mass distribution in X-direction

The maximum stress in X-direction in function of the mass distribution in X-direction is shown in Figure 6.10. The calculated correlation coefficient is equal to 0.6741, The analysis of variation results in a p-value of 0.0452.

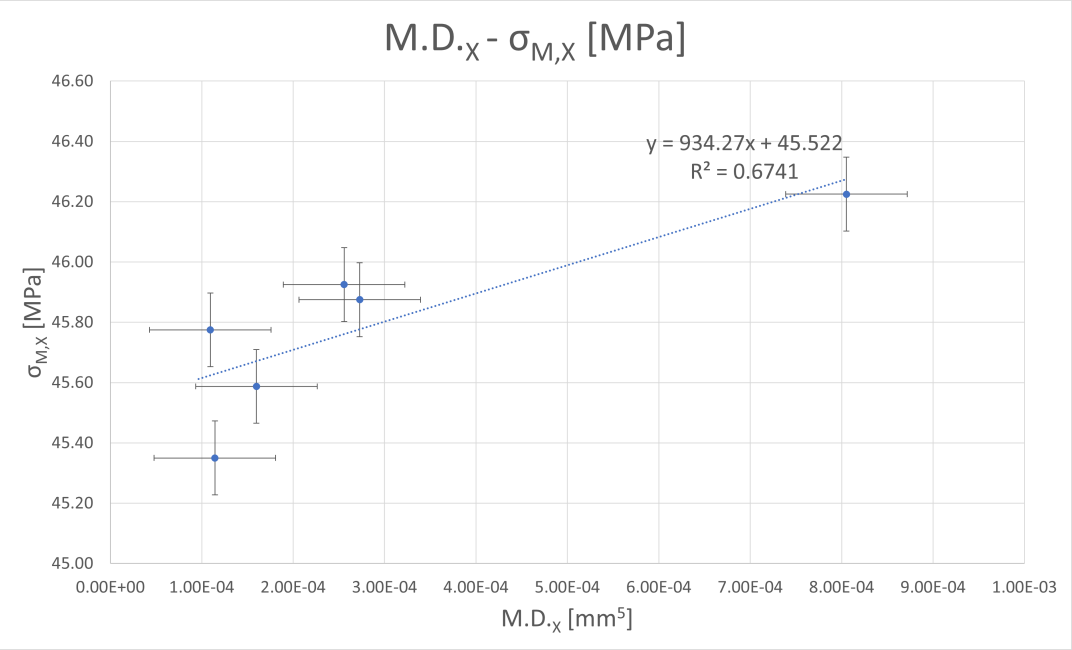

Figure 6.10: Graphical representation of maximum stress in X-direction in function of the mass distribution in X-direction

In Figure 6.11 the average maximum stress in function of the mass distribution in Z-direction is shown. The calculated correlation coefficient however is only equal to 0.0003.The p-value is calculated to be equal to 0.9627.

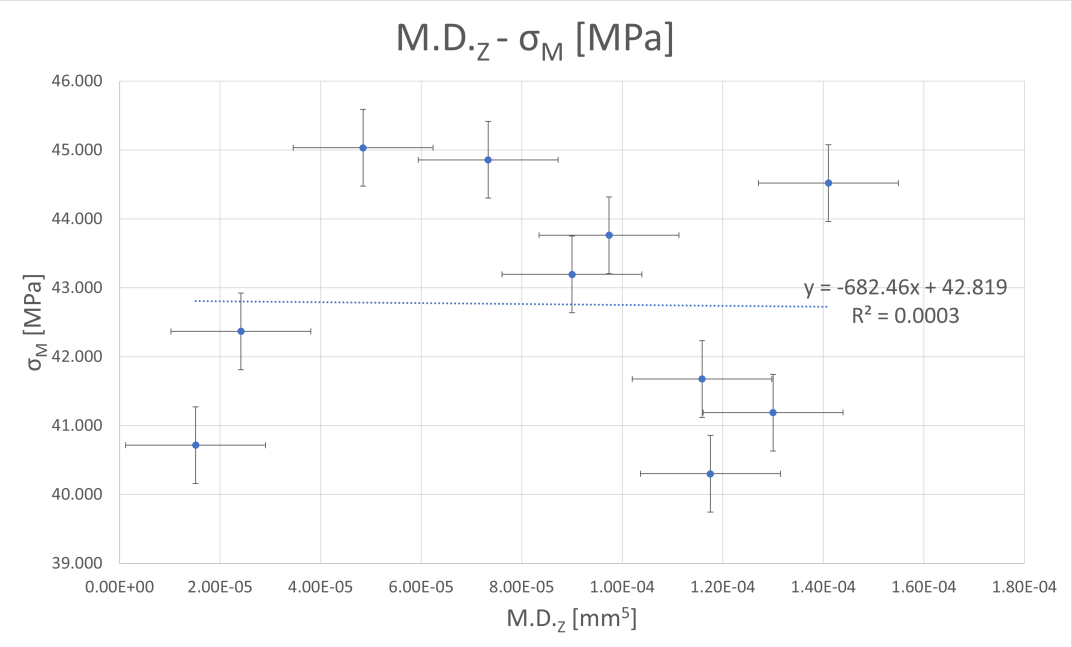

Figure 6.11: Graphical representation of average maximum stress in function of the mass distribution in Z-direction

Figure 6.12 shows the maximum stress in Z-direction in function of the mass distribution in Z-direction. The calculated correlation coefficient however is only equal to 0.0018. The analysis of variation results in a p-value of 0.9079.

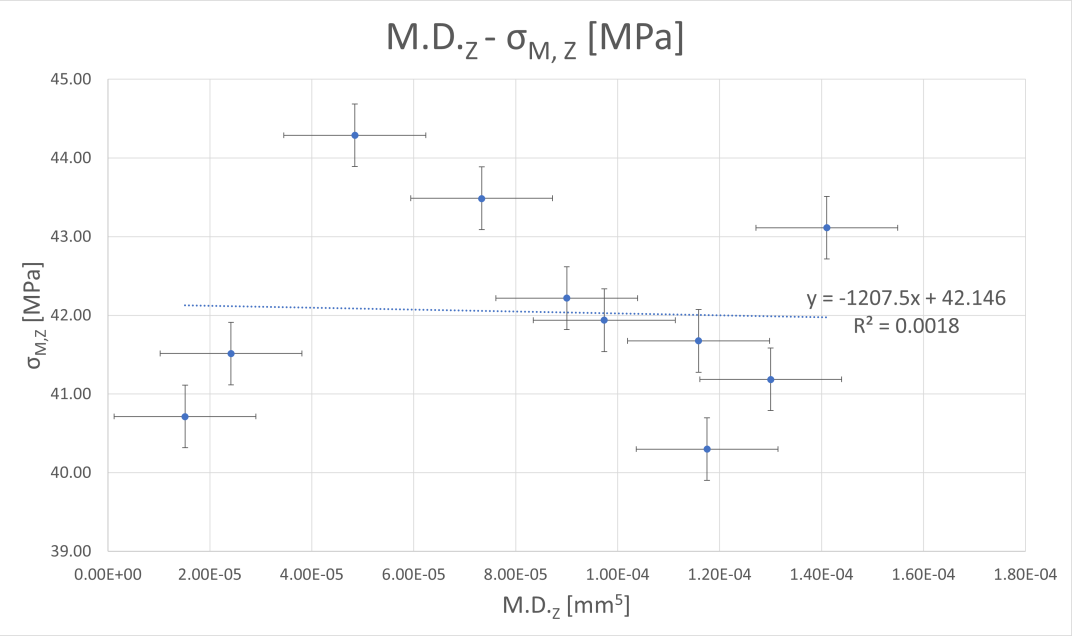

Figure 6.12: Graphical representation of maximum stress in Z-direction in function of the mass distribution in Z-direction

The final parameter that needs to be discussed is the effect of the weighted average of the ratio of surface area over volume on the average maximum stress. This can be seen in Figure 6.13. The calculated correlation coefficient however is only equal to 0.1609. The p-value is calculated to be equal to 0.2506.

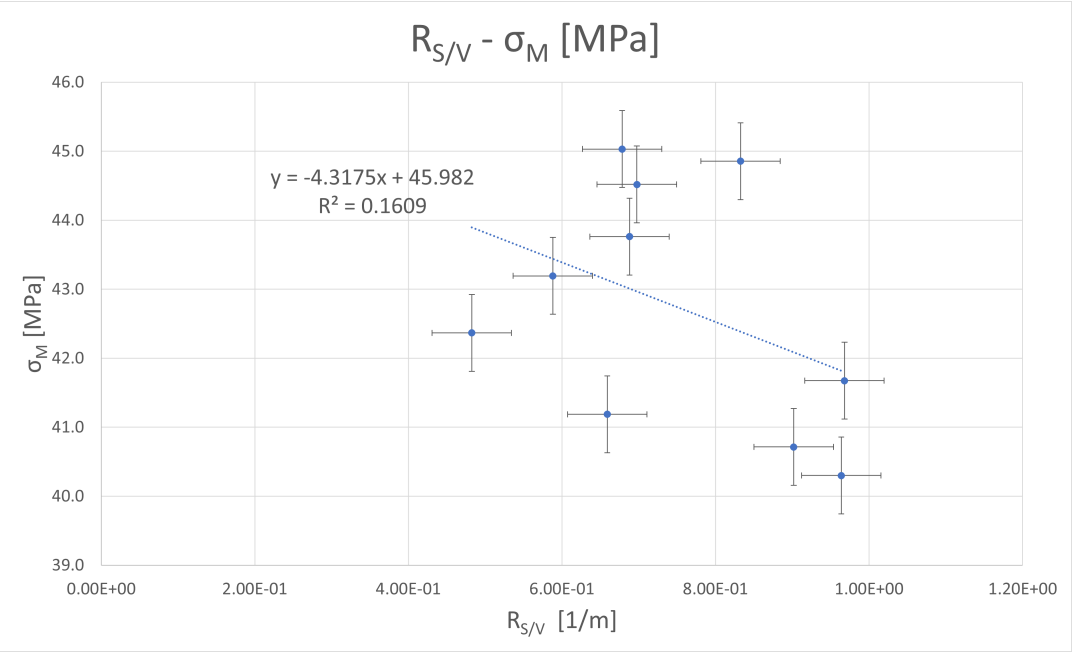

Figure 6.13: Graphical representation of maximum stress in function of the weighted average of the ratio of surface area over volume

Chapter 7
Discussion

In the previous chapter, the results obtained from the experiments are presented. This chapter focuses on discussing these results and analysing them with a critical eye. The limitations of the results, as well as how the result compare to the state-of-the-art are discussed. This discussion will follow the same structure as the section above. In order, a discussion will occur on the results of the:

- Degree of Crystallinity & Porosity
- Flame Retardant Additive
- Geometrical Properties

7.1 Degree of Crystallinity & Porosity

The first research question is aimed at determining the effect of the crystallinity of Selective Laser Sintered PA2241FR on two mechanical properties: the ultimate tensile strength and the tensile modulus. Several hypothesis are made and tested, see Section 3.3, and the results can be observed in Section 6.1.

To commence the analysis, the two dimensional cases are investigated in which the crystallinity is correlated to a mechanical property for a certain printing orientation. Both the correlation coefficient and the p-value are calculated for these cases, see Chapter 6 for the results. More information on the methodology can be found in Chapter 5.

The maximum stress in horizontal orientation is plotted in function of the degree of crystallinity in Figure 6.1. The calculated R^2-value is very low. According to [52] and [31], this is considered to have no or a very weak effect size, since $R^2 \leq 0.3$. The relationship between tensile modulus in horizontal orientation and the degree of crystallinity has an even worse result. This is presented in Figure 6.2. The R^2-value is almost equal to zero, it can thus be assumed that there is no scientific ground for the linear trend.
For the horizontal direction, the analysis of variance is performed on the maximum stress and the degree of crystallinity and an interesting result is obtained. It can be seen that the effect of the crystallinity on the ultimate tensile strength is significant. Unfortunately, the proposed linear model is not relevant. The p-value for this case is equal to 0.045524. The null hypothesis can thus be rejected and the alternative hypothesis can be accepted. The maximum stress is affected by the degree of crystallinity for the horizontal orientation.
In contrast to the effect on the maximum stress, the degree of crystallinity is not a significant parameter for the tensile modulus. It cannot be stated beyond any reasonable doubt that the null hypothesis is true and can thus not be rejected, since the p-value for this case is equal to 0.40996. The tensile modulus is unaffected by the degree of crystallinity for the horizontal orientation.

Figure 6.3, depicts the effect of the degree of crystallinity on the maximum stress in vertical direction. The R^2-value is extremely low. It can be considered to have no or a very weak effect size, since $R^2 \leq 0.3$. In the plot of the tensile modulus in function of the degree of crystallinity, see Figure 6.4, again, an even worse result is obtained. The R^2-value is extremely small, there is no scientific basis for this relationship.
The results of the analysis of variance indicate that the degree of crystallinity has a significant effect on the maximum stress in vertical orientation, since the p-vale is smaller than 0.05. However, the proposed linear model is not relevant. The null hypothesis can be rejected and the alternative hypothesis can be accepted. The maximum stress is affected by the degree of crystallinity for the vertical orientation.
The tensile modulus in vertical orientation and the degree of crystallinity are also subjected to an analysis of variance. Once again, the degree of crystallinity is not a significant parameter for the tensile modulus in this printing orientation. The null hypothesis cannot be rejected, since the p-value for this case is too high. The tensile modulus is unaffected by the degree of crystallinity for the vertical orientation.

To summarise the discussion above, the null hypothesis could not be rejected, meaning that the tensile modulus is unaffected by the degree of crystallinity in both directions. There is no correlation between the tensile

modulus and the degree of crystallinity.
On the other hand, the alternative hypothesis is accepted: the maximum stress is affected by the degree of crystallinity in both directions. But in both cases there is a very low correlation as stated earlier. This may imply that there is another variable that is more significant or that in combination with the degree of crystallinity may result in a better model. Because of this the porosity of the tensile specimens is determined.

The analysis of the porosity measurements, seen in Figure 6.5, result in a very low p-value. The effect of the porosity on the ultimate tensile strength is considered to be significant. Additionally, the linear approximation has a R^2 that is equal to 0.4653. The porosity can be considered to have a weak effect size on the maximum stress of the samples, since the 0.3 $R^2 \leq 0.5$. [31, 52]
A interesting trend can be seen in Figure 6.6, the proposed linear relationship between porosity and the ultimate tensile strength in vertical direction has a R^2 that is equal to 0.6285. The porosity can be considered to have a moderate effect size on the maximum stress of the samples, since the 0.5 $/R^2 \leq 0.7$. [31, 52] Since the p-value for this case is equal to 0.0465, the porosity can also be considered to have a significant effect on the ultimate strength in vertical direction.

Both the degree of crystallinity and the porosity have a significant effect on the maximum stress. When either the degree of crystallinity or the porosity is correlated to the ultimate tensile strength, the correlation has room for improvement. The 3D model that combines the effect of these parameters is generated. This graphical representation of the data allow for a better understanding of the relative effect on the tensile strength of both the degree of crystallinity and the porosity.
In Figure 7.2, the model is shown for the vertical orientation. The combination of the porosity and the degree of crystallinity can be considered to have a strong effect size on the maximum stress of the samples in the vertical direction, since the R^2 0.7. [31, 52].
Figure 7.1 shows the model for the horizontal orientation. The combination of the porosity and the degree of crystallinity can be considered to have a moderate effect size on the maximum stress of the samples in the vertical direction.

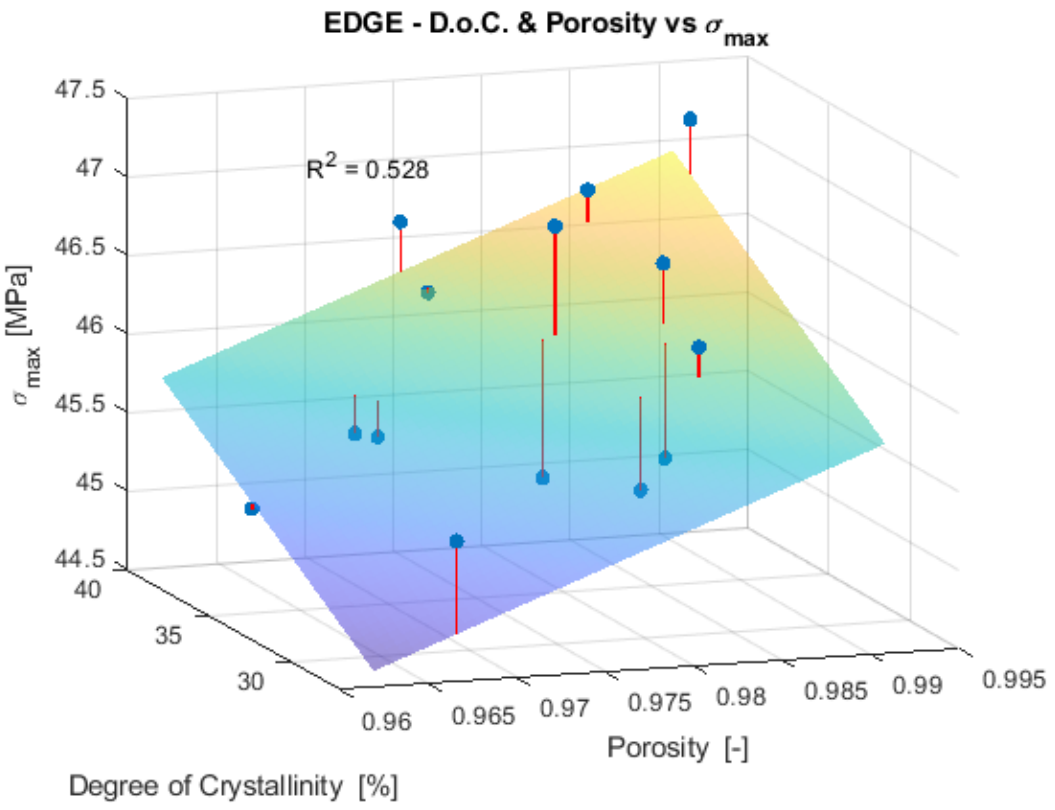

Figure 7.1: 3D model of the degree of maximum stress in function of the degree of crystallinity and the porosity in horizontal direction

In Figure 7.2, a graphical representation on the effect of the porosity and the degree of crystallinity of a sample, with vertical orientation, on its ultimate tensile strength is presented. The R^2 is equal to 0.71480 and the fit can be considered to be good. The equation that describes the trend plane is given by Equation 7.1.

$$\sigma_M = 147.324 \cdot X_{porosity}\ 0.0806737 \cdot X_{D.o.C.} - 104.744 \tag{7.1}$$

It is interesting to see that if the porosity goes up by 1%, the effect is much more pronounced compared to when the degree of crystallinity goes up by 1%. The increase in level op porosity would result in an addition of 1.47 MPa, while the increase in degree of crystallinity results in an increase of only 0.08 MPa. This does corresponds with what is found in literature, in which it is stated that porosity has the most significant effect on the mechanical properties of the printed material, see Chapter 2.

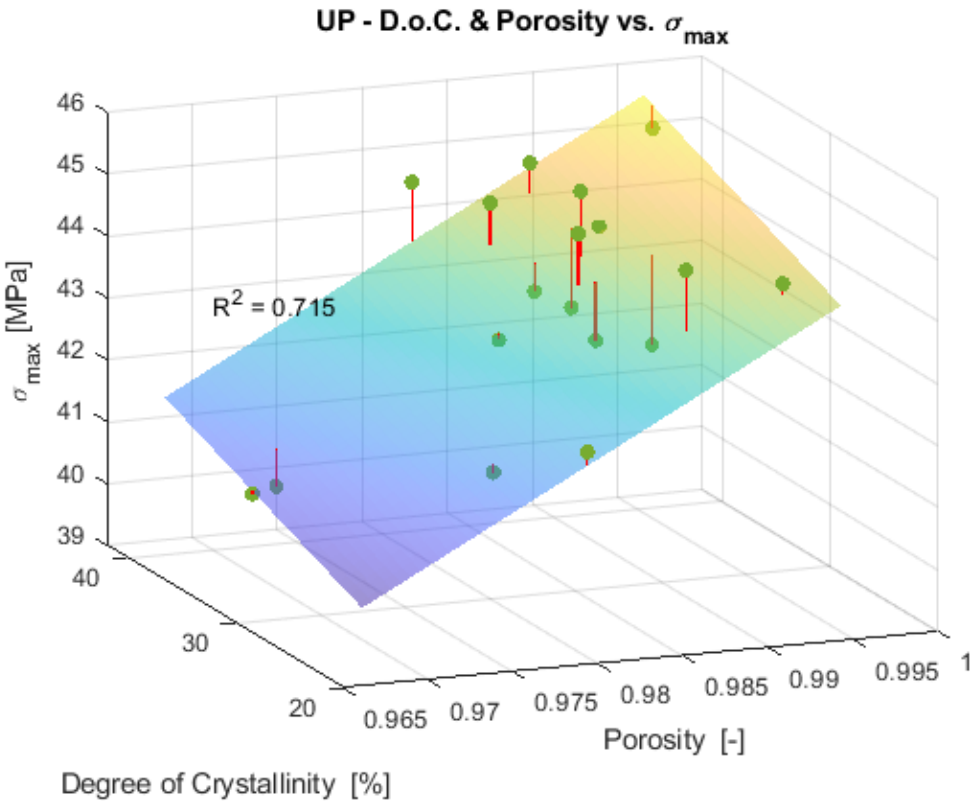

Figure 7.2: 3D model of the degree of maximum stress in function of the degree of crystallinity and the porosity in vertical direction

Figure 7.1 shows the model for the horizontal direction. Its R^2 value is equal to 0.52795. This is less than for the vertical trend. The combination of the porosity and the degree of crystallinity can be considered to have a moderate effect size on the maximum stress of the samples in the vertical direction. The equation that corresponds to the trend plane is given by Equation 7.2.

$$\sigma_M = 42.5809 \cdot X_{porosity}\ 0.0845861 \cdot X_{D.o.C.}\ 1.36385 \tag{7.2}$$

Again, the same interesting phenomenon can be seen, that if the porosity goes up by 1%, the effect is much more clear-cut compared to when the degree of crystallinity goes up by 1%. The increase in porosity would result in an addition of 0.426 MPa, while the increase in degree of crystallinity results in an increase of only 0.084 MPa. This can also be explained by the findings in literature, in which it is stated that porosity has a more significant effect on the mechanical properties of the printed material, see Chapter 2.

Combining all of the above, of the three proposed null hypotheses, two are rejected. Only one could not be rejected: The tensile modulus is unaffected by the degree of crystallinity.

The two alternative hypotheses that can be accepted are:

1. The maximum stress is affected by the degree of crystallinity.
2. The maximum stress is affected by the porosity.

Accepting the null hypothesis, that the degree of crystallinity does not affect the tensile modulus, is in contradiction with [41]. This source explicitly mentions that an increase in crystal size results in an increased modulus of elasticity. In [7], it is also stated that an increase of in crystallinity will result in an increased modulus of elasticity. However, from the data of PA2241FR and PA2200, presented in Table 2.1, it can clearly be seen that the additive has a very large impact on the elastic modulus. A variation on the mount of additive, may be the cause of the lack of correlation and low significance found here.

However, there are some important notes that must be made on these findings. According to [41], a growth in crystal size has a negative effect on the maximum stress. On the other hand, [6] confirms these findings, stating that an increase in degree of crystallinity will result in a higher maximum stress. It is important to note that the findings in [6] are true for thermoplastic polymers in general. The findings presented in [41] are specifically true for laser sintered polymers. Because of this, the findings of [41] can be expected to be similar to the conditions of this research. When comparing the obtained results to the state-of-the-art, several observations can be made. There are multiple ways for achieving a high degree of crystallinity. Either there is a low amount of crystals with a large crystal size or there are many crystals that do not have a large crystal size. Unfortunately, since only differential scanning calorimetry was performed on the samples, only data is obtained on the degree of crystallinity and not on the crystal size. The samples need to be tested using X-ray diffraction in order to obtain data on the crystal size.
The degree of crystallinity does have a significant and positive effect on the ultimate tensile strength. This trend is in accordance with the state-of-the-art presented in [6], but the correlation coefficient leaves room for improvement. A possible explanation for this might be the presence of the flame retardant additive and this is elaborated upon in section 7.2. However, it is possible that the crystal size is also an important parameter. The combination of degree of crystallinity, crystal size, and number of crystals results several possible cases. The first case is that the crystal size is the same for all crystals in a sample. The effect of the crystal size can thus neglected. An increase in degree of crystallinity can than be explained by an increase in the amount of crystals present in the sample. According to the state-of-the-art presented in [6], this will result in an increase in the ultimate tensile strength.
In a second possible case, the degree of crystallinity will remain constant. A sample with a higher crystal size can be expected to have an lower amount of crystals. The effect of the crystal size, discussed in [41], predicts a decrease in tensile strength.
The third possible case is the most relevant, since it is probably more in line with the conditions of the used samples. There is an increase in degree of crystallinity. But since the crystal size is not measured, it is impossible to know, how it is affected. The samples in this case can either have a decrease in tensile strength, if the especially the crystal size is increased and the number of crystals remained more or less constant. On the other hand, the samples can also experience an increase in tensile modulus, if the number of crystals have increased, but the crystal size remained more or less constant. An combination of both a higher number of crystals and an increased crystal size can result in a sample that has no significant increase of decrease in tensile strength. The degree of crystallinity does not give sufficient information to shine more light on this variation. Additional tests on the crystal size of the sample can give a better understanding of the local conditions. This allows for a more accurate characterisation of the effect.

Both [41] and [14] state that the effect of the porosity is more pronounced in the vertical direction, compared to the horizontal direction. This can be confirmed by the findings of this research. The maximum strength is influenced three to four times as much in vertical direction compared to the horizontal direction. The magnitude of this increase can be compared to literature. In [51] it is determined that an increase in porosity level of 1%, will result in an increase of 2.2 MPa. This increase is in the same order of magnitude as the findings of this research. This research did use another manufacturing technique, not selective laser sintering, and normal PA12 is used and not PA2241FR. The differences in experimental setup between this research and [51] may explain the difference in the magnitude of the effect. The porosity in this research is measured using X-ray computed

tomography. This technique is much more accurate compared to the approach used in this research.
The reason for the more pronounced effect of the porosity in vertical direction, can be explained using the sintering window, see Section 2.2.2. After a layer is scanned, a layer of fresh powder is introduced upon the sintered areas. This will result in a small thermal shock of the sintered area below. They will experience a slight drop in temperature. When the laser passes over the new layer and melts the powder, the new top layer will have a slightly higher temperature compared to the area below. When the process is finished, the build volume can cool down. The fact that the part is build layer-by-layer results in the fact that the mechanical properties are significantly less in the build orientation.

As cited throughout the discussion, the state-of-the-art presented in literature has some limitations. The conditions in these sources are not exactly the same as the conditions used in this research. It is possible that a difference in these conditions may have a significant effect on the results.
The method used to obtain the porosity measurements can be improved upon. For example, using microscopy to analyse multiple cross sections of a single sample will allow for a more accurate approximation of the porosity. X-ray CT-scanning can also be used for obtaining data on the porosity. This method is the most accurate, but also the most expansive. It is also important to have a good signal-to-noise ratio in order to obtain accurate results.
Additionally, the obtained data used in this research also has some limitations. To start off, the tensile strength of the samples did experience some significant variation. However, in the vertical orientation the ultimate tensile strength has a maximum value of 45 MPa and a minimum of only 40.5 MPa. This is a significant difference, but this research and its findings are limited to the high end of the material properties, since the maximum tensile stress is considered to be 46 MPa in vertical direction. [14] For the horizontal orientation, the ultimate tensile strength has a maximum value of 47.2 MPa and a minimum of only 45.2 MPa. This variation is less significant, but it is not as close to the maximum value of 49 MPa. [14] The trends found in this research can only be considered to be valid for this region of tensile strength. The tensile modulus varies between 1700 MPa and 1800 MPa, while the maximum is considered to be 1900 MPa. [14] It is important to note that the exact conditions are not known in which these extreme values are obtained. It could be the case that these extremes are not obtained using normal processing conditions. The test standard ISO 527, does not allow for any actions during the test that may have improved the results. But the processing parameters used for manufacturing these samples may be unrepresentative of the conditions used in this research.
Similar limitations are introduced by the range of the crystallinity and porosity. The degree of crystallinity of all samples lies within a range of 20% and 45%. No amorph or highly crystalline samples are investigated. This limits the results of this research to this region. Data with a significantly higher or lower degree of crystallinity can be useful for a more complete model. However, the samples used in this research are representative on the actual conditions and properties of selective laser sintered PA2241FR using the EOS P770. The measured porosity also only has a limited window of 96% to 100%. This is definitely a desirable result for Materialise NV, but there is room for improvement. For the porosity also holds that samples with more extreme/lower results can be useful for obtaining a more complete model. But on the other hand, the samples used in this research are representative of the actual manufactured parts.
The linear trends established in this research must be assumed to only be valid when using the same processing parameters as Materialise NV.

7.2 Flame Retardant Additive

The effect of the flame retardant additive is attempted to be investigated using nuclear magnetic resonance scanning. As mentioned earlier, a couple of issues have been experienced. Even though the NMR spectra could not be obtained, there are some results. PA 2241 FR does not dissolve in the same solvents which are able to solve regular PA12. The exact reason for this is unknown. If sulphuric acid is used, an additional problem would have arisen. Sulphuric acid is very strong and would in all likelihood have completely destroyed the polymer structure. There is a large possibility that the obtained spectra are useless, since the additive is not longer bonded.

Even tough, the nuclear magnetic resonance spectra are not obtained. There is reason to believe that the flame retardant additive has a significant impact on the tensile strength and especially on the tensile modulus. In the previous chapter in Section 7.1, the effect of degree of crystallinity and the porosity was discussed. A clear effect of both these parameters was determined on the tensile strength but not on the tensile modulus. In this section, we also discuss the possibility that the crystal size is an important factor. But there is still a variation that could not

be explained. Literature indicates that for PA12, or any other semi-crystalline polymer, the degree of crystallinity does have a significant effect on the tensile modulus. There is no reason to believe, that the variation in degree of crystallinity has no impact due to the addition of the additive. Even tough the obtained results do indicate that the degree of crystallinity is insignificant. However, it is possible that the presence of the additive has a much larger and pronounced effect on the tensile modulus. If this is the case the effect of the degree of crystallinity can be insignificant compared to effect of the presence of the additive.

By process of elimination, it can be concluded that the flame retardant content has a significant effect on the both the tensile modulus and the ultimate tensile strength. In Table 2.1, the direct effect of the addition of the halogenated additive can be seen. The ultimate tensile strength increases with 2.1% but more importantly, the tensile modulus increases by more than 15%. The impact of the additive on the tensile strength is significant, but it is limited. If the variation of this parameter is included in the proposed model, a better correlation is expected. The impact of the additive on the tensile modulus is much more pronounced. The presence of this filler material causes a larger increase of the tensile modulus than the range in which the used samples vary. A significant variation of the additive can be expected to have a substantial and overpowering effect on the modulus. The fact that the crystallinity has an insignificant effect on the tensile modulus, even tough this is in contradiction with the state-of-the-art for PA12, can be explained if the effect of the additive is dominating. The effect of the halogenated additive is also inline with the findings presented in Section 2.2.1. Since this is the case, there is a solid basis to believe that the presence of the additive is the cause of the large variation in the tensile modulus. Additionally, there is also reason to believe that the additive has a significant effect on the tensile stress.

7.3 Geometrical Properties

This section focuses on the influence of several geometrical parameters on the mechanical strength of the material. In Section 6.3, the results are presented. Since the p-value of almost all parameters are above the threshold of 0.05, only one null hypothesis can be rejected. All other null hypothesis are considered to be valid. These hypothesis are presented below:

1. The maximum stress is unaffected by the proximity of a part.
2. The maximum stress is unaffected by the total printed volume.
3. The maximum stress is unaffected by the local printed volume.
4. The maximum stress in Z-direction is unaffected by the mass distribution in Z-direction.
5. The maximum stress is unaffected by the mass distribution in Z-direction.
6. The maximum stress in X-direction is unaffected by the mass distribution in X-direction.
7. The maximum stress is unaffected by the weighted aspect ratio of surface area over volume.

The maximum stress in X-direction in function of the mass distribution in X-direction has a correlation coefficient of 0.6741, this value is relatively high and the mass distribution in X-direction can be considered to moderate strong effect on the maximum stress in X-direction. Even when one of the points, such as the outlier that can be seen on the right hand side of the graph, a similar result is obtained. The analysis of variation resulted in a p-value of 0.0452. The effect must thus be considered to be statistically significant. The null hypothesis can be rejected and the alternative hypothesis is considered to be valid. The maximum stress in X-direction is affected by the mass distribution in X-direction.
Even though, both the p-value and the correlation coefficient indicate that there is a linear trend present, it was chosen not to accept this hypothesis. This is the case since only a limited set of data points are available for this case. It advised to gather additional data points before a conclusion can be composed on the effect of this process parameter. Additionally, since none of the other processing parameter that investigate the mass distribution can be considered to be significant, it is also chosen not the reject the null hypothesis.

Even though no null hypotheses could be rejected, the results from this research are still informative. The proximity of a part to the tensile bars are proven with a high degree of certainty to not have an effect on the mechanical properties of the heat shield. This is very interesting for the selective laser sintering process. As discussed earlier, the printed parts are nested throughout the build volume. This nesting is optimised to allow for the maximum number of parts in a single batch. It is interesting to know that the proximity of a part to another part does not influence the tensile strength. Nesting parts closer together will thus not result in a better mechanical performance.

For the range of data available for this research, the total printed volume has no effect on the maximum stress of the tensile specimens in a build. Several remarks must be made for this data. Only ten data points were available, a higher amount may result in a better model. But more importantly, the range in which in these data points lie is very narrow and this can cause misleading results. The total printed volume is between 2% and $\pm 5\%$. If builds with a larger printed volume are included, the results may vary. For Materialise NV, this factor can be considered to be irrelevant, since their builds are always in this range. For the available data, it must be considered that the total printed volume does not affect the maximum stress.

A similar explanation can be given to the local printed volume. Here, there is a larger variation in data. The printed volume ranges from $\pm 1.9\%$ to $\pm 7.1\%$. This is a broader range, but is still considered to be relatively narrow and because of this, potentially misleading. If batches with a higher local printed volume are added, the results may vary. Using the available data, it must unfortunately also be stated that the local printed volume has no effect the maximum stress.

None of the presented trends between the mass distribution and the maximum stress are useful. The p-values for all of these trends is too high, and must be discarded.

The last factor that needs to be elaborated upon is the surface area to volume ratio. The idea behind this parameter is that a large part, with less surface area will lose its heat slower, which results in a slower cooling rate. A higher degree of crystallinity is expected as a result and this will increase the maximum tensile strength. However when performing the analysis on this data, the trend has a low correlation coefficient and the p-value indicates this trend is insignificant. This ratio can thus be stated to have no significant effect on the maximum stress of a build. This is surprising, since a large surface area for a given volume is know to radiate more heat to its surroundings. A higher cooling rate is thus suspected for the parts with a higher surface area. This is not the case, unfortunately. It is possible that there is another factor that is more pronounced and as a result this factor is insignificant relative to the other factor. The current picture of the situation may be misleading, since an important factor is missing.

It is interesting that none of the above null hypothesis can be rejected. The idea behind these parameters is that they would have an impact on the cooling rate of the material. A lower cooling rate, will result in improved mechanical properties. This is confirmed by several sources. [8, 19] As established in Section 7.1, this increase in maximum stress can be explained by the increased crystallinity, since the degree of crystallinity is affected by the cooling rate. Unfortunately, it is not possible to relate the aforementioned parameters to any changes in mechanical behaviour. A possible reason for this might be that the discussed parameters are an oversimplification of the parameters that may actually have an effect on the cooling rate. It is definitely possible that more complex parameters can predict the mechanical behaviour of a batch.
Another important factor is the fact that the tensile bars are always printed close to the edge of the build volume. It is certainly possible that the boundary conditions at the edge of the build volume have a stronger impact on the mechanical properties than the aforementioned parameters. For example, the walls of the build chamber consist of insulation and heating elements. The heat added by these heaters may have a dominant effect of the tensile strength compared to the geometrical parameters of that batch. It is very likely that printing sacrificial parts throughout the build volume will allow for more useful data, especially if the parts are located further away from the heaters at the edge.

Nevertheless, none of these parameters can be stated to have a significantly affect on the maximum strength of the tensile specimens. This does not mean that the general idea, that geometrical properties of a build will affect the mechanical strength, must be discarded. There may be other parameters that have a more significant impact. The research performed by [8, 19] did indicate the effect of the cooling rate on the mechanical strength. And other geometrical parameters may still influence the cooling rate of the build. If parameters are found that have a significant effect, a more complex multi-variable model may need to determined.

Additionally, the geometrical data used in this model was based on point volumes, bounding boxes,... since the data was exported this way by Materialise Magics. A more precise model and data of a batch could be used to improve the reliability of the data. If an accurate CAD model of the entire build could be analysed to obtain data on the mass distribution and proximity, significant trend involving the aforementioned geometrical parameters may be discovered.

Parameters such as the time per layer, scanning speed, scanning pattern,... may have an affect on the cooling rate. These parameters are influenced by the geometry present in the print volume. Future research should also focus on creating, verifying and validating a model for the cooling rate of a printed batch.

Chapter 8
Conclusion

The purpose of the MSc Thesis report was firstly to identify knowledge gaps in the field of selective laser sintering. Secondly, its goal was to investigate these gaps and to gain insight into the results.

After studying the behaviour of semi-crystalline polymers and going into further detail on the processing parameters of selective laser sintering, it was chosen to investigate these research questions:

1. How does the crystallinity correlate with strength and stiffness of Selective Laser Sintered PA2241FR?
2. How does the amount of FR-additive correlate with strength and stiffness of Selective Laser Sintered PA2241FR?
3. What is the influence of the geometrical properties of a printed batch on the strength of Selective Laser Sintered PA2241FR?

8.1 Importance of Research

Additive manufacturing is a relatively new family of manufacturing processes. Because of this there is still a lot to be investigated about Selective Laser Sintering. Specifically concerning the characteristics of the material PA2241FR a lot can still be investigated. The more that is known about a manufacturing process or the behaviour of a material, the better the repeatability in a production environment. This is specifically useful for a material such as PA2241FR which is used solely for aerospace applications. The better the repeatability of the process, the more this material and process can be used for more components within the aircraft.

Materialise NV experiences a variation in mechanical properties of the selective laser sintered PA2241FR parts. This variation raised the question what the cause might be of this variation. The results from this research may allow Materialise NV to make the SLS printing process more efficient.

8.2 Main Conclusions

When finalising the research, several conclusions can be drawn. These conclusions are presented per research question in the following sections.

Degree of Crystallinity & Porosity

A three dimensional model was established in which the effect on the tensile strength in function of the degree of crystallinity and the porosity is plotted. Two models are made, since the tensile strength is different in the printing direction. Both these models are shown to be statistically significant and has a decent correlation coefficient. The model for the vertical orientation has a better fit. This is explained by the fact the effect of the porosity is more pronounced in the printing direction.
However, there is room for improvement. The crystal size of the samples is determined to be an additional factor that may have a significant impact. The range in which these models can be considered to be valid is also limited. This is the case since the available data and the obtained results have a limited range. More extreme data can be used to establish a stronger model. The current range of the model is in accordance with the processing parameters used by Materialise NV.

Additionally, it is determined that the degree of crystallinity has no apparent effect on the tensile modulus of the material. However, this does not necessarily mean that the degree of crystallinity has no impact on the tensile modulus. It is expected that there is a different parameter which has a much stronger effect on the tensile modulus than the degree of crystallinity has. A possible explanation for this is a variation in the flame retardant content.

Flame Retardant Additive

No results on the flame retardant additive could be obtained using NMR spectroscopy, since PA2241FR could not be dissolved in a solvent that is suitable for NMR spectroscopy.
Fortunately, the analysis of the effect of the degree of crystallinity and porosity on the mechanical properties indicates that there is an important factor which is not yet identified. The presence of the flame retardant additive is a possible candidate. The most important argument for this is the fact that the addition of the additive in the powdered PA12, causes for an increase in stiffness of more than 15%. This is a very significant increase. A possible variation in the flame retardant content can also be expected to have a large impact on the mechanical properties and especially the stiffness. Since literature does support the effect of the flame retardant additive on the material, it is recommended to find a method in which the variation in content can be evaluated. A possible method may be to find a solvent which is usable for NMR tests and that will dissolve the PA2241FR powder.

Geometrical Properties

The final research question investigates the influence of the geometrical properties of a printed batch on the maximum stress. None of the proposed hypotheses could be rejected. This has some interesting implications. The proximity of a part to a tensile bars does not influence its mechanical performance. A more dense nesting of parts can thus be considered to not have a significant result.
The effect of the local and total printed volume is also shown to be insignificant. A possible reason for this is that the range in which the build volume varies is very limited. The mass distribution parameters are all proven to be insignificant.
The surface area to volume ratio is also proven to be insignificant. This is not the expected result. A part with a larger surface area will radiate more heat and this is expected to have a higher cooling rate. This would result in a lower degree of crystallinity. The fact that this effect is not observed, indicates that there is an other factor that has a more significant effect on the mechanical properties.

The idea behind all the aforementioned geometrical parameters is that they would have an impact on the cooling rate of the material. A lower cooling rate, will result in improved mechanical properties. Literature support this hypothesis. [8, 19] Possible reasons for the lack of any significant trend is that the proposed parameters are an oversimplification of the actual situation. A set of more complex parameters may be able to predict reliable results.
The proximity of the witness specimens to the edge of the build volume, may also have an impact. The walls of the build chamber house several heaters to keep the build volume at a constant temperature. Their presence may have a more pronounced effect on the other parameters. Printing sacrificial parts throughout the build volume is expected to result in more useful data.

None of the geometrical parameters are shown to have significantly affect on the maximum strength of the tensile specimens. However, this does not mean that the influence of geometrical parameters on the mechanical properties must be discarded. If parameters are found that have a significant effect, a more complex multi-variable model may need to determined.

8.3 Recommendations for Future Research

Research is never completed, and there is always room for improvement. The recommendations for future research are presented and bundled per research question.

Degree of Crystallinity & Porosity

In order to improve upon this part of the research, several topics can be improved upon. To start of, the degree of crystallinity was determined using differential scanning calorimetry. This is an useful and relatively easy method to obtain results on the crystallinity. A technique like X-ray Diffraction can be used to obtain more accurate results on the degree of crystallinity, the size and the type of the crystals. This will allow for a more complete overview of the characteristics of the material. As discussed earlier, the size of the crystals has an undesirable effect on the tensile strength. Measuring the crystal size will thus allow for a more complete picture and a more accurate model.
The porosity could also be determined using X-ray computed tomography, which is very accurate, or by using microscopy to investigate the porosity in several sections of a sample. This last method is less accurate as the

X-ray CT-scan, but is still more accurate as the method used in this research. If X-ray CT-scanning is used, it is important to determine a good signal to noise ration, in order to have accurate results.

Flame Retardant Additive

In order to investigate the effect of flame retardant additive in the material, it is recommended to look for a suitable solvent for PA2241FR. If a usable solvent is found, the quantitative solution NMR spectroscopy tests can be performed. It is preferred to use solution nuclear magnetic resonance spectroscopy compared to its solid state counterpart, since quantitative results are required and this testing method is less expensive.

It is recommended to first determine the degree of crystallinity and porosity of the samples, and select samples that are outliers. Since the effect is more significant on the elastic modulus, it is recommended to focus the efforts on the effect of the additive on the elastic modulus.

Geometrical Properties

The geometrical data used in this model was based on point volumes, bounding boxes,... since the data was exported this way by Materialise Magics. It is expected that more precise results can be obtained if a CAD model of the entire build could be analysed layer by layer. An accurate CAD model of the entire build can be used to obtain data on the mass distribution and proximity. This can allow for the discovering of a significant trend involving the aforementioned geometrical parameters.
Parameters such as the time per layer, scanning speed, scanning pattern,... may have an affect on the cooling rate. These parameters are influenced by the geometry present in the print volume. Future research should also focus on creating, verifying and validating a model for the cooling rate of a printed batch.

Bibliography

[1] Alessandro Airoldi. Evaluation of SLS-made PA12 Under Uniaxial Tensile Test. Technical report, SCHOOL OF INDUSTRIAL AND INFORMATION ENGINEERING, 2017.

[2] Saleh Ahmed Aldahash. Optimum manufacturing parameters in selective laser sintering of PA12 with white cement additives. *International Journal of Advanced Manufacturing Technology*, 96(1-4):257–270, 4 2018. ISSN 14333015. doi: 10.1007/s00170-018-1584-y.

[3] Jiaming Bai, Shangqin Yuan, Wanlu Chow, Chee Kai Chua, Kun Zhou, and Jun Wei. Effect of surface orientation on the tribological properties of laser sintered polyamide 12. *Polymer Testing*, 48:111–114, 12 2015. ISSN 01429418. doi: 10.1016/j.polymertesting.2015.09.017.

[4] A.J. Brandolini and D.D. Hills. *NMR Spectra of Polymers and Polymer Additives*. Taylor & Francis, 2000. ISBN 9780824789701. URL https://books.google.nl/books?id=3GGmtOKk4RsC.

[5] G. Camino, L. Costa, and M.P. Luda di Cortemiglia. Overview of fire retardant mechanisms. *Polymer Degradation and Stability*, 33(2):131 – 154, 1991. ISSN 0141-3910. doi: https://doi.org/10.1016/0141-3910(91)90014-I. URL http://www.sciencedirect.com/science/article/pii/014139109190014I. Thermal Stabilisation and Flammability of Polymers and Composites.

[6] E. Charles and Jr. Carraher. *Polymer Chemistry*. Marcel Dekker, Inc, 2004. ISBN 0834708067.

[7] M Citation Pavan, T ; Craeghs, P V Puyvelde, J.-P ; Kruth, and W Dewulf. Understanding The Link Between Process Parameters, Microstructure And Mechanical Properties Of Laser Sintered Pa12 Parts Through X-ray Computed Tomography. Technical report, 2016.

[8] Garrett Craft, Justin Nussbaum, Nathan Crane, and J. P. Harmon. Impact of extended sintering times on mechanical properties in pa-12 parts produced by powderbed fusion processes. *Additive Manufacturing*, 22:800–806, 8 2018. ISSN 22148604. doi: 10.1016/j.addma.2018.06.028.

[9] Garrett Craft, Justin Nussbaum, Nathan Crane, and J. P. Harmon. Impact of extended sintering times on mechanical properties in PA-12 parts produced by powderbed fusion processes. *Additive Manufacturing*, 22:800–806, 8 2018. ISSN 22148604. doi: 10.1016/j.addma.2018.06.028.

[10] Sasan Dadbakhsh, Leander Verbelen, Olivier Verkinderen, Dieter Strobbe, Peter Van Puyvelde, and Jean Pierre Kruth. Effect of PA12 powder reuse on coalescence behaviour and microstructure of SLS parts. *European Polymer Journal*, 92:250–262, 7 2017. ISSN 00143057. doi: 10.1016/j.eurpolymj.2017.05.014.

[11] N A Darwish, Adel Bassuoni Shehata, Nabil Lawandy, Ahmed I Abou-Kandil, A B Shehata, S N Lawandy, and A I Abou-Kandil. Preparation of Quality Control Material for Assuring Quality of Electrical Conductivity Measurements in Soil View project Improving Efficiency of Crystalline Silicon Photovoltaic Devices View project Effect of Non-Oiled Sulfur Concentration on the Adhesion Between Nitrile Rubber and Nylon Cord. *Article in Journal of Applied Polymer Science*, 74:762–771, 1999. doi: 10.1002/(SICI)1097-4628(19991024)74:43.0.CO;2-W. URL https://www.researchgate.net/publication/239097610.

[12] Dietmar Drummer, Dominik Rietzel, and Florian Kühnlein. Development of a characterization approach for the sintering behavior of new thermoplastics for selective laser sintering. In *Physics Procedia*, volume 5, pages 533–542. Elsevier B.V., 2010. doi: 10.1016/j.phpro.2010.08.081.

[13] EOS. EOS P 770 - Laser Sintering System with Two Lasers for the Production of Large Parts and for Industrial High-Throughput Manufacturing. Technical report, Headquarters EOS GmbH, Munich, Germany, 2018.

[14] *Product Information*. EOS GmbH - Electro Optical Systems, September 2013. URL https://www.materialdatacenter.com/mb/file/show/653/0/Product_information_PA2241FR_2013-09-26_en.pdf.

[15] Jeffrey W. Gilman, Steven J. Ritchie, Takashi Kashiwagi, and Sergey M. Lomakin. Fire-retardant additives for polymeric materials—i. char formation from silica gel–potassium carbonate. *Fire and Materials*, 21(1):23–32, 1997. doi: 10.1002/(SICI)1099-1018(199701)21:1<23::AID-FAM591>3.0.CO;2-O. URL https://onlinelibrary.wiley.com/doi/abs/10.1002/%28SICI%291099-1018%28199701%2921%3A1%3C23%3A%3AAID-FAM591%3E3.0.CO%3B2-O.

[16] A.F. Grand and C.A. Wilkie. *Fire Retardancy of Polymeric Materials*. CRC Press, 2000. ISBN 9781420027099. URL https://books.google.nl/books?id=BOIlen8ZqP4C.

[17] Sandra Greiner, Lydia Lanzl, Katrin Wudy, and Dietmar Drummer. A new approach for getting more homogeneous temperature fields in selective laser sintering of polymers. In *AIP Conference Proceedings*, volume 2055. American Institute of Physics Inc., 1 2019. ISBN 9780735417830. doi: 10.1063/1.5084907.

[18] Eva C. Hofland, Ismet Baran, and Dagmar A. Wismeijer. Correlation of Process Parameters with Mechanical Properties of Laser Sintered PA12 Parts. *Advances in Materials Science and Engineering*, 2017, 2017. ISSN 16878442. doi: 10.1155/2017/4953173.

[19] B. Van Hooreweder, F. De Coninck, D. Moens, R. Boonen, and P. Sas. Microstructural characterization of sls-pa12 specimens under dynamic tension/compression excitation. *Polymer Testing*, 29:319–326, 5 2010. ISSN 01429418. doi: 10.1016/j.polymertesting.2009.12.006.

[20] Robert L. Johnson and Klaus Schmidt-Rohr. Quantitative solid-state 13c nmr with signal enhancement by multiple cross polarization. *Journal of Magnetic Resonance*, 239:44 – 49, 2014. ISSN 1090-7807. doi: https://doi.org/10.1016/j.jmr.2013.11.009. URL http://www.sciencedirect.com/science/article/pii/S1090780713003005.

[21] T. Jollivet, A. Darfeuille, B. Verquin, and S. Pillot. Rapid manufacturing of polymer parts by selective laser sintering. *International Journal of Material Forming*, 2(SUPPL. 1):697–700, 12 2009. ISSN 19606206. doi: 10.1007/s12289-009-0604-8.

[22] Shafi Ullah Khan, Arshad Munir, Rizwan Hussain, and Jang-Kyo Kim. Fatigue damage behaviors of carbon fiber-reinforced epoxy composites containing nanoclay. *Composites Science and Technology*, 70 (14):2077 – 2085, 2010. ISSN 0266-3538. doi: https://doi.org/10.1016/j.compscitech.2010.08.004. URL http://www.sciencedirect.com/science/article/pii/S0266353810003003.

[23] F. Laoutid, L. Bonnaud, M. Alexandre, J.-M. Lopez-Cuesta, and Ph. Dubois. New prospects in flame retardant polymer materials: From fundamentals to nanocomposites. *Materials Science and Engineering: R: Reports*, 63(3):100 – 125, 2009. ISSN 0927-796X. doi: https://doi.org/10.1016/j.mser.2008.09.002. URL http://www.sciencedirect.com/science/article/pii/S0927796X08000892.

[24] Menachem Lewin and Edward D. Weil. 1 - introduction: polymer combustion, condensed phase pyrolysis and smoke formation. In A.R. Horrocks and D. Price, editors, *Fire Retardant Materials*, pages 1 – 30. Woodhead Publishing, 2001. ISBN 978-1-85573-419-7. doi: https://doi.org/10.1533/9781855737464.31. URL http://www.sciencedirect.com/science/article/pii/B9781855734197500068.

[25] Menachem Lewin and Edward D. Weil. 2 - mechanisms and modes of action in flame retardancy of polymers. In A.R. Horrocks and D. Price, editors, *Fire Retardant Materials*, pages 31 – 68. Woodhead Publishing, 2001. ISBN 978-1-85573-419-7. doi: https://doi.org/10.1533/9781855737464.31. URL http://www.sciencedirect.com/science/article/pii/B9781855734197500068.

[26] Mo lin Chan, Kin tak Lau, Tsun tat Wong, Mei po Ho, and David Hui. Mechanism of reinforcement in a nanoclay/polymer composite. *Composites Part B: Engineering*, 42(6):1708 – 1712, 2011. ISSN 1359-8368. doi: https://doi.org/10.1016/j.compositesb.2011.03.011. URL http://www.sciencedirect.com/science/article/pii/S1359836811001089.

[27] Yi Fan Lv, Wayne Thomas, Rodger Chalk, and Sarat Singamneni. Flame retardant polymeric materials for additive manufacturing. *Materials Today: Proceedings*, 2020. ISSN 2214-7853. doi: https://doi.org/10.1016/j.matpr.2020.05.081. URL http://www.sciencedirect.com/science/article/pii/S2214785320336373.

[28] Shadpour Mallakpour and Mehdi Taghavi. Molten tetrabutylammonium bromide as eco-friendly media for the synthesis of optically active and thermal stable polyamides under microwave irradiation. *Polymer Journal - POLYM J*, 40:1049–1059, 08 2008. doi: 10.1295/polymj.PJ2008056.

[29] *Datasheets 3D Printing Materials*. Materialise NV, june 2020. URL https://www.materialise.com/system/files/resources/materialise_datasheets_25_06_20.pdf.

[30] *Operating instructions AB-S/FACT, PB-S/FACT*. Mettler Toledo, 2007. URL https://www.mt.com/be/nl/home/library/operating-instructions/laboratory-weighing/AB-S-FACT_PB-S-FACT_Operating_instructions.html.

[31] D.S. Moore. *The Basic Practice of Statistics*. W. H. Freeman, 2011. ISBN 9781464119392. URL https://books.google.nl/books?id=CbUVAAAAQBAJ.

[32] Javier Munguia and Kenny Dalgarno. Fatigue behaviour of laser-sintered PA12 specimens under four-point rotating bending. *Rapid Prototyping Journal*, 20(4):291–300, 6 2014. ISSN 13552546. doi: 10.1108/RPJ-07-2012-0064.

[33] Ben Ottenbourgs, Peter Adriaensens, Robert Carleer, Dirk Vanderzande, and Jan Gelan. Quantitative carbon-13 solid-state n.m.r. and ft–raman spectroscopy in novolac resins. *Polymer*, 39(22):5293 – 5300, 1998. ISSN 0032-3861. doi: https://doi.org/10.1016/S0032-3861(97)10283-X. URL http://www.sciencedirect.com/science/article/pii/S003238619710283X.

[34] M. Pavan, M. Faes, D. Strobbe, B. Van Hooreweder, T. Craeghs, D. Moens, and W. Dewulf. On the influence of inter-layer time and energy density on selected critical-to-quality properties of PA12 parts produced via

laser sintering. *Polymer Testing*, 61:386–395, 8 2017. ISSN 01429418. doi: 10.1016/j.polymertesting.2017.05.027.

[35] Michele Pavan. CT-based quality optimization of Laser Sintering of Polyamide-12. Technical report, ARENBERG DOCTORAL SCHOOL FACULTY OF ENGINEERING TECHNOLOGY, Leuven, Belgium, 2018.

[36] Michele Pavan, Piet Van Den Ecker, Tom Craeghs, Jean-Pierre Kruth, and Wim Dewulf. Investigating the influence of the energy density distribution on the quality of laser sintered polyamide-12 parts by using X-Ray Computed Tomography. Technical report. URL `http://www.ndt.net/?id=20880`.

[37] Michele Pavan, Tom Craeghs, Raf Verhelst, Olivier Ducatteeuw, Jean Pierre Kruth, and Wim Dewulf. CT-based quality control of Laser Sintering of Polymers. *Case Studies in Nondestructive Testing and Evaluation*, 6:62–68, 11 2016. ISSN 22146571. doi: 10.1016/j.csndt.2016.04.004.

[38] Michele Pavan, Tom Craeghs, Jean Pierre Kruth, and Wim Dewulf. Investigating the influence of X-ray CT parameters on porosity measurement of laser sintered PA12 parts using a design-of-experiment approach. *Polymer Testing*, 66:203–212, 4 2018. ISSN 01429418. doi: 10.1016/j.polymertesting.2018.01.037.

[39] T. N.A.T. Rahim, A. M. Abdullah, H. Md Akil, D. Mohamad, and Z. A. Rajion. The improvement of mechanical and thermal properties of polyamide 12 3d printed parts by fused deposition modelling. *Express Polymer Letters*, 11:963–982, 12 2017. ISSN 1788618X. doi: 10.3144/expresspolymlett.2017.92.

[40] D RIETZEL, D DRUMMER, and F KUEHNLEIN. *INVESTIGATION OF THE PARTICULAR CRYSTALLIZATION BEHAVIOUR OF SEMI-CRYSTALLINE THERMOPLASTIC POWDERS PROCESSED BY SELECTIVE LASER SINTERING*. DAAAM, 2010. ISBN 9783901509735.

[41] M. Schmid. *Laser Sintering with Plastics - Technology, Processes, and Materials*. Hanser Publishers, Munich, 2015. ISBN 978-1-56990-683-5.

[42] Manfred Schmid, Rob Kleijnen, Marc Vetterli, and Konrad Wegener. Influence of the origin of polyamide 12 powder on the laser sintering process and laser sintered parts. *Applied Sciences (Switzerland)*, 7(5), 2017. ISSN 20763417. doi: 10.3390/app7050462.

[43] Thomas Stichel, Thomas Frick, Tobias Laumer, Felix Tenner, Tino Hausotte, Marion Merklein, and Michael Schmidt. A Round Robin study for selective laser sintering of polymers: Back tracing of the pore morphology to the process parameters. *Journal of Materials Processing Technology*, 252:537–545, 2 2018. ISSN 09240136. doi: 10.1016/j.jmatprotec.2017.10.013.

[44] Lei Wang, Ke Wang, Ling Chen, Yongwei Zhang, and Chaobin He. Preparation, morphology and thermal/mechanical properties of epoxy/nanoclay composite. *Composites Part A: Applied Science and Manufacturing*, 37(11):1890 – 1896, 2006. ISSN 1359-835X. doi: https://doi.org/10.1016/j.compositesa.2005.12.020. URL `http://www.sciencedirect.com/science/article/pii/S1359835X06000054`.

[45] Yueqi Wang, K U Leuven, and David Moens. Variability in the mechanical properties of Laser Sintered PA-12 Components. Technical report. URL `https://www.researchgate.net/publication/280941822`.

[46] Shaoxiong Wu. Lecture notes: Introduction to solid state nmr, 2015.

[47] Hideki Yamamoto, Sadao Araki, Yuki Nagano, Kotaro Mizuta, Tetsuya Huruike, and Hiroshi Tamura. Development of a regeneration process for nylon-6 and nylon-6,6 from felt wastes. *KAGAKU KOGAKU RONBUNSHU*, 39:238–243, 05 2013. doi: 10.1252/kakoronbunshu.39.238.

[48] R. J. Young and P. A. Lovell. *Introduction to Polymers*. CRC PRess, third edition edition, 2011. ISBN 9780849339295.

[49] Way Yusoff, Hanafi Ani, and DT Pham. Influence of Molecular Weight Average, Degree of Crystallinity, and Viscosity of Different Polyamide PA12 Powder Grades on the Microstructures of Laser Sintered Part. doi: 10.1051/C. URL `http://www.matec-conferences.org`.

[50] Meng Zhao, Katrin Wudy, and Dietmar Drummer. Crystallization kinetics of polyamide 12 during Selective laser sintering. *Polymers*, 10(2), 2 2018. ISSN 20734360. doi: 10.3390/polym10020168.

[51] Zicheng Zhu and Candice Majewski. Understanding pore formation and the effect on mechanical properties of high speed sintered polyamide-12 parts: A focus on energy input. *Materials and Design*, 194, 9 2020. ISSN 18734197. doi: 10.1016/j.matdes.2020.108937.

[52] W.G. Zikmund. *Business Research Methods*. Dryden Press series in management. Dryden Press, 2000. ISBN 9780030258176. URL `https://books.google.nl/books?id=LP1R7I20xjIC`.

Appendix A
Data Tensile Tests

Table A.1: Data from Tensile tests for Batch 138448

Phys Part ID	**Orientation**	**Spare?**	**Tag**	**Build ID**	**Counter**	E_T **[MPa]**	σ_Y **[MPa]**	σ_M **[MPa]**	ε_M **[%]**	σ_B **[MPa]**	ε_B **[%]**
9682337	EDGE	SPARE	AERO	138448	11						
9682338	EDGE	-	AERO	138448	12	1780	46.1	46.1	9.3	45.3	10
9682339	EDGE	-	AERO	138448	13	1760	-	45.2	8.2	45	8.7
9682340	EDGE	-	AERO	138448	14	1770	45.5	45.5	8.8	43	9.6
9682341	EDGE	-	AERO	138448	15	1770	-	45.8	8.8	45.4	9.6
9682342	UP	SPARE	AERO	138448	16						
9682343	UP	-	AERO	138448	17	1790	-	43.4	4.6	42.7	4.6
9682344	UP	-	AERO	138448	18	1780	-	43.3	4.7	43.3	4.7
9682345	UP	-	AERO	138448	19	1780	-	43.1	4.4	42.7	4.4
9682346	UP	-	AERO	138448	20	1780	-	43.4	4.7	43.3	4.7
9682347	EDGE	SPARE	AERO	138448	21						
9682348	EDGE	-	AERO	138448	22	1780	47.2	47.2	10	46.7	12.3
9682349	EDGE	-	AERO	138448	23	1750	-	46.6	10.3	46.2	12.6
9682350	EDGE	-	AERO	138448	24	1760	46.7	46.7	10	46.2	12.6
9682351	EDGE	-	AERO	138448	25	1760	46.7	46.7	9.8	44.4	10.7
9682352	UP	SPARE	AERO	138448	26						
9682353	UP	-	AERO	138448	27	1780	-	43.2	4.6	43.1	4.6
9682354	UP	-	AERO	138448	28	1790	-	44.1	4.6	43.9	4.6
9682355	UP	-	AERO	138448	29	1780	-	44.3	5.5	44.1	5.6
9682356	UP	-	AERO	138448	30	1790	-	43.1	4.3	41.8	4.3

Table A.2: Data from Tensile tests for Batch 138297

Phys Part ID	**Orientation**	**Spare?**	**Tag**	**Build ID**	**Counter**	E_T **[MPa]**	σ_Y **[MPa]**	σ_M **[MPa]**	ε_M **[%]**	σ_B **[MPa]**	ε_B **[%]**
9671765	EDGE	Spare	AERO	138297	11						
9671766	EDGE	-	AERO	138297	12	1760	45.4	45.4	9.2	43.6	9.9
9671767	EDGE	-	AERO	138297	13	1760	45.7	45.7	7.7	44.6	8.2
9671768	EDGE	-	AERO	138297	14	1750	-	45.3	7.7	43.6	7.9
9671769	EDGE	-	AERO	138297	15	1750	-	45.3	8.2	45.1	8.8
9671770	UP	Spare	AERO	138297	16						
9671771	UP	-	AERO	138297	17	1790	-	43.5	4.3	43.2	4.3
9671772	UP	-	AERO	138297	18	1790	-	44.1	4.8	42.5	4.8
9671773	UP	-	AERO	138297	19	1790	-	42.6	3.8	40.9	3.8
9671774	UP	-	AERO	138297	20	1800	-	44.3	4.7	43.1	4.7
9671775	EDGE	Spare	AERO	138297	21						
9671776	EDGE	-	AERO	138297	22	1730	-	45.9	9.8	45.6	11.8
9671777	EDGE	-	AERO	138297	23	1760	46.6	46.6	9.8	45.9	11.9
9671778	EDGE	-	AERO	138297	24	1760	-	46.8	9.8	46.7	10.8
9671779	EDGE	-	AERO	138297	25	1750	46.4	46.4	9.6	45.5	11.1
9671780	UP	Spare	AERO	138297	26						
9671781	UP	-	AERO	138297	27	1780	-	41.3	3.5	41.2	3.5
9671782	UP	-	AERO	138297	28	1790	-	43.9	4.7	43.9	4.7
9671783	UP	-	AERO	138297	29	1790	-	42.5	3.9	40.6	3.9
9671784	UP	-	AERO	138297	30	1790	-	42.7	4	41.1	4

Table A.3: Data from Tensile tests for Batch 138456

Phys Part ID	**Orientation**	**Spare?**	**Tag**	**Build ID**	**Counter**	E_T **[MPa]**	σ_Y **[MPa]**	σ_M **[MPa]**	ε_M **[%]**	σ_B **[MPa]**	ε_B **[%]**
9682690	EDGE	Spare	AERO	138456	9						
9682691	EDGE	-	AERO	138456	10	1750	45.5	45.5	8.7	44.6	9.5
9682692	EDGE	-	AERO	138456	11	1690	-	44.5	8	44.5	8.3
9682693	EDGE	-	AERO	138456	12	1700	-	44.2	7.3	42	7.7
9682694	EDGE	-	AERO	138456	13	1730	-	45.2	8.3	44.8	9.1
9682695	UP	Spare	AERO	138456	14						
9682696	UP	-	AERO	138456	15	1730	-	42	4.3	41.4	4.4
9682697	UP	-	AERO	138456	16	1720	-	40.5	3.6	40.5	3.6
9682698	UP	-	AERO	138456	17	1700	-	40.6	3.6	40.3	3.7
9682699	UP	-	AERO	138456	18	1710	-	41.4	4	41.4	4
9682700	EDGE	Spare	AERO	138456	19						
9682701	EDGE	-	AERO	138456	20	1740	46.2	46.2	10	44.3	12.1
9682702	EDGE	-	AERO	138456	21	1700	46.1	46.1	10.7	45	12.9
9682703	EDGE	-	AERO	138456	22	1710	-	46.2	10.2	45.8	13.2
9682704	EDGE	-	AERO	138456	23	1730	46.8	46.8	10.1	44.4	12.6
9682705	UP	Spare	AERO	138456	24						
9682706	UP	-	AERO	138456	25	1740	-	42.3	4.3	41.1	4.3
9682707	UP	-	AERO	138456	26	1710	-	43	5	43	5
9682708	UP	-	AERO	138456	27	1720	-	42.7	4.6	42	4.6
9682709	UP	-	AERO	138456	28	1720	-	43	5.2	42.9	5.2

Table A.4: Data from Tensile tests for Batch 137470

Phys Part ID	**Orientation**	**Spare?**	**Tag**	**Build ID**	**Counter**	E_T **[MPa]**	σ_Y **[MPa]**	σ_M **[MPa]**	ε_M **[%]**	σ_B **[MPa]**	ε_B **[%]**
9613543	EDGE	Spare	AERO	137470	11						
9613544	EDGE	-	AERO	137470	12	1750	-	45.6	9.6	45.4	10.6
9613545	EDGE	-	AERO	137470	13	1730	-	45.2	8.8	43.2	9.1
9613546	EDGE	-	AERO	137470	14	1740	45.7	45.7	9.4	43.7	10.4
9613547	EDGE	-	AERO	137470	15	1750	45.4	45.4	9.1	44.6	10.6
9613548	UP	Spare	AERO	137470	16						
9613549	UP	-	AERO	137470	17	1810	-	44.7	5.3	43.6	5.3
9613550	UP	-	AERO	137470	18	1770	-	44.5	6.4	44.4	6.5
9613551	UP	-	AERO	137470	19	1770	-	44.5	6.2	44.3	6.3
9613552	UP	-	AERO	137470	20	1780	-	44.8	5.8	44.5	5.9
9613553	EDGE	Spare	AERO	137470	21						
9613554	EDGE	-	AERO	137470	22	1740	46.2	46.2	9.8	45.4	11.9
9613555	EDGE	-	AERO	137470	23	1720	45.9	45.9	9.8	44.4	11.8
9613556	EDGE	-	AERO	137470	24	1730	-	46.1	9.8	45.7	12.1
9613557	EDGE	-	AERO	137470	25	1730	46.1	46.1	10.1	45.1	11.7
9613558	UP	Spare	AERO	137470	26						
9613559	UP	-	AERO	137470	27	1780	-	45	6.2	44.8	6.3
9613560	UP	-	AERO	137470	28	1750	-	44.4	6.1	44.4	6.1
9613561	UP	-	AERO	137470	29	1760	-	43.7	5.1	42.2	5.1
9613562	UP	-	AERO	137470	30	1750	-	42.7	4.2	42.5	4.3

Appendix B
Results Differential Scanning Calorimetry

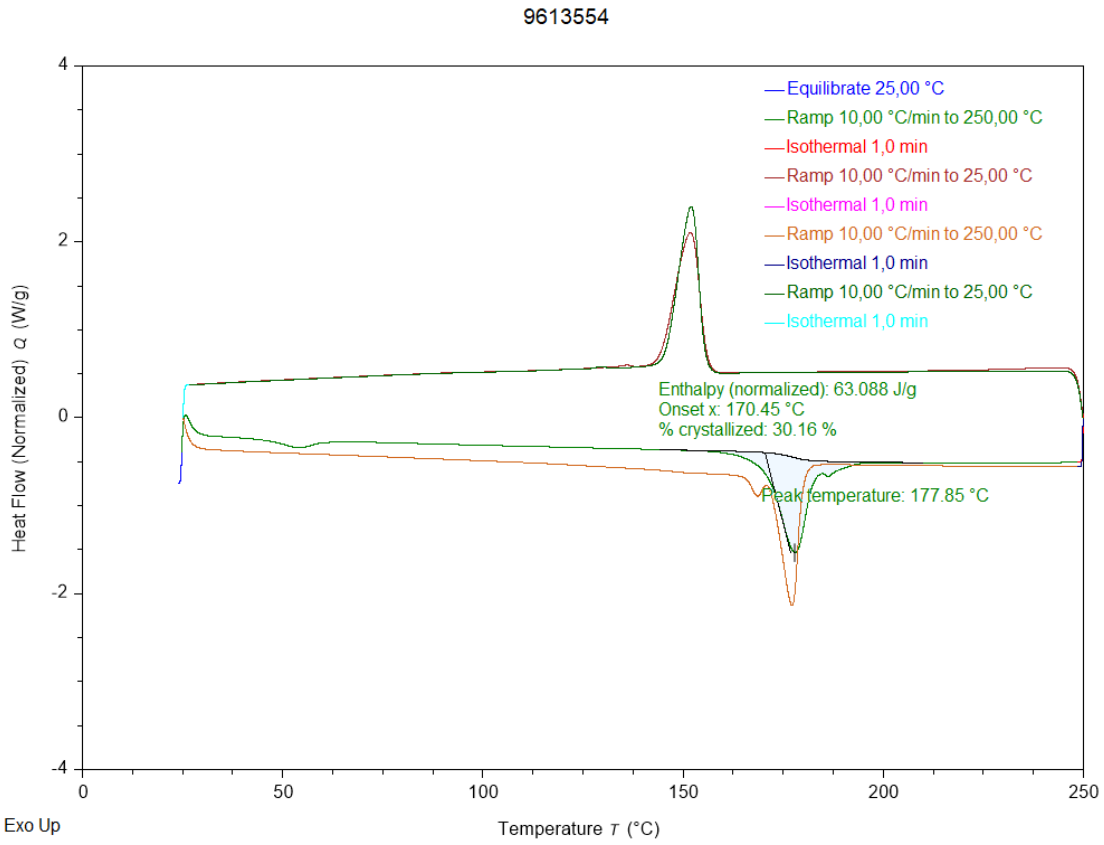

Figure B.1: Graphical representation of DSC data of specimen 9603554

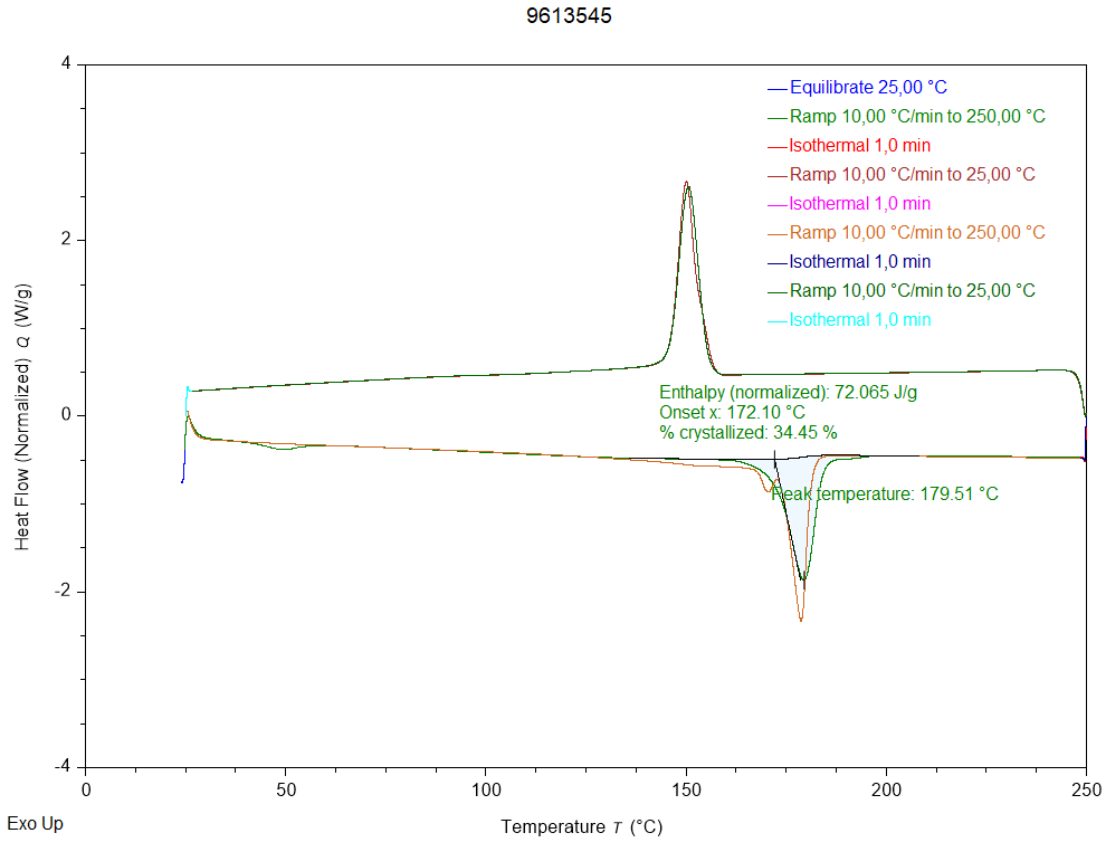

Figure B.2: Graphical representation of DSC data of specimen 9613545

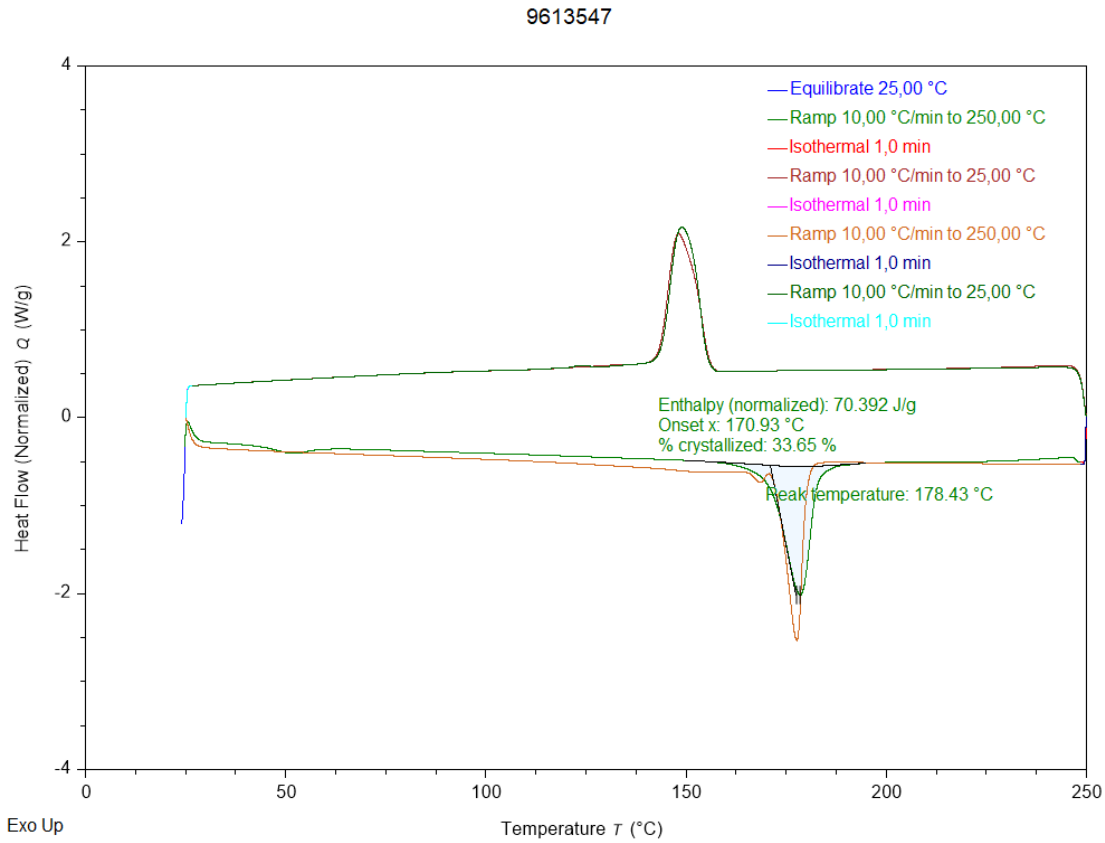

Figure B.3: Graphical representation of DSC data of specimen 9613547

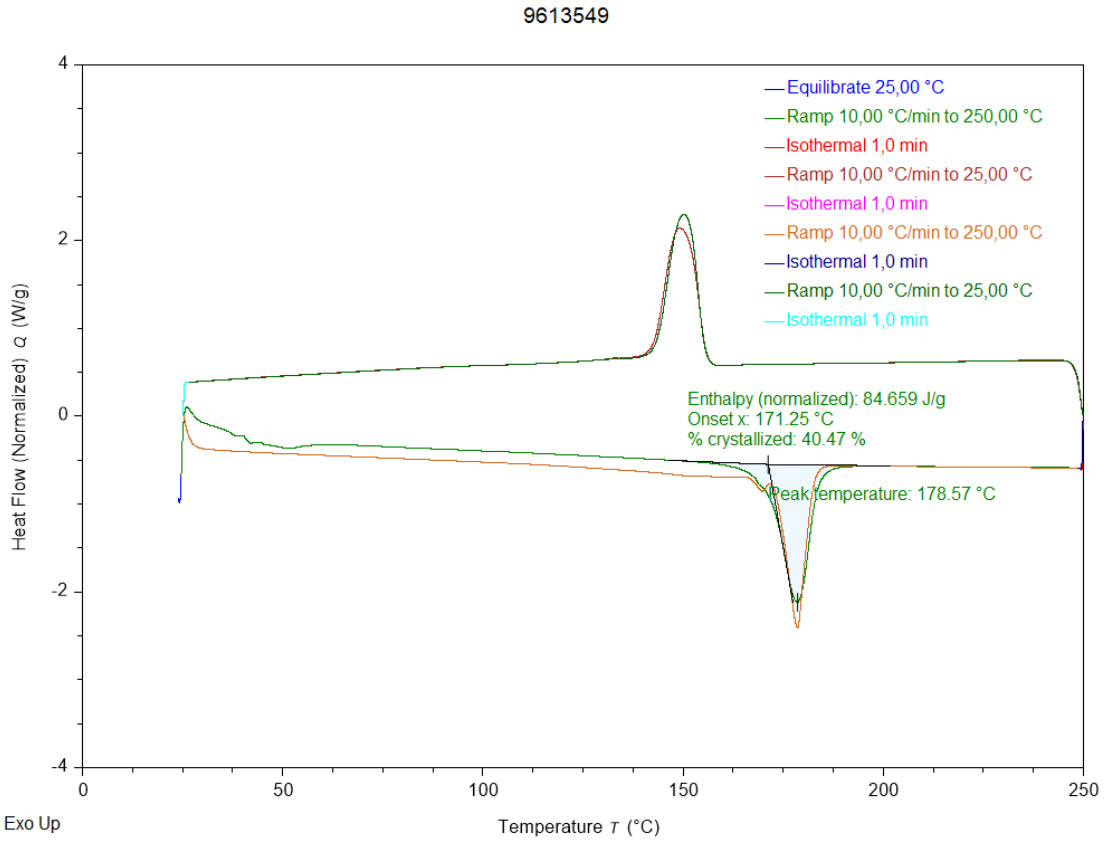

Figure B.4: Graphical representation of DSC data of specimen 9613549

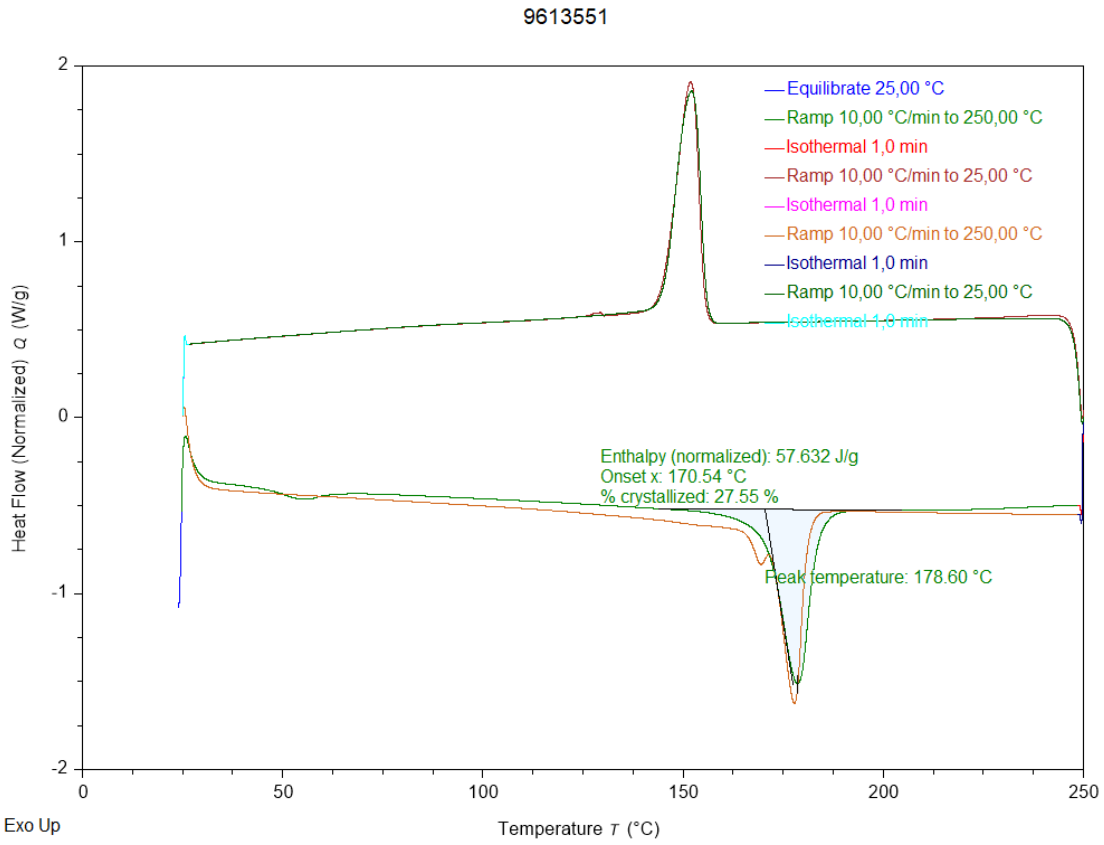

Figure B.5: Graphical representation of DSC data of specimen 9613551

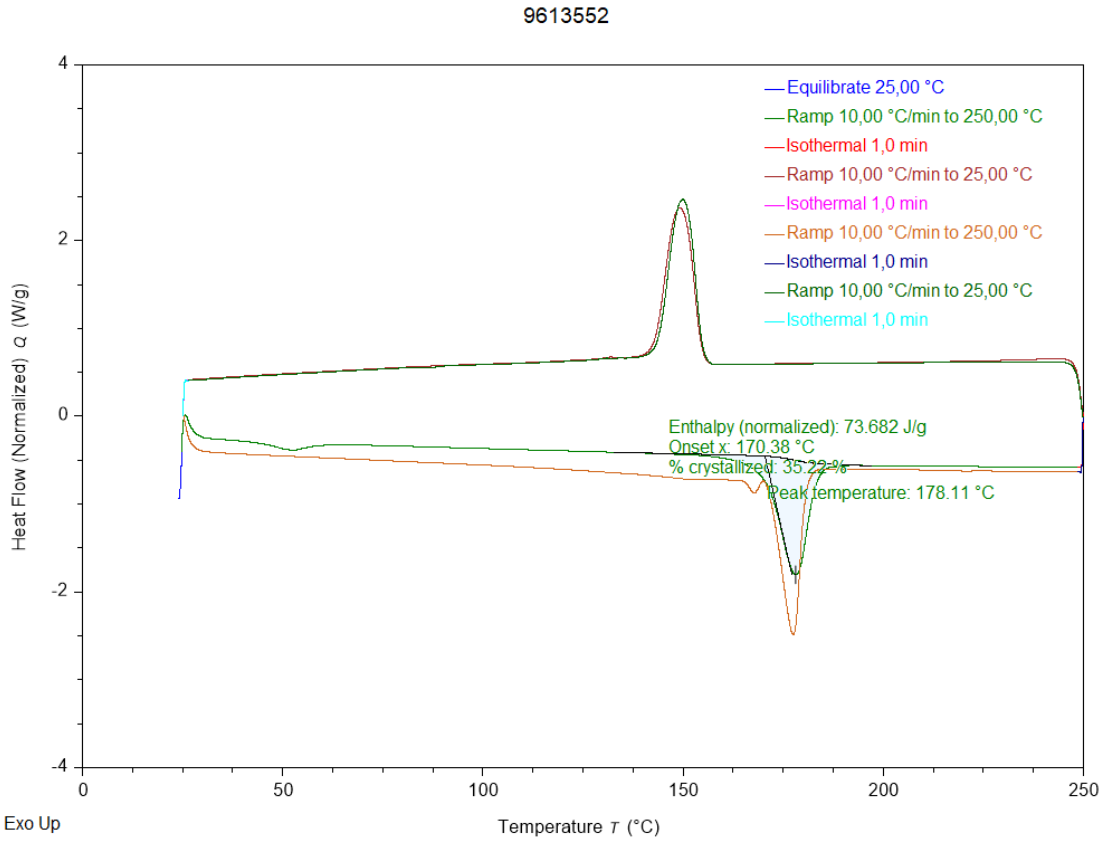

Figure B.6: Graphical representation of DSC data of specimen 9613552

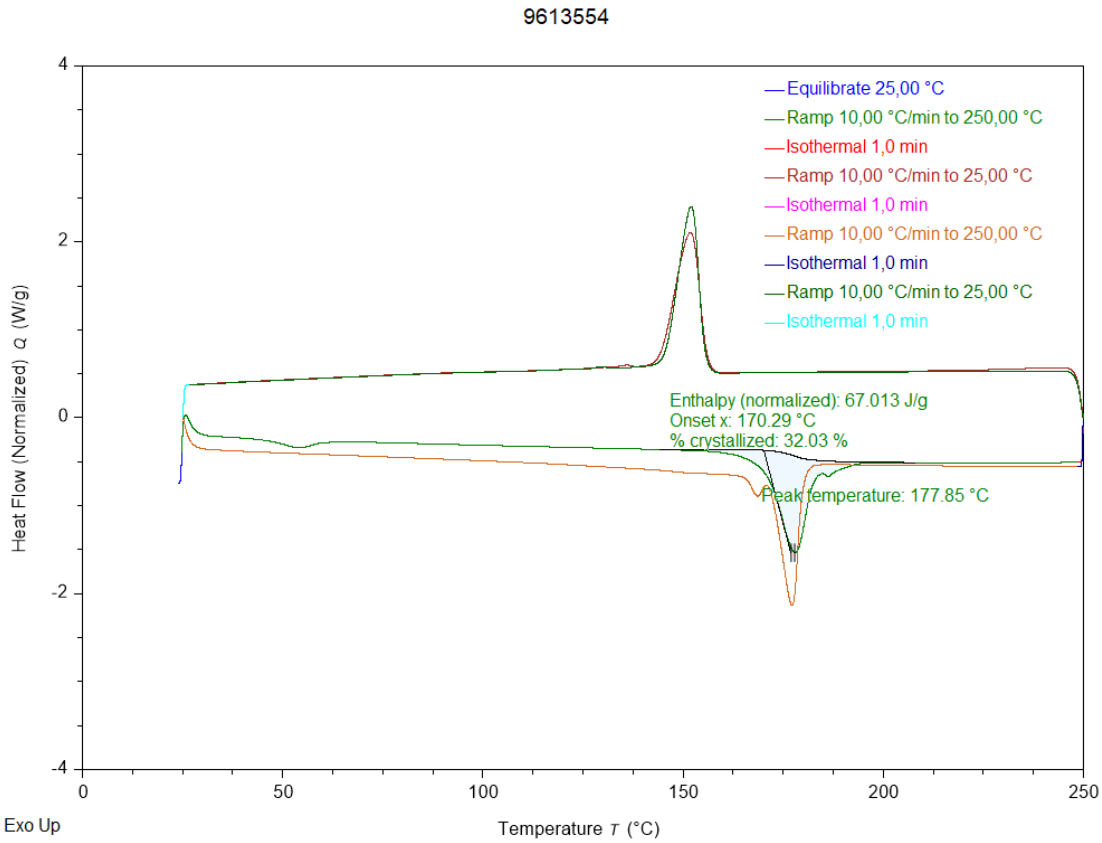

Figure B.7: Graphical representation of DSC data of specimen 9613554

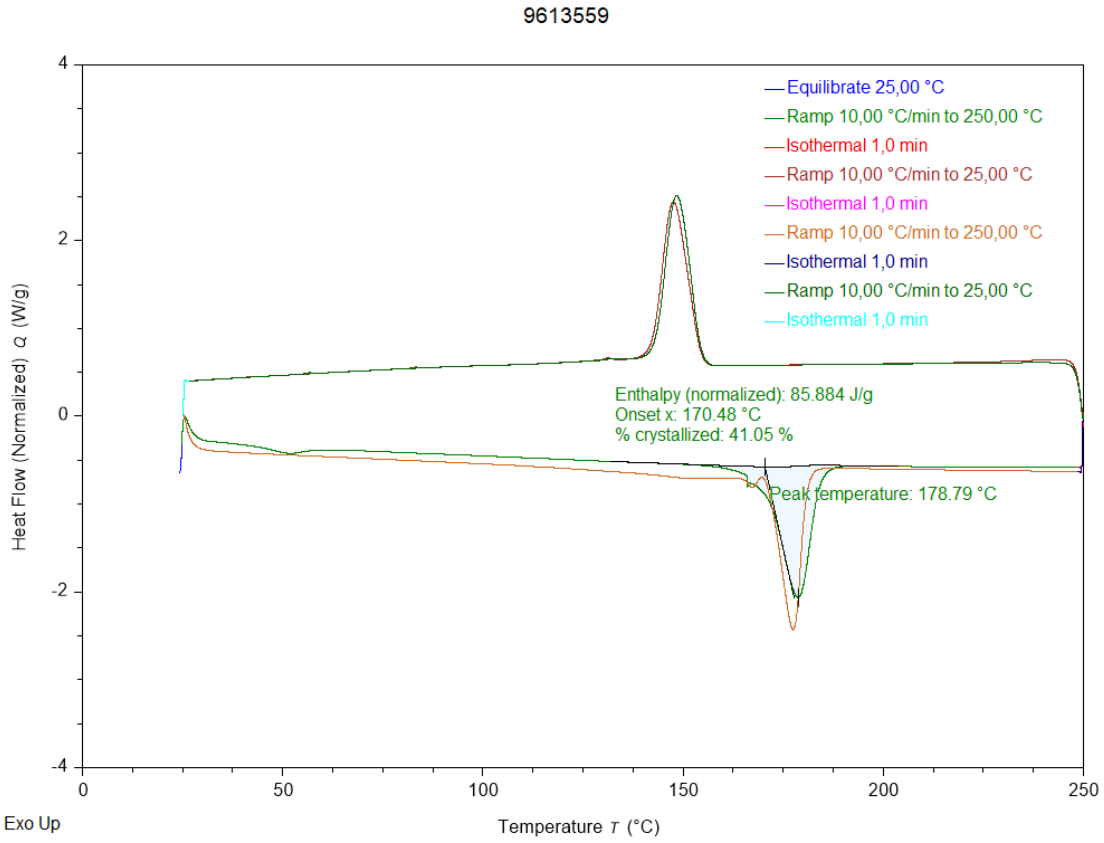

Figure B.8: Graphical representation of DSC data of specimen 9613559

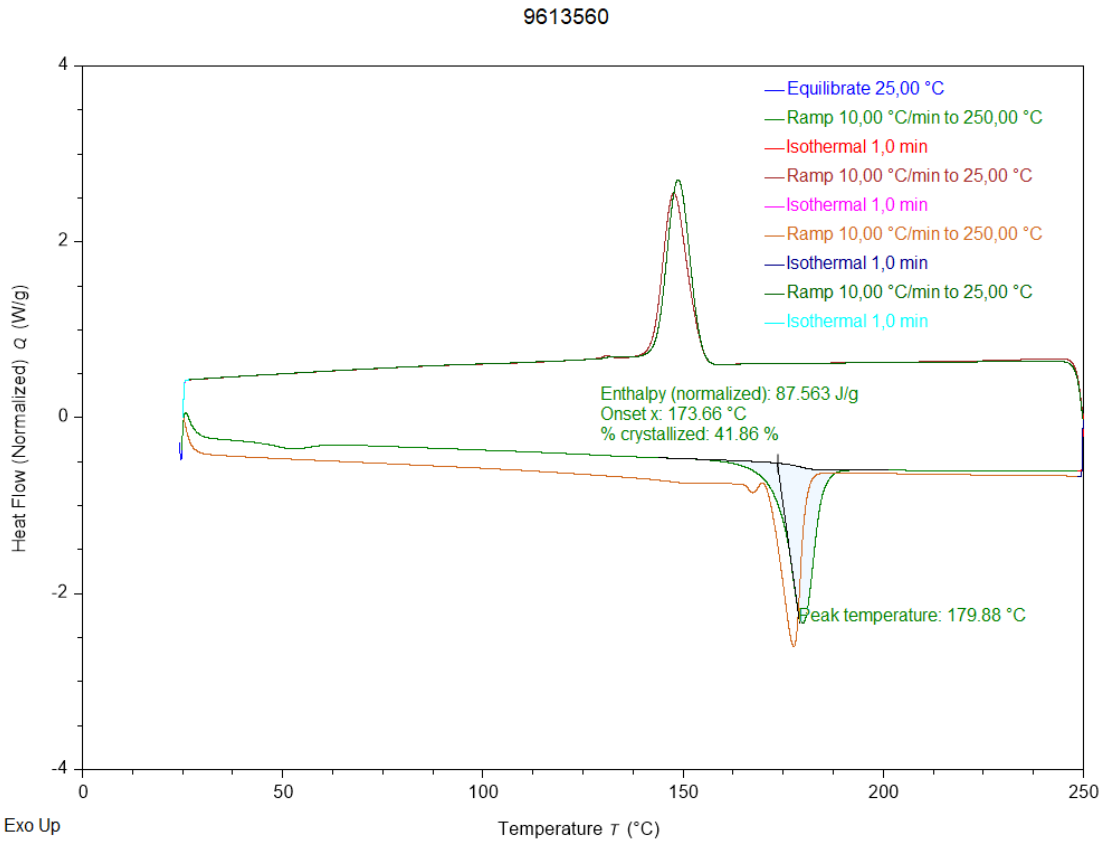

Figure B.9: Graphical representation of DSC data of specimen 9613560

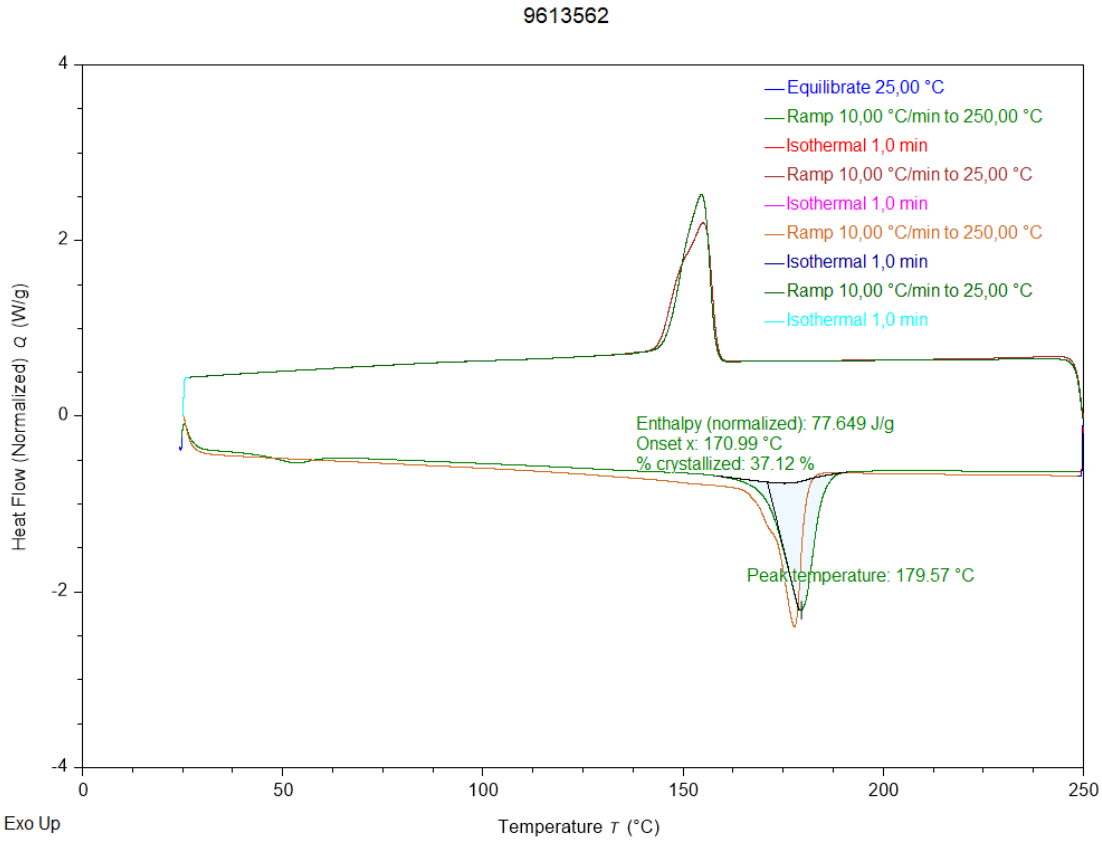

Figure B.10: Graphical representation of DSC data of specimen 9613562

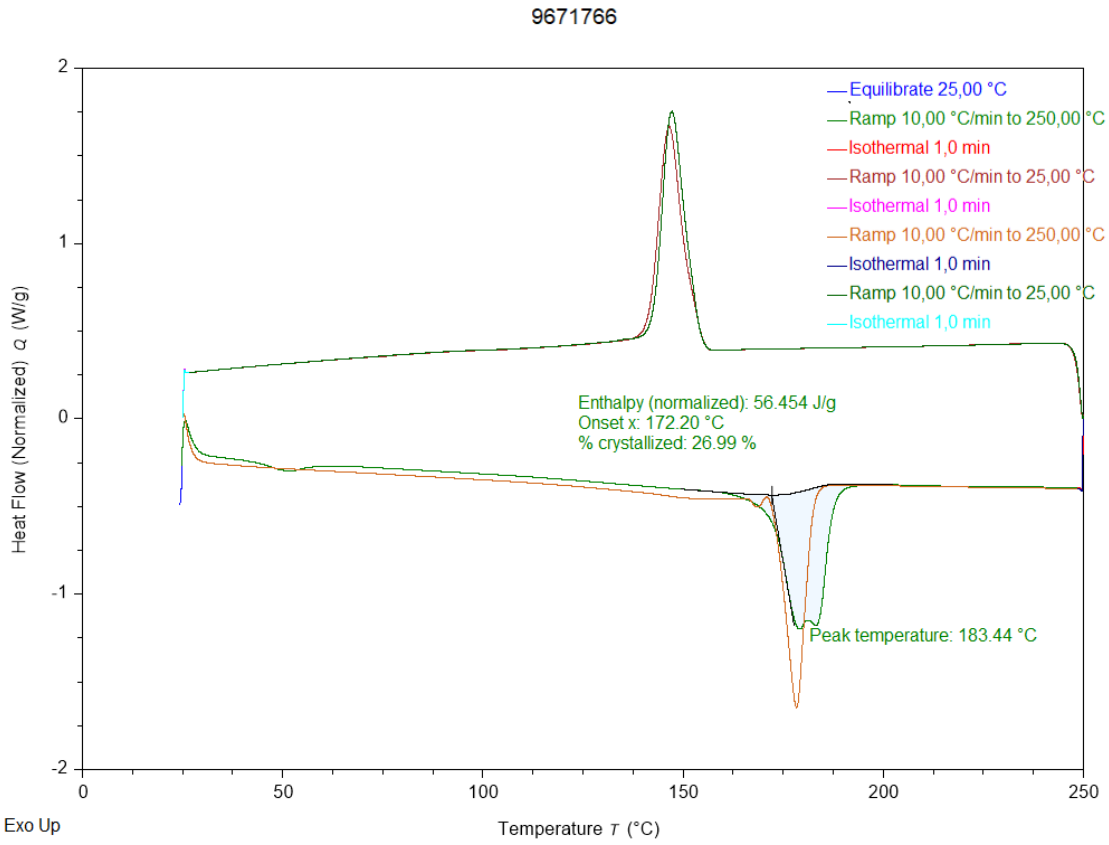

Figure B.11: Graphical representation of DSC data of specimen 9671766

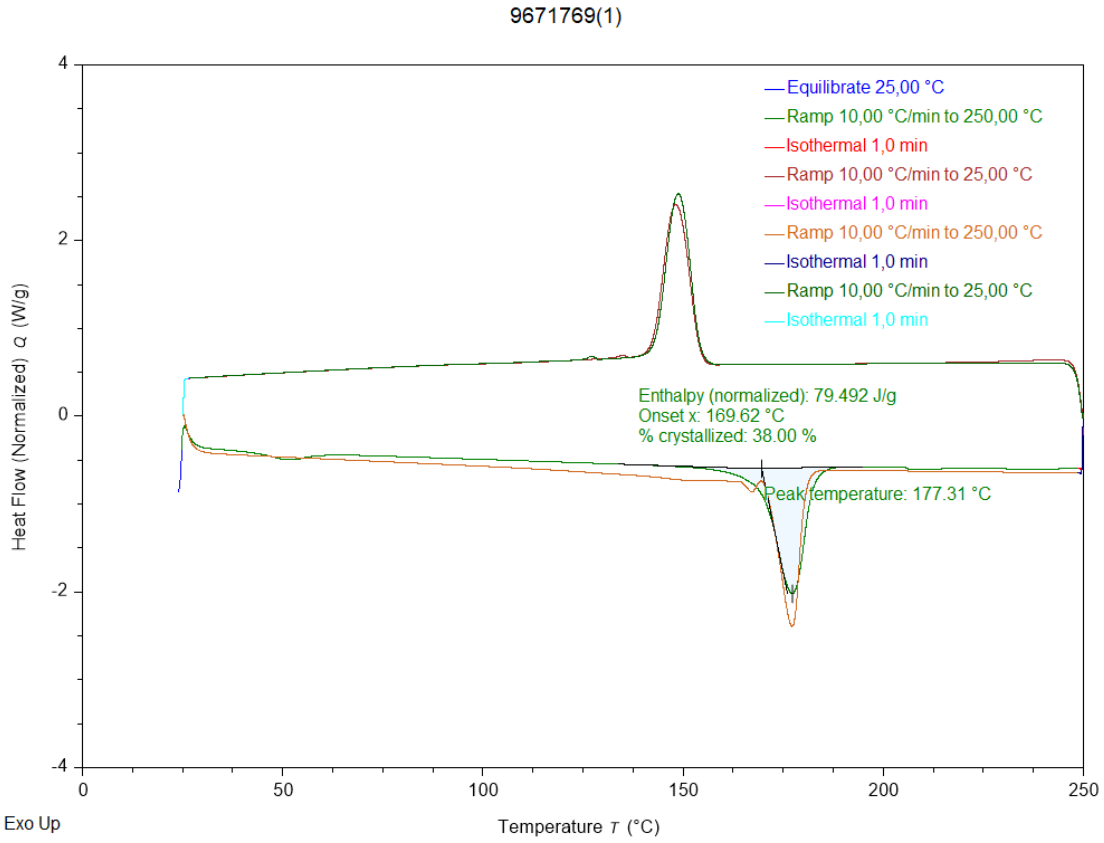

Figure B.12: Graphical representation of DSC data of specimen 9671769

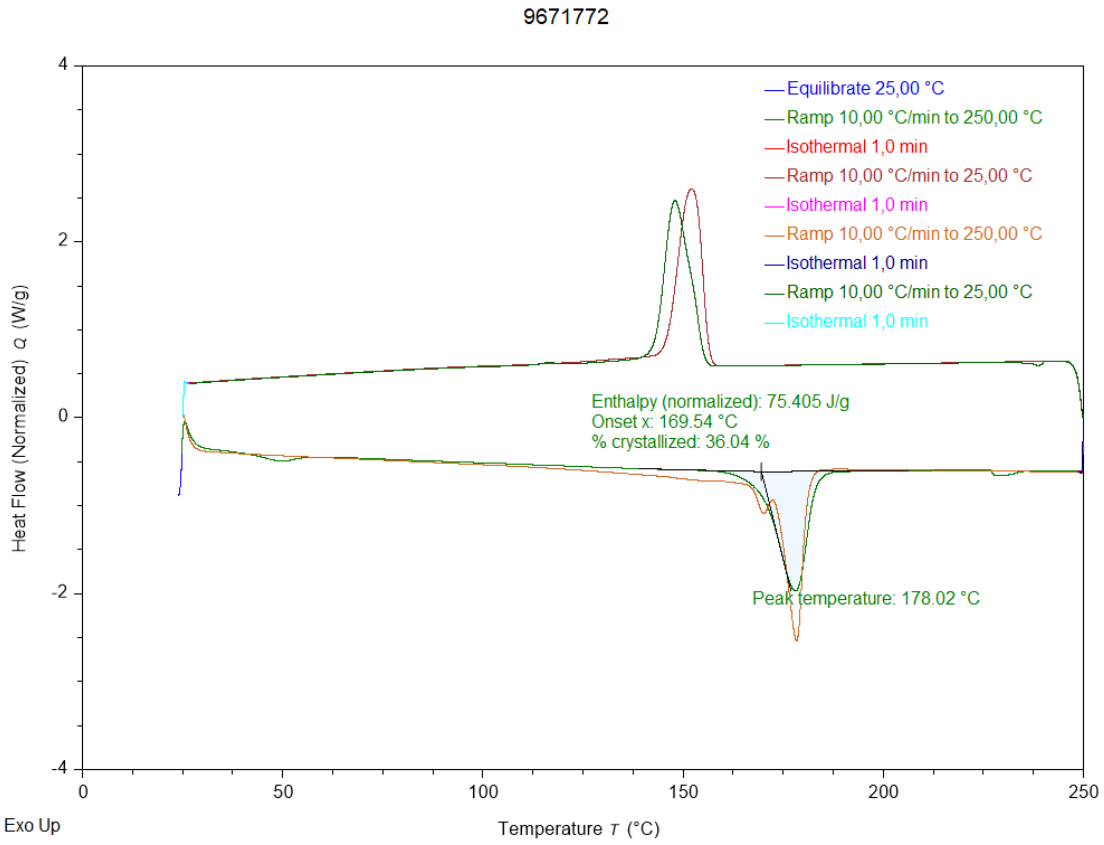

Figure B.13: Graphical representation of DSC data of specimen 9671772

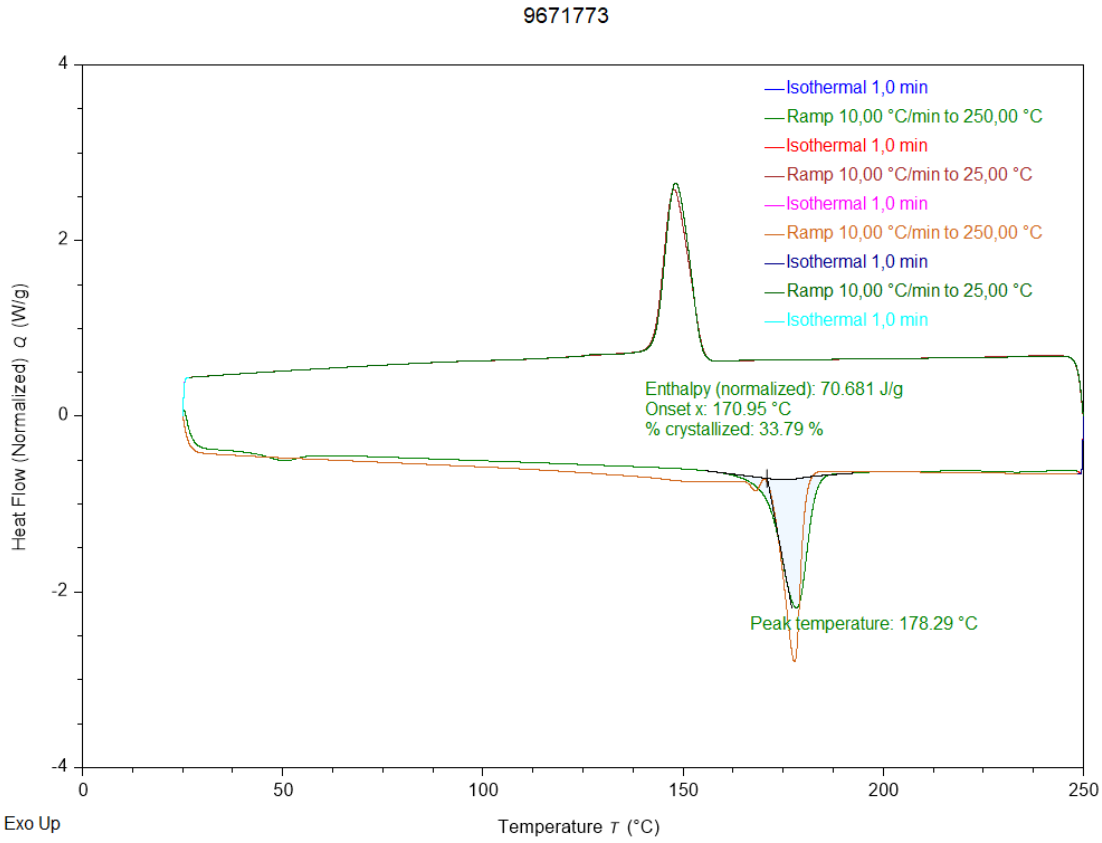

Figure B.14: Graphical representation of DSC data of specimen 9671773

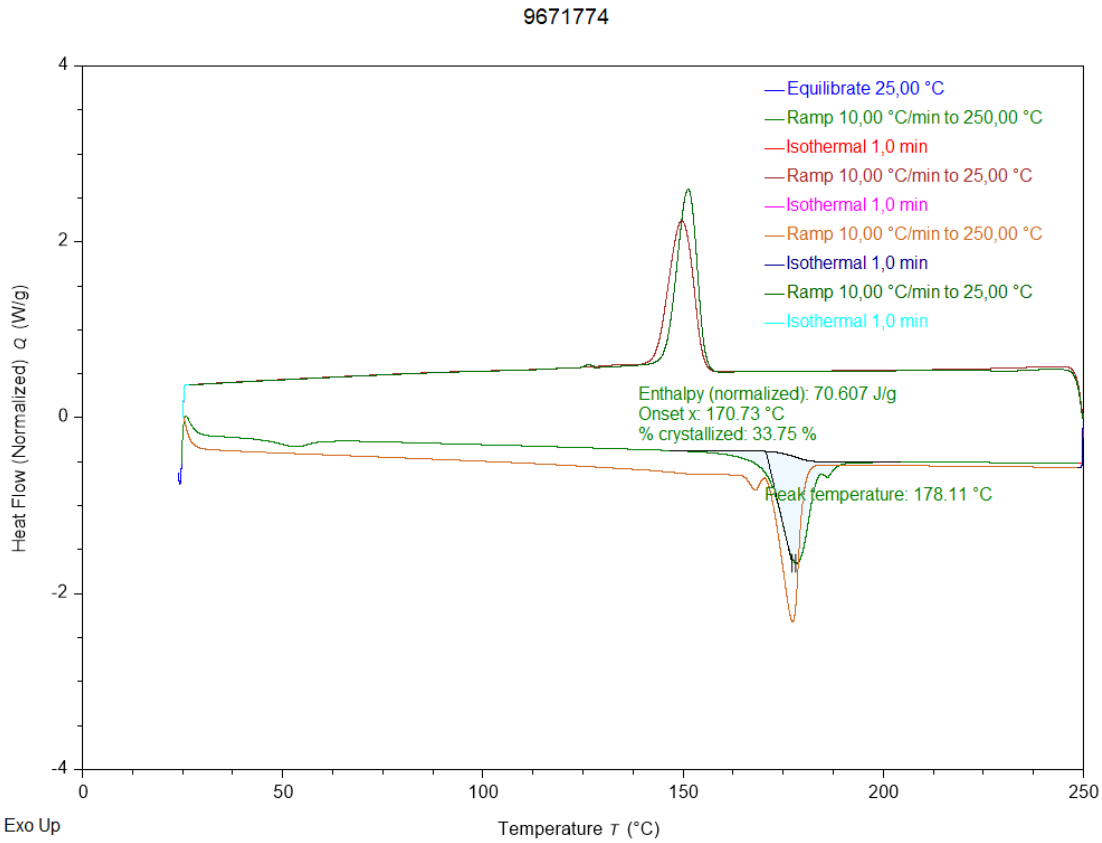

Figure B.15: Graphical representation of DSC data of specimen 9671774

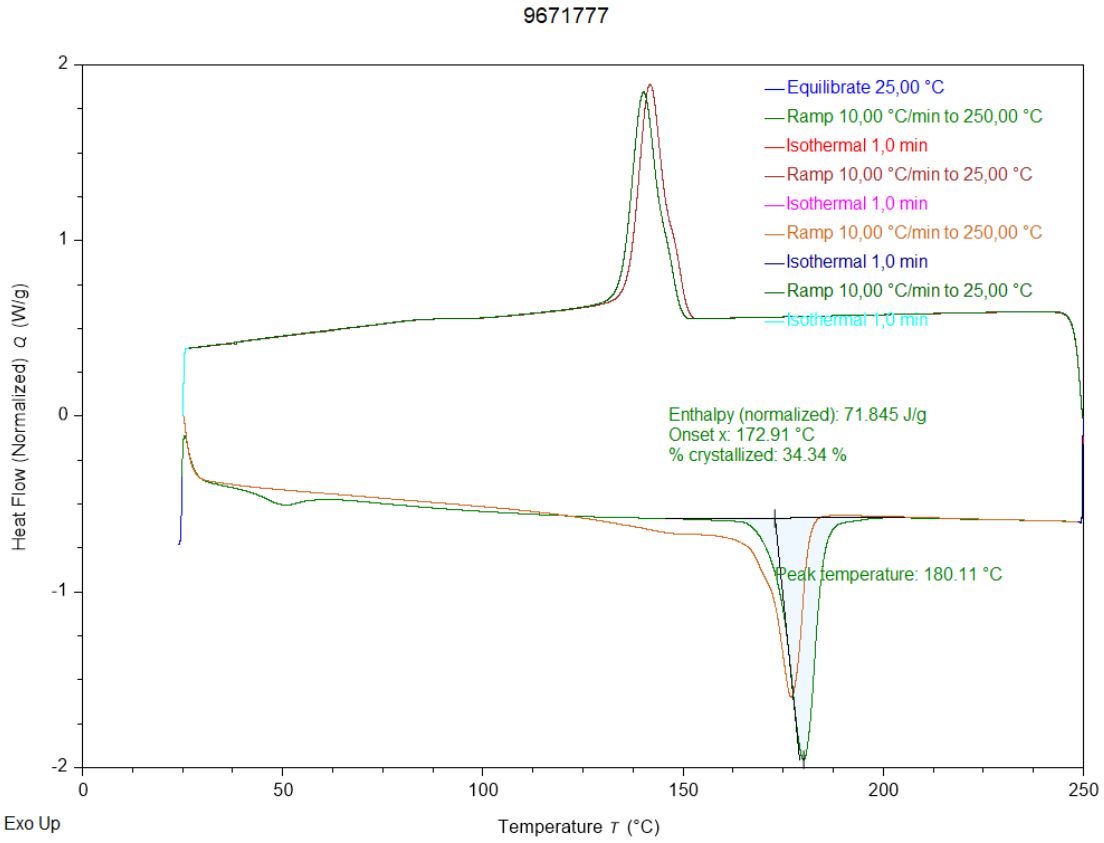

Figure B.16: Graphical representation of DSC data of specimen 9671777

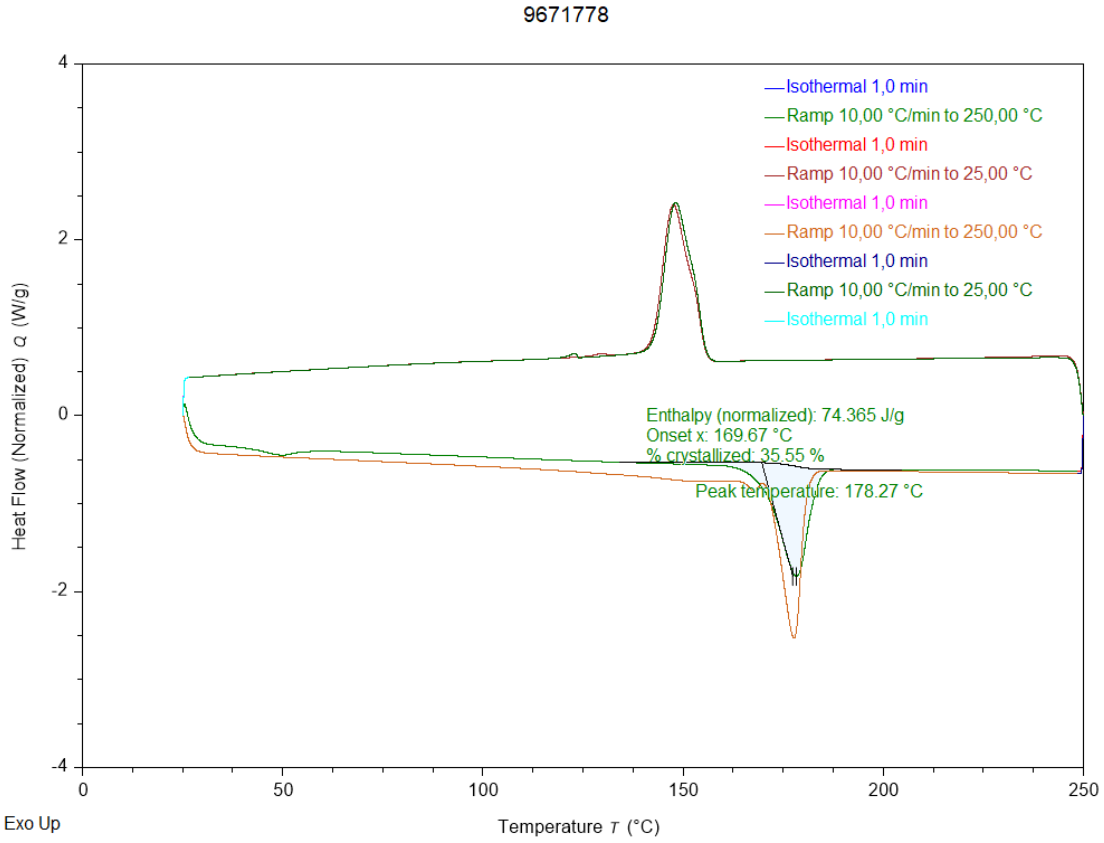

Figure B.17: Graphical representation of DSC data of specimen 9671778

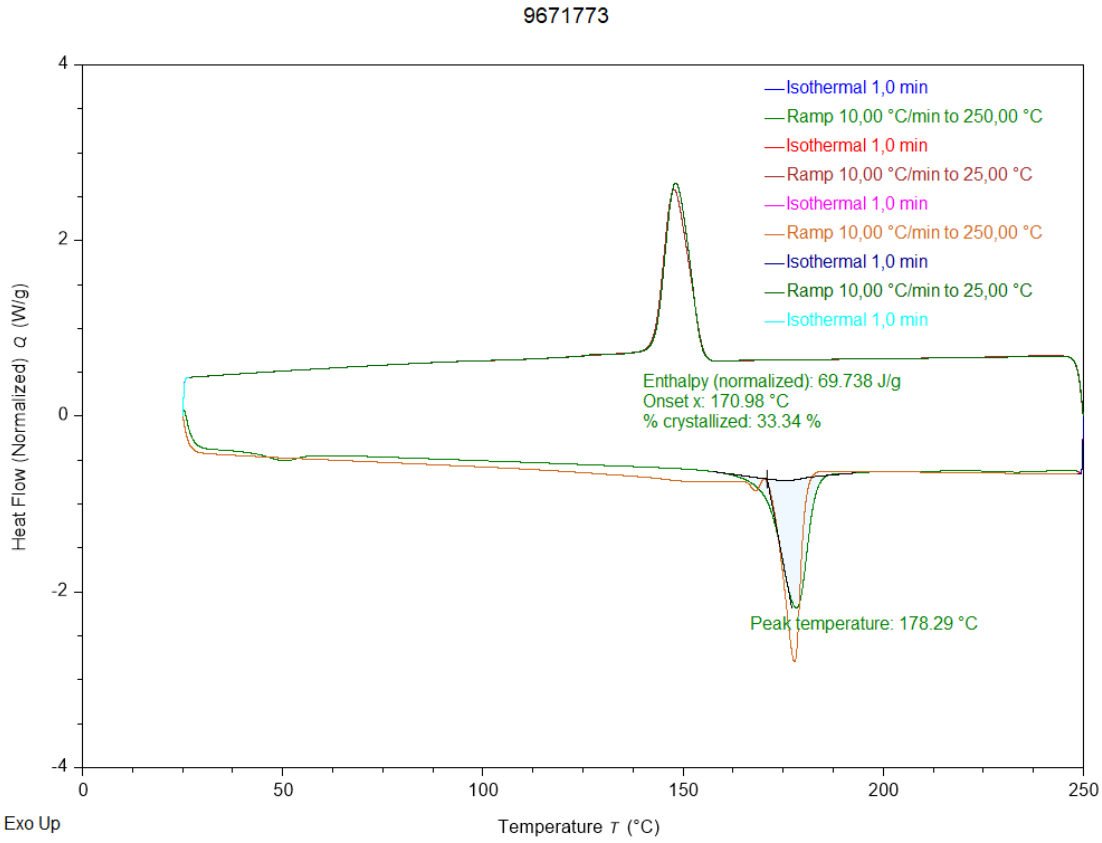

Figure B.18: Graphical representation of DSC data of specimen 9671783

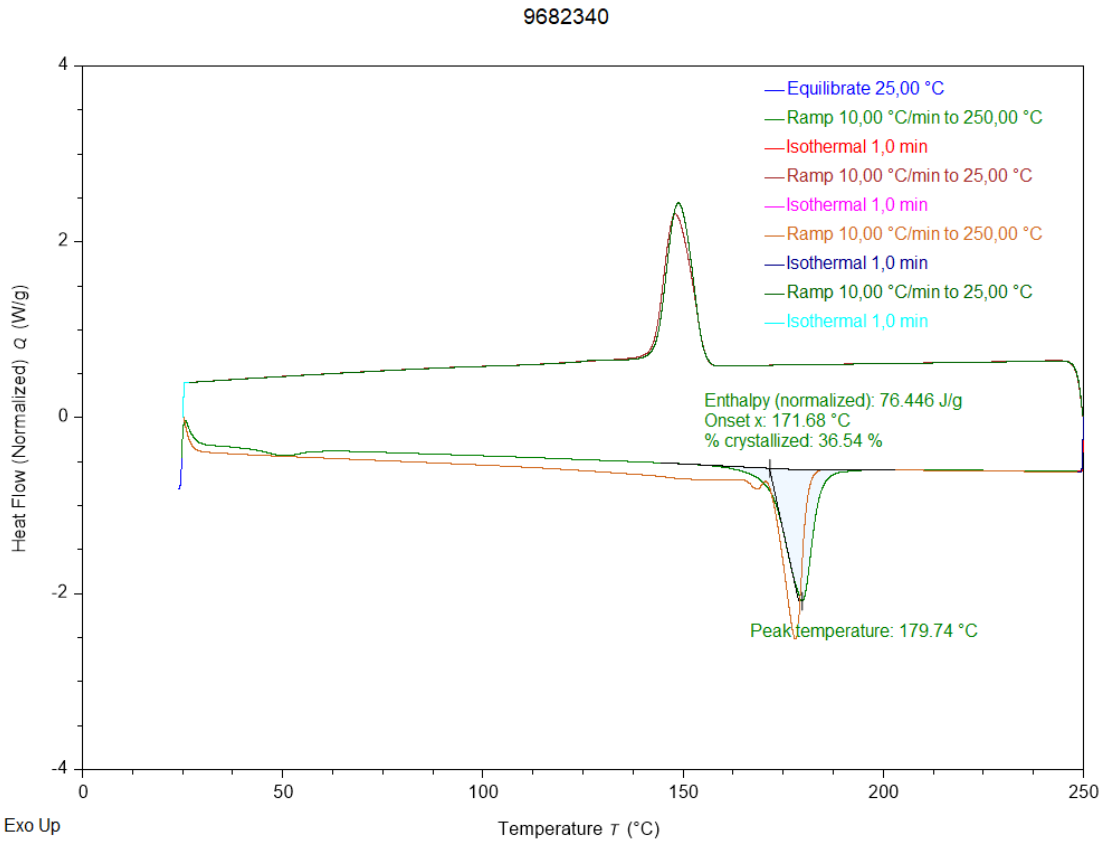

Figure B.19: Graphical representation of DSC data of specimen 9682340

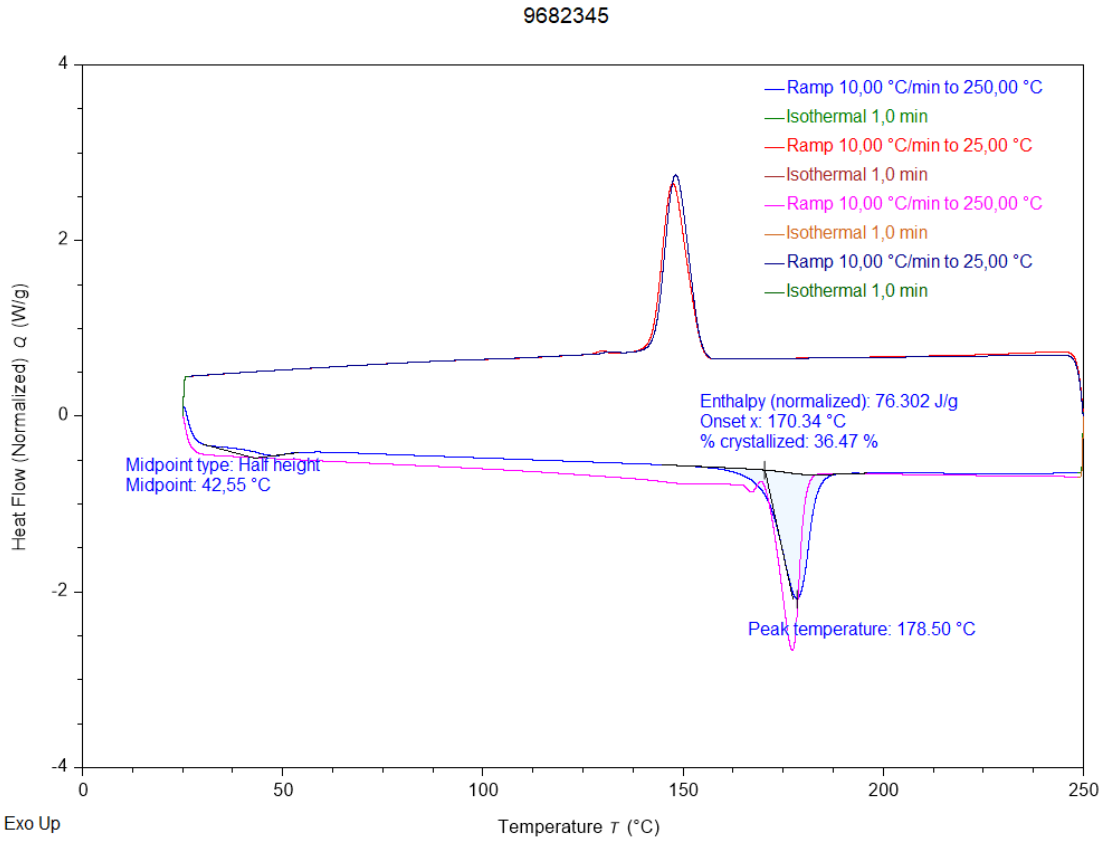

Figure B.20: Graphical representation of DSC data of specimen 9682345

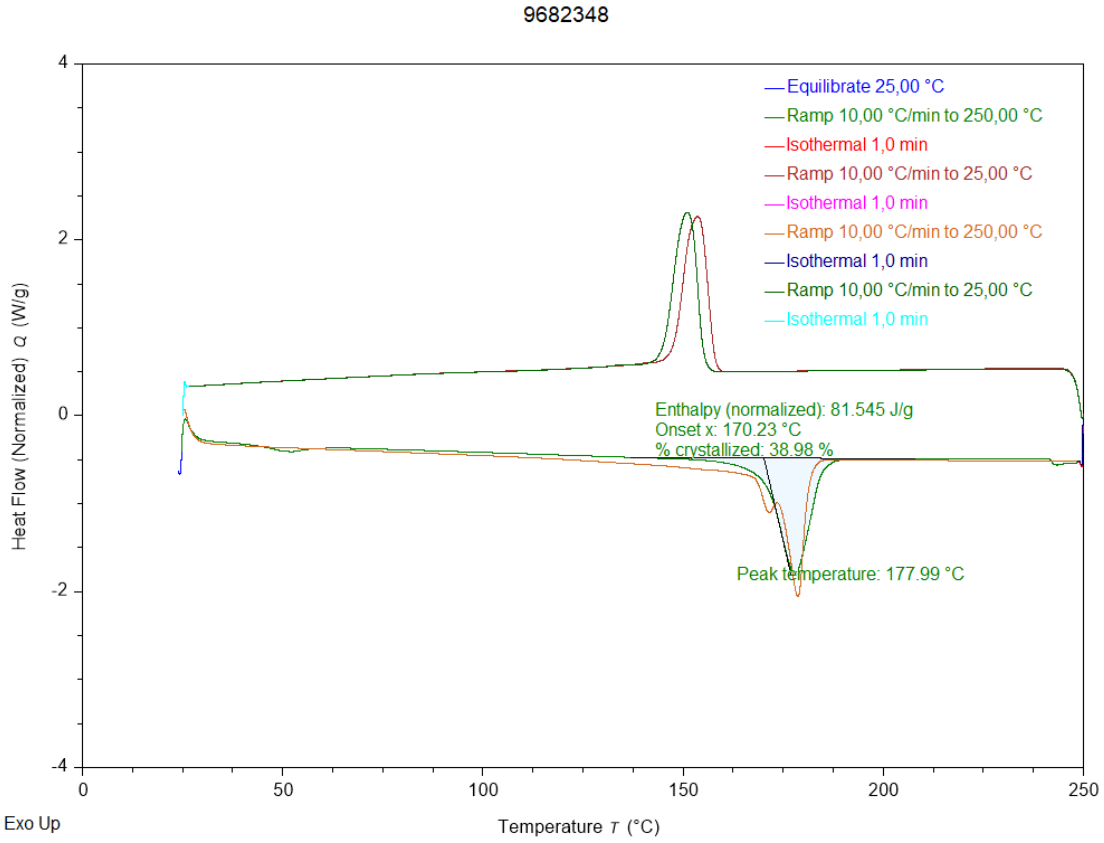

Figure B.21: Graphical representation of DSC data of specimen 9682348

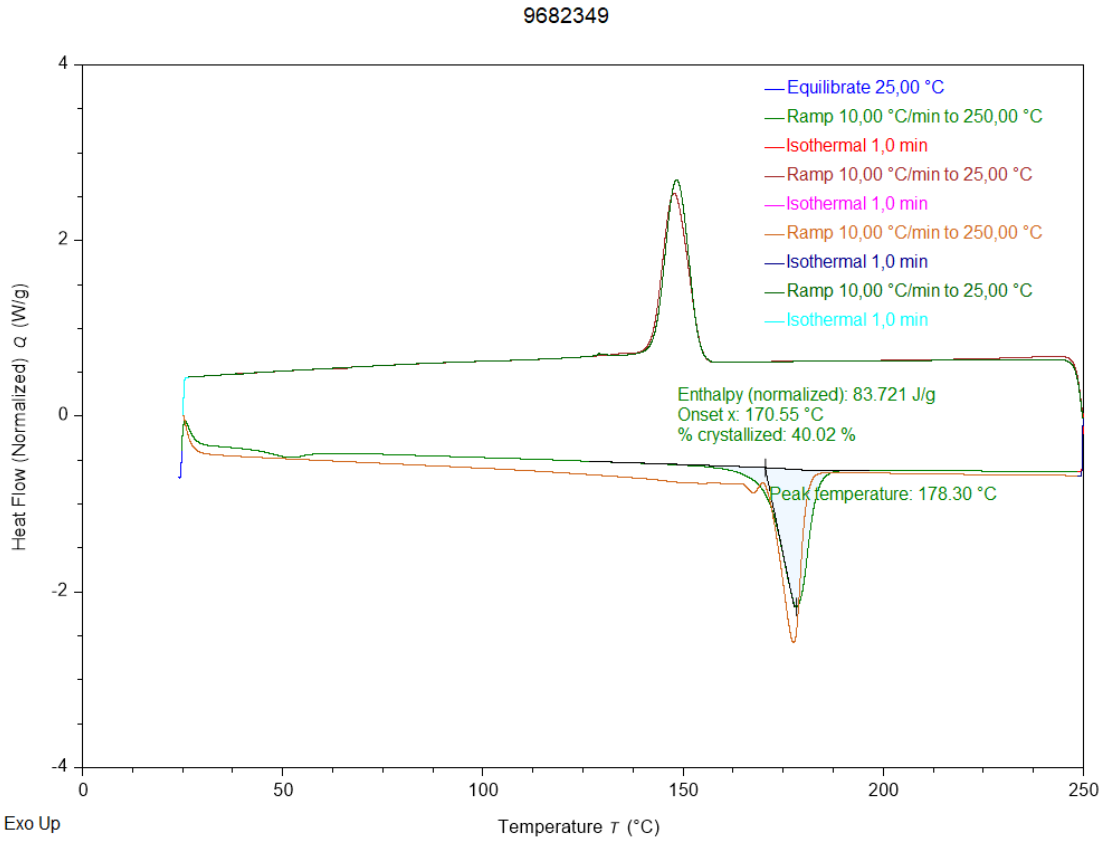

Figure B.22: Graphical representation of DSC data of specimen 9682349

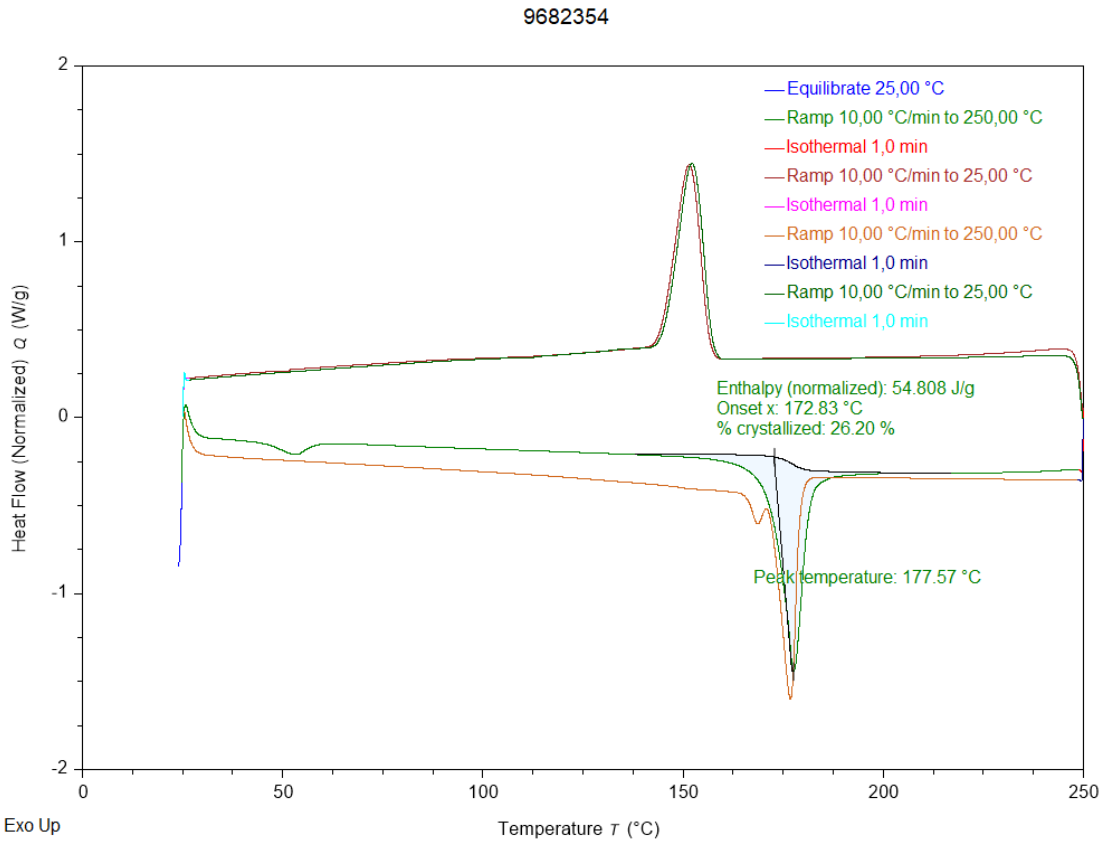

Figure B.23: Graphical representation of DSC data of specimen 9682354

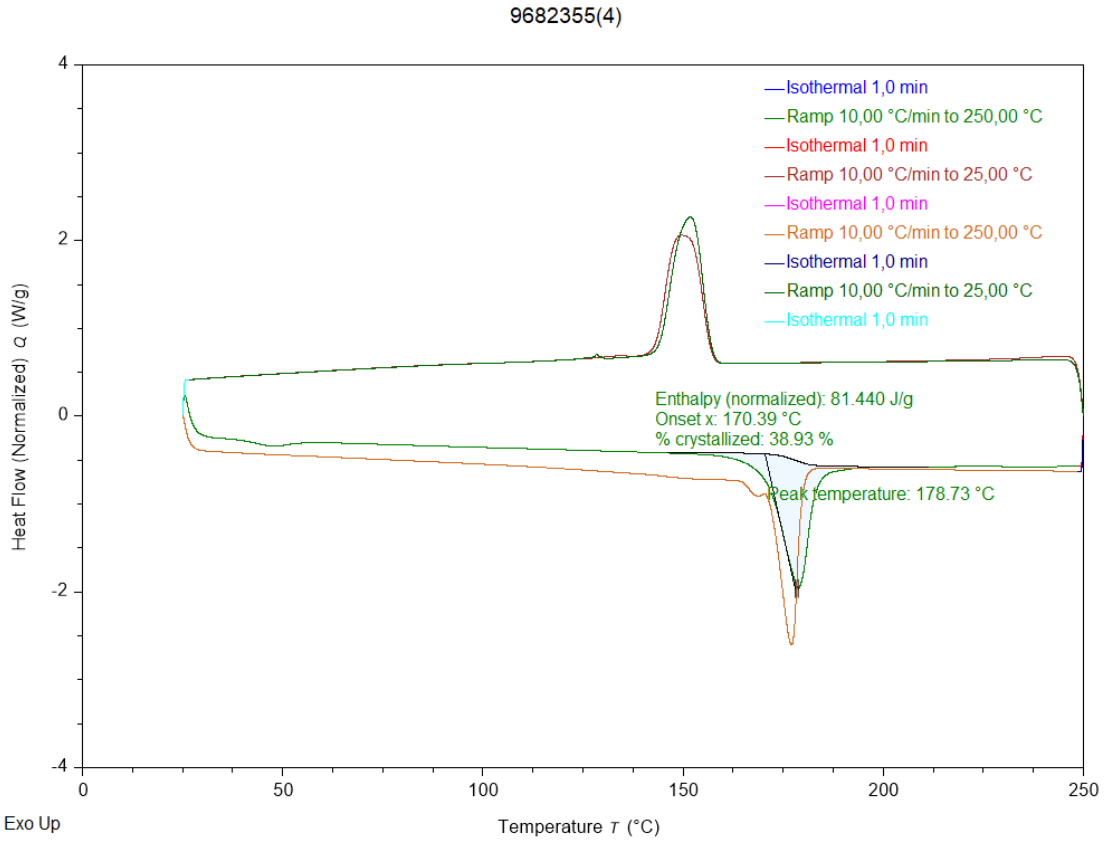

Figure B.24: Graphical representation of DSC data of specimen 9682355

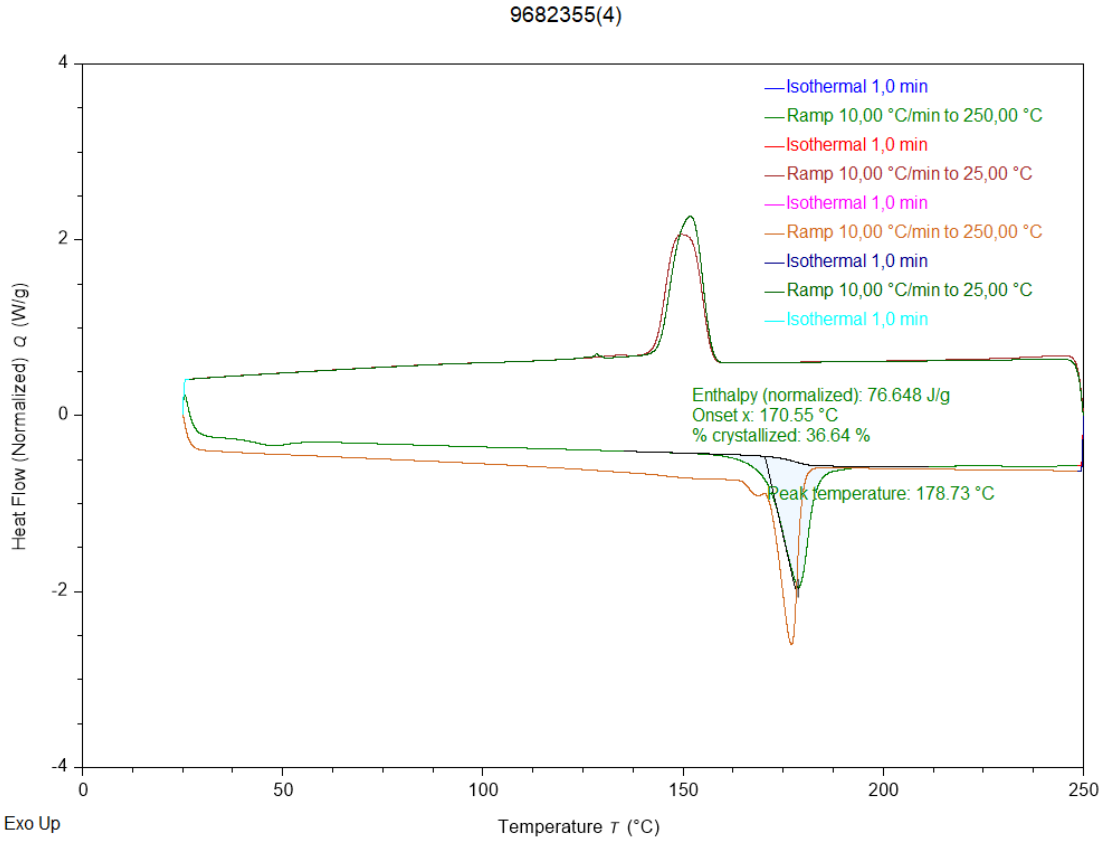

Figure B.25: Graphical representation of DSC data of specimen 9682655

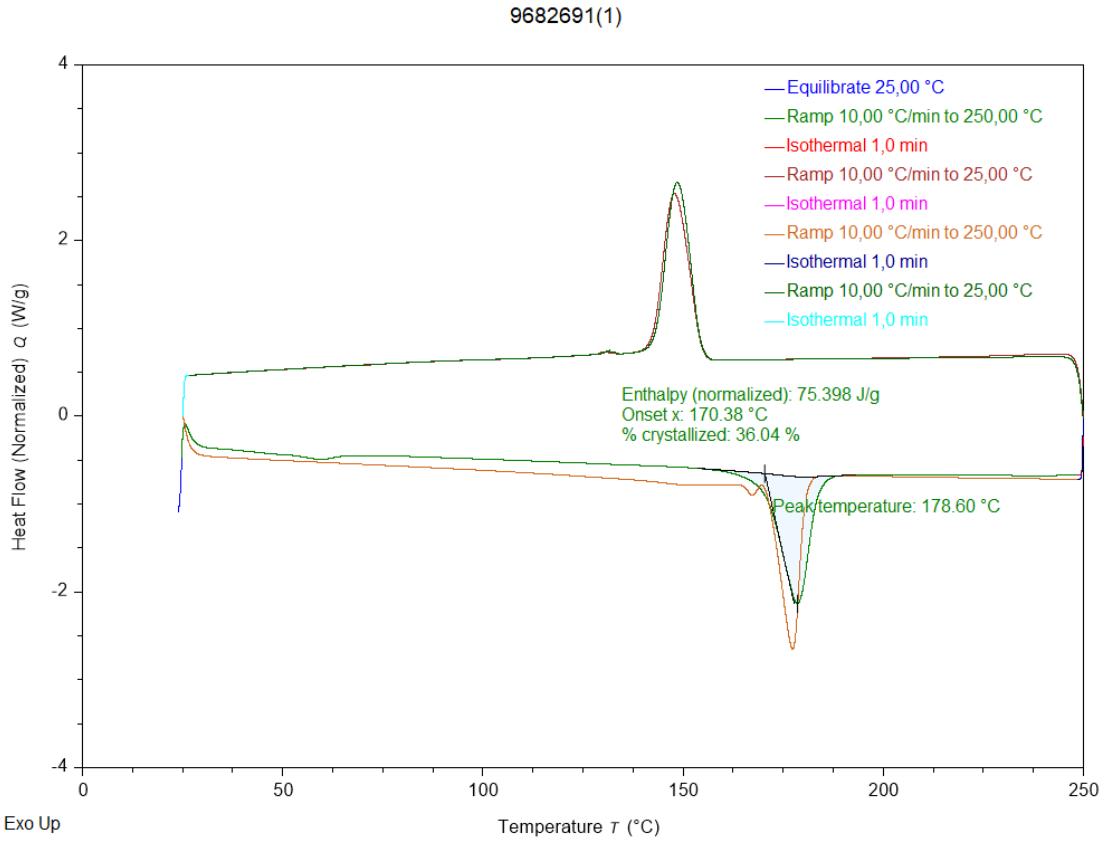

Figure B.26: Graphical representation of DSC data of specimen 9682691

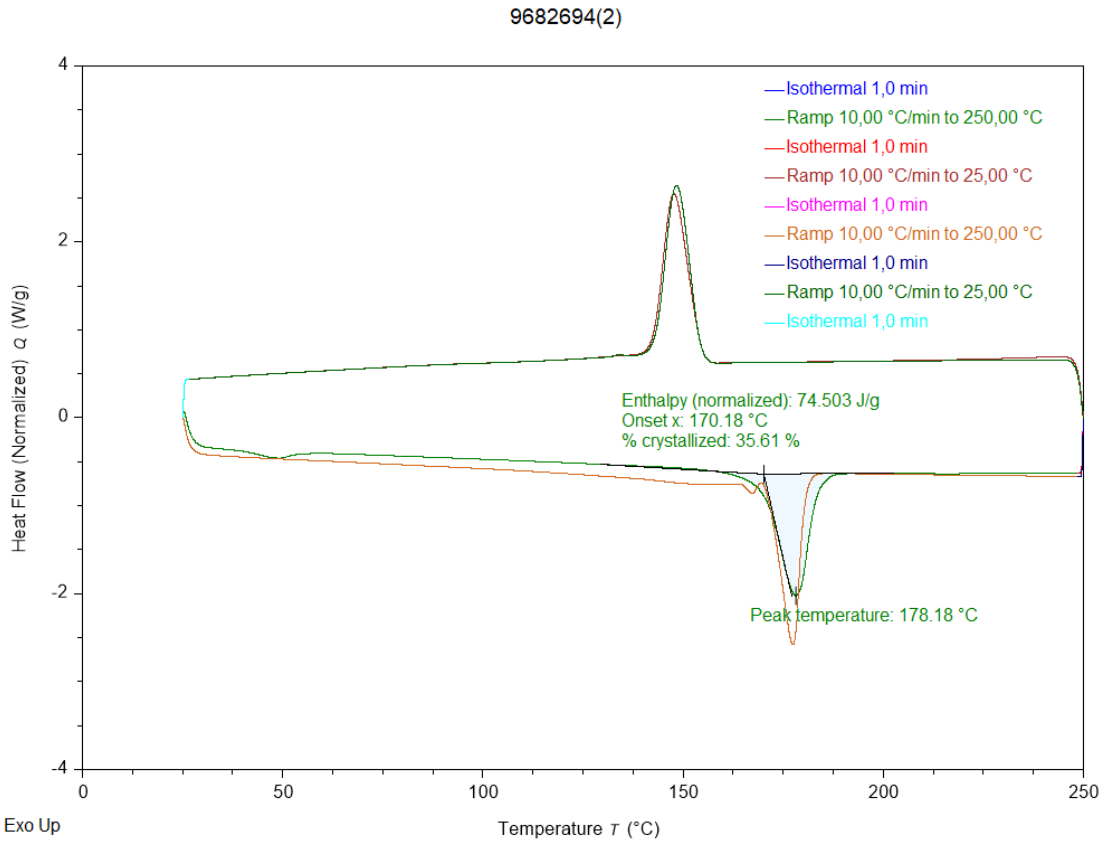

Figure B.27: Graphical representation of DSC data of specimen 9682694

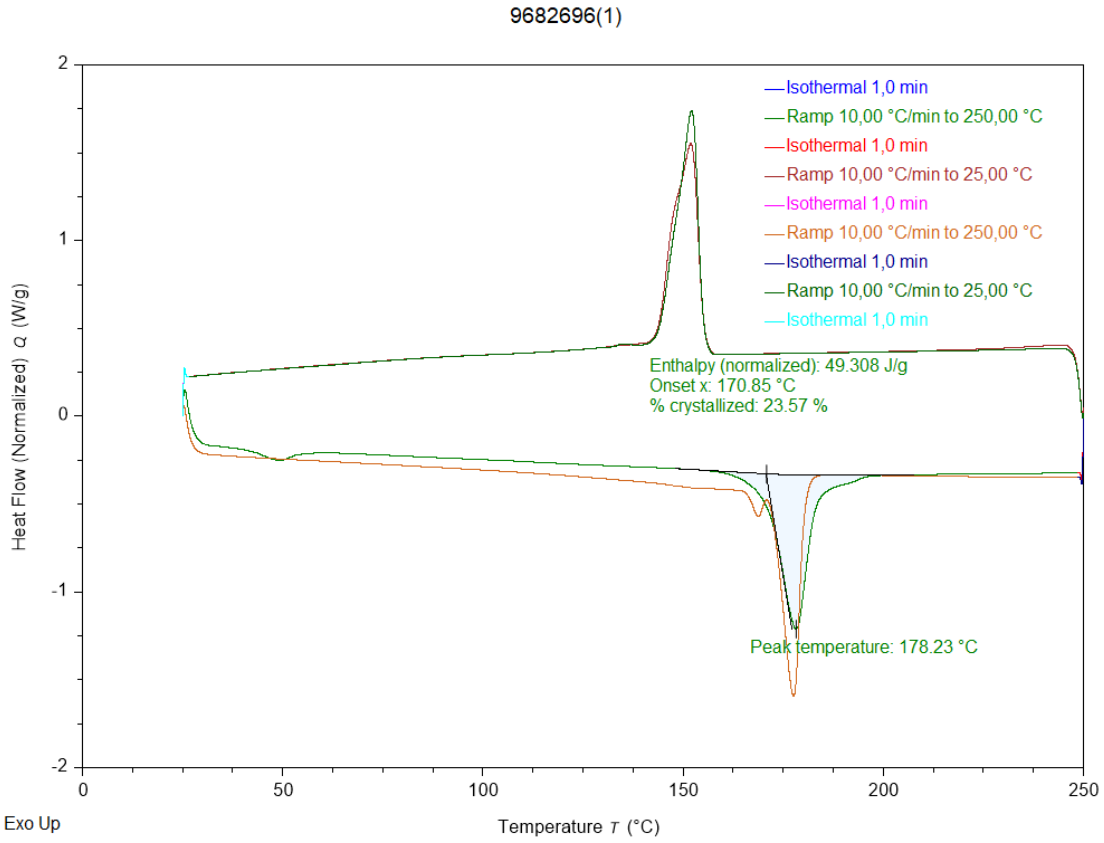

Figure B.28: Graphical representation of DSC data of specimen 9682696

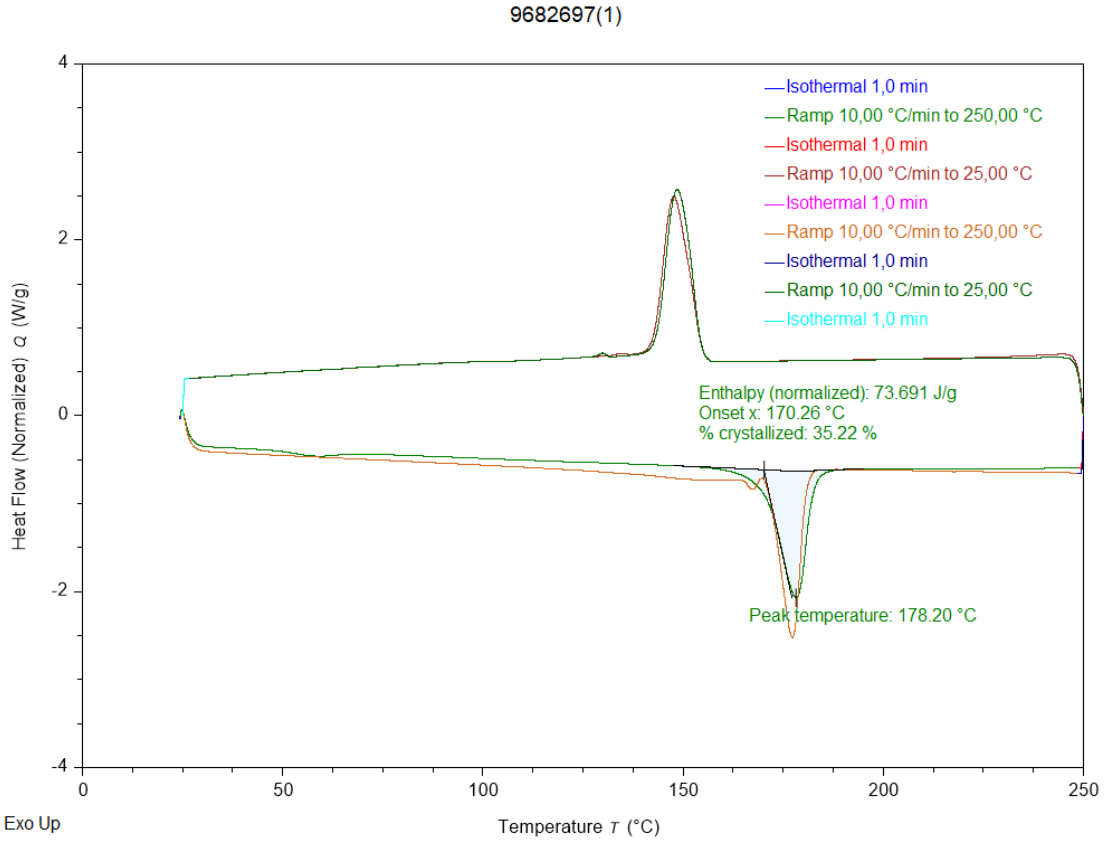

Figure B.29: Graphical representation of DSC data of specimen 9682697

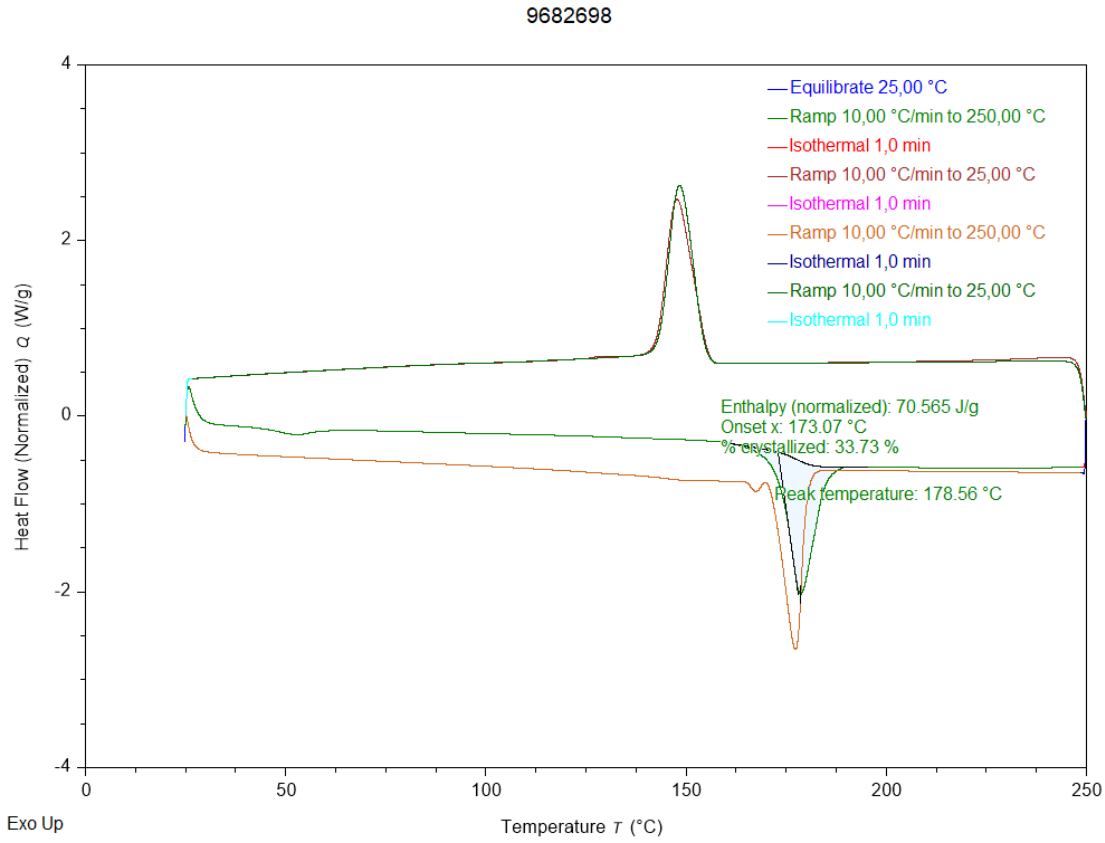

Figure B.30: Graphical representation of DSC data of specimen 9682698

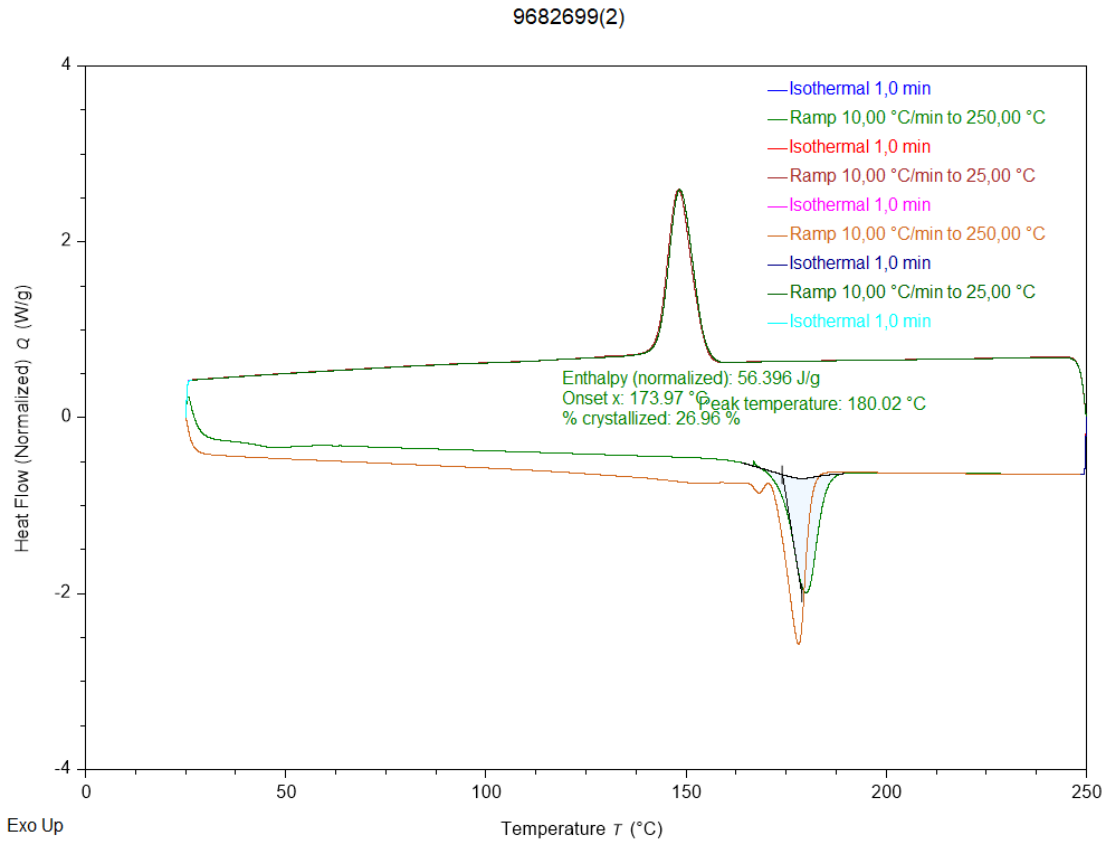

Figure B.31: Graphical representation of DSC data of specimen 9682699

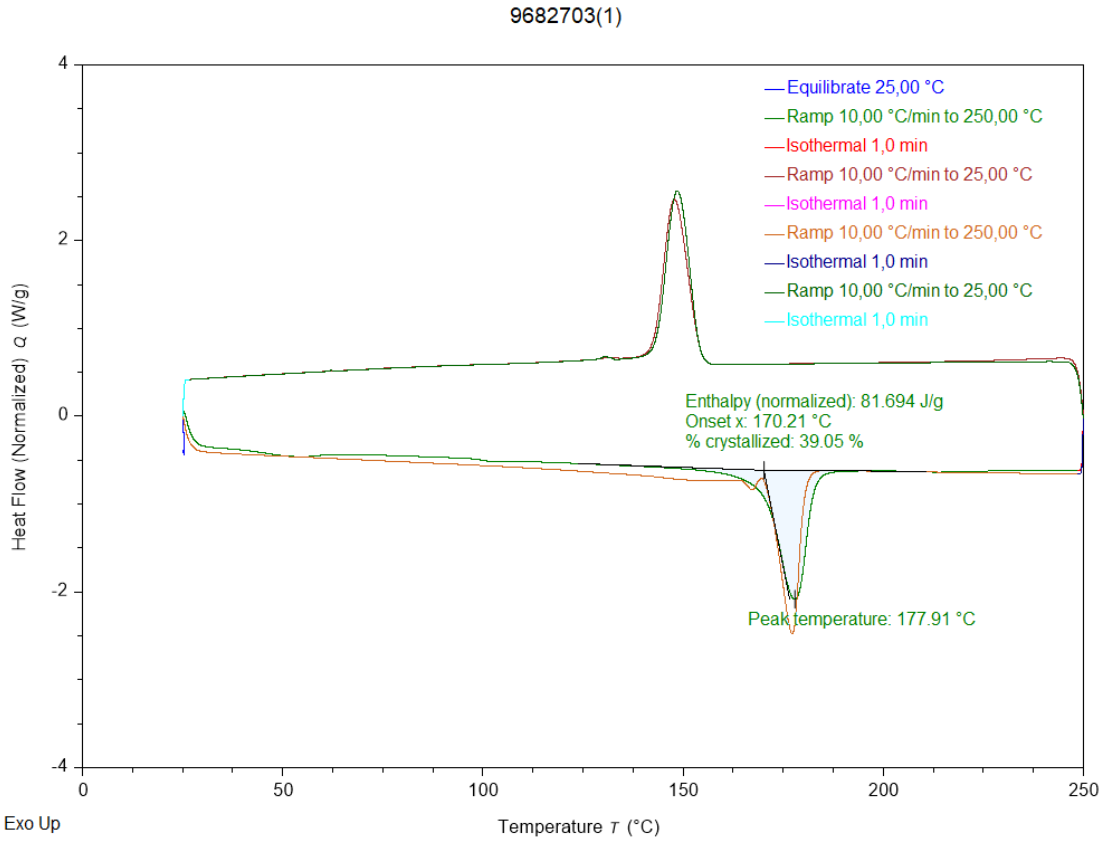

Figure B.32: Graphical representation of DSC data of specimen 9682703

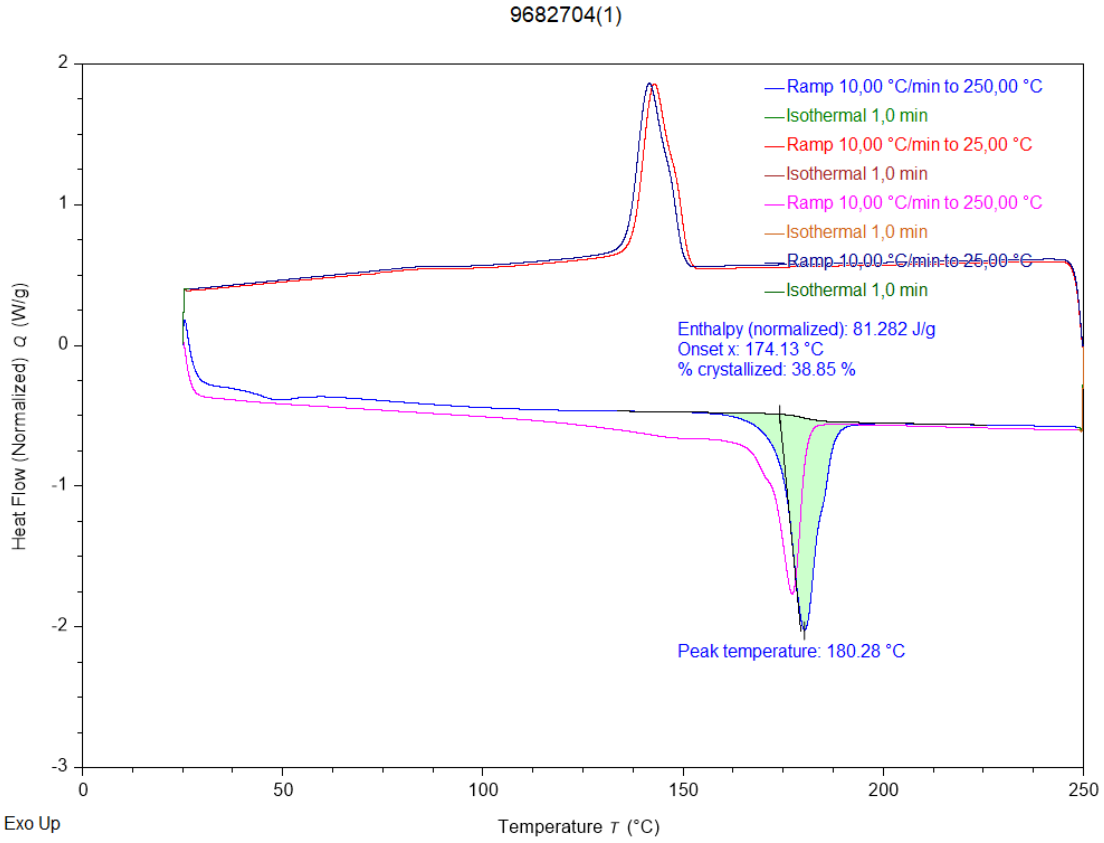

Figure B.33: Graphical representation of DSC data of specimen 9682704

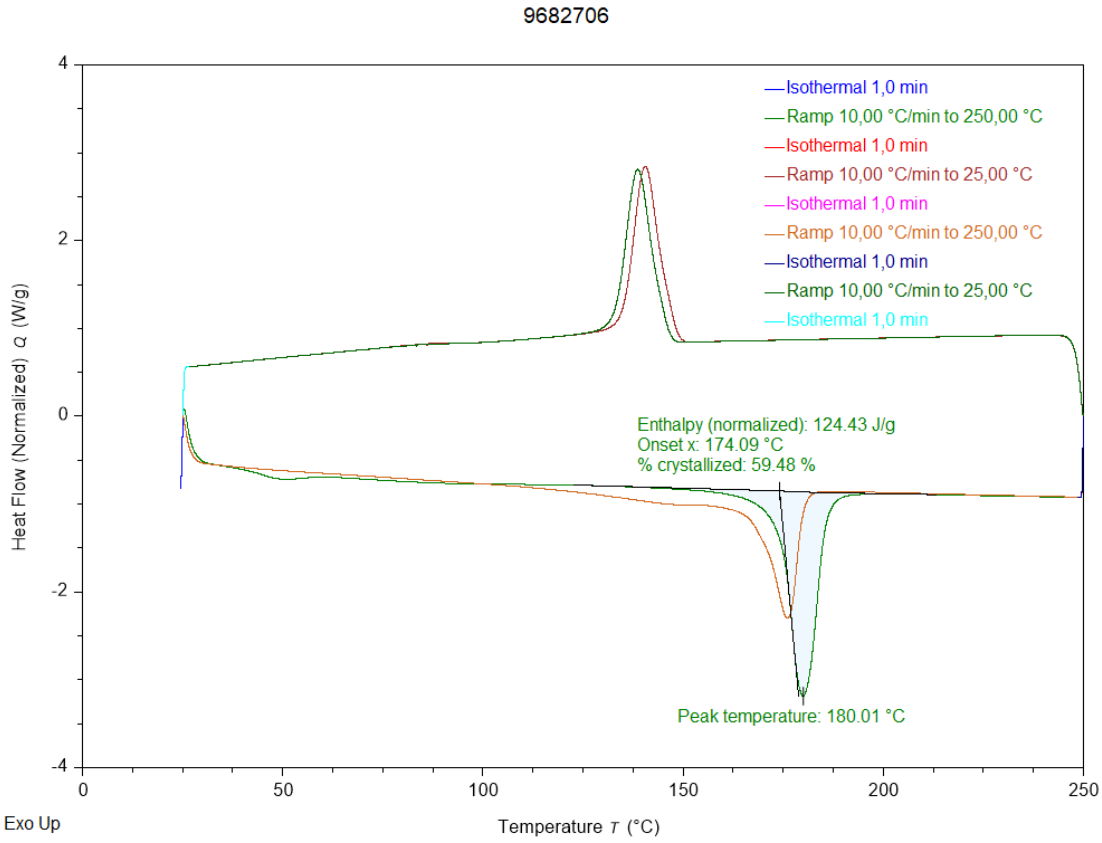

Figure B.34: Graphical representation of DSC data of specimen 9682706

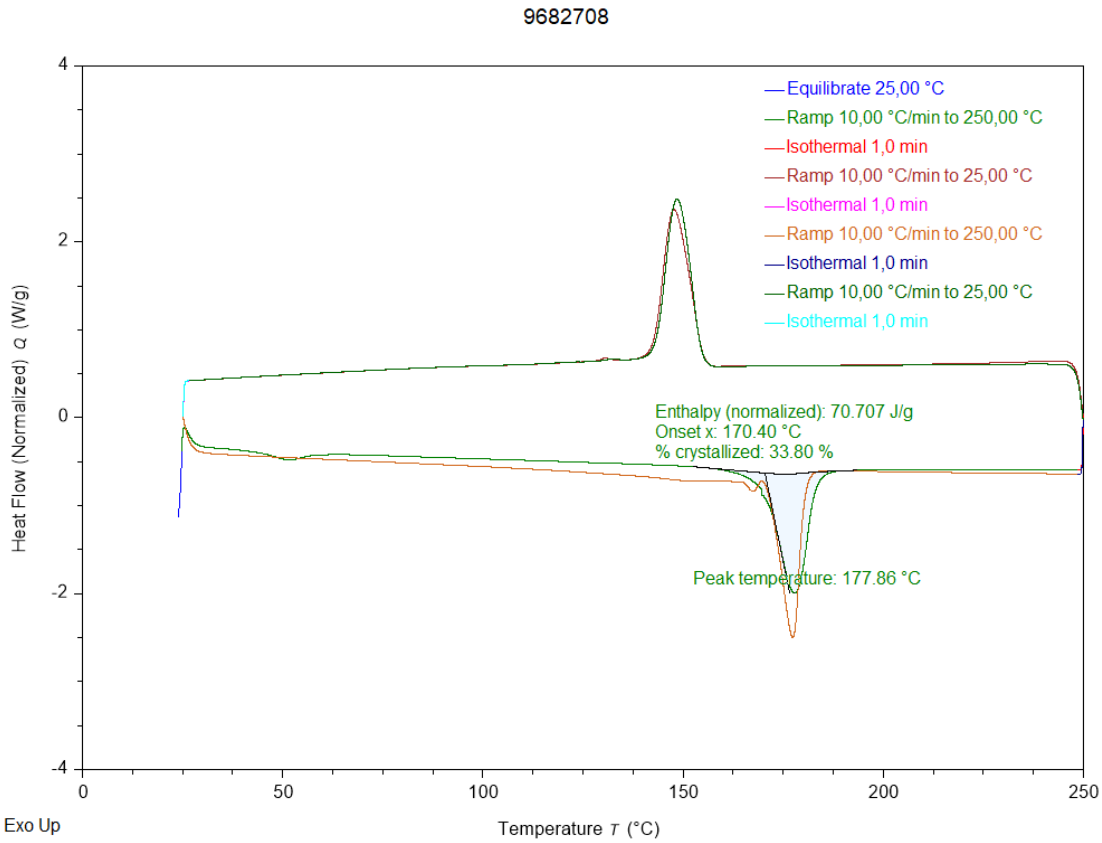

Figure B.35: Graphical representation of DSC data of specimen 9682708

Appendix C
Testing Equipment

In this chapter, an overview is given of the equipment used in this research. This chapter includes technical data on the accuracy and capabilities of the used equipment. In Section C.1, the DSC machine is elaborated upon. Section C.2 presents the different options for NMR spectroscopy. In Section C.3, the CAM software of Materialise NV will be presented. It is called Materialise Magics.

Both the DSC and NMR machines will need a powdered form of the sample. Because of this, the samples will need to be grounded to a fine powder, without increasing the temperature to much, since this will affect the crystallinity of the material. Because of this, a cryogenic grinder will be used to ground the samples. This piece of equipment will be presented in Section C.4. Finally, a scale is needed to measure the samples for determination of the porosity.

C.1 Differential Scanning Calorimetry

The Differential Scanning Calorimetry machine used in this research is the TA Instruments DSC 250. It is shown in Figure C.1[1]. Although it is not visible in this figure, the machine that is present in the laboratory, has an auto-sampler. This facilitates the testing of a large number of samples, as the machine can autonomously replace the specimen that needs to be tested. The machine is also coupled to an external liquid nitrogen tank, which is needed for a more rapid and controlled cool down of the samples.

Figure C.1: TA Instrument DSC 250

In Table C.1, technical specifications are given on the accuracy of of the used equipment. As can be seen, the precision and accuracy of the DSC250 is very small. The enthalpy measurements are also very accurate and only have a range of inaccuracry of $\pm 0.08\%$. The sampling rate of 600 data points per minute, any fluctuations, imprecision, and inaccuracies in the measured data have a small effect. As a result of all this, the data points obtained from these tests has a high credibility.

The raw results are processed using the software of TA Instruments called Trios. This software performs the baseline integration needed for the determination of the degree of crystallinity. This baseline must be selected manually. Trios determines the melting enthalpy and can also give the degree of crystallinity if the melting

[1] `https://www.tainstruments.com/dsc-250/`

Table C.1: Specifications of DSC 250

	DSC25	**DSC250**	**DSC2500**
Baseline Flatness (-50 to 300°C)	≤100 μW	≤10 μW	≤5 μW
Baseline Repeatability (-50 to 300°C)	40μW	20μW	10μW
Temperature Range	-180°C to 725°C	-180°C to 725°C	-180°C to 725°C
Temp Accuracy	±0.1°C	±0.05°C	±0.025°C
Temp Precision	±0.01°C	±0.008°C	±0.005°C
Enthalpy Precision	±0.1%	±0.08%	±0.04%

enthalpy is given of a sample with 100% crystallinity. It is important to note that a small change in the baseline, may have a significant impact on the degree of crystallinity. In Figure C.2, the raw results of the test of sample 9671778 are shown.

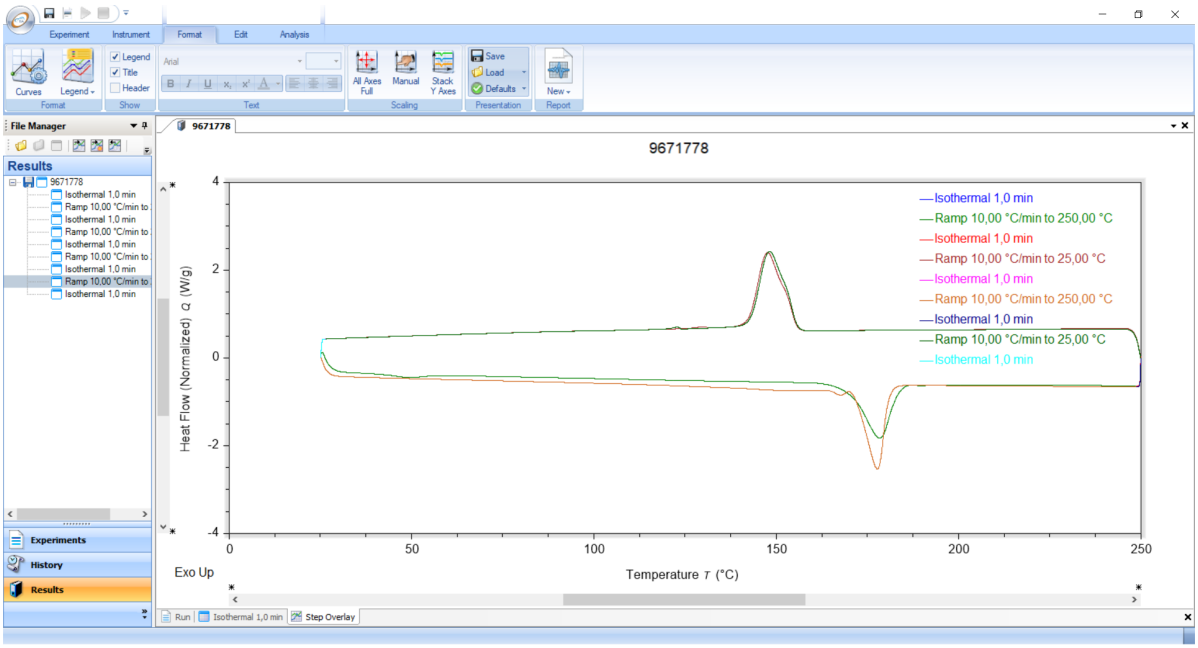

Figure C.2: Example of results shown in TRIOS

C.2 Nuclear Magnetic Resonance Spectroscopy

This section is split into two parts. An in depth explanation of Solution NMR spectroscopy and solid-state NMR spectroscopy in Sections C.2.1, and C.2.2, respectively. A general explanation of Nuclear Magnetic Resonance Spectroscopy can be found in Section C.2.

C.2.1 Solution Nuclear Magnetic Resonance Spectroscopy

Solution based Nuclear Magnetic Resonance Spectroscopy is the most common used type of NMR. The sample is dissolved into a solution, since this will allow a free motion of the molecules. As a result the material can easily be investigated both qualitatively and quantitatively. The use of a powdered sample is advised since this will facilitate the dissolving of the sample into the solvent.
The solvents used for solution NMR may not have any ^{1}Hydrogen atoms in its molecular structure, since the presence of these atoms will interfere with the results of spectroscopy due to the presence of the ^{1}H atom in the structure of most polymers. Because of this, a variation of these solvents are used where the ^{1}Hydrogen atoms are replaced by deuterium. Deuterium, or ^{2}H or mostly refered to by the symbol D, is a stable isotope of hydrogen with instead of having only one proton in its core, it has one additional neutron present. Because of this, the nuclear spin properties differ form that of the lighter ^{1}Hydrogen. Because of that the NMR spectra of hydrogen and deuterium are highly differentiable.

In Solution NMR, the obtained spectra consists of a series of very sharp and clearly distinguishable peaks. This is because of the averaging of the anisotropic NMR interactions caused by the random movement of the molecules in the solution. These peaks can be observed in the top part of Figure C.3. [46]

It is important to have a solvent in which the sample can completely dissolve. The solubility of polyamide was tested quantitatively in several solvents in [28]. The results indicate that polyamides are soluble in organic solvents such as DMF, DMAc, dimethyl sulfoxide, NMP, Py and in H_2SO_4. Polyamides are insoluble in chloroform, tetrahydrofuran, methylene chloride, cyclo-hexane, acetone and water.

C.2.2 Solid-State Nuclear Magnetic Resonance Spectroscopy

The second type of Nuclear Magnetic Resonance Spectroscopy is called solid-state NMR Spectroscopy. As the name of this technique may suggest, is the powder in a solid state and not in solution. This limits the motion of the molecules and because of this the effect of the orientation-dependant interactions are observed. This is the cause of the very broad spectra that are obtained using solid-state NMR. An example of such a spectra can be seen in Figure C.3.

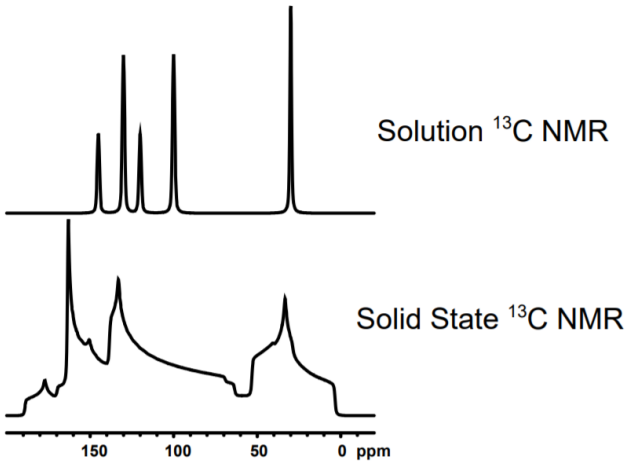

Figure C.3: Comparison of solution and solid state NMR spectra [46]

If the tests are performed with a sufficiently high resolution, the obtained spectra can provide the same type of information as solution NMR spectroscopy. This also requires a number of specialised techniques and equipment, such as magic-angle spinning (or MAS), cross polarisation (or CP), ... Standard solid-state NMR tests only give qualitative data on the composition of a material, not quantitative data. However, there are complex techniques that make it possible to obtain quantitative spectra, such as described in [33] and [20].

Magic Angle spinning in a technique used in solid-state NMR in order to increase the resolution of the obtained spectra. When applying this technique, the sample is spinning at a frequency between 1 to 130 kHz at an the so-called magic angle σ_m. This angle is between the axis of rotation of the sample and the direction of the magnetic field, and is approximately 54.74°. This spinning makes the recorded peaks more narrow. Which makes the identification and analysis of the spectrum easier. Cross polarisation is a very important technique that is used to enhance the signal to noise ratio of the results. This technique transfers the abundant spins, like those of ^{1}H and ^{19}F, to the dilute spins such as ^{13}C or ^{15}N. This is because the abundant spins are strongly dipolar coupled. As a result of this, they are subject to significant fluctuating magnetic fields resulting from motion of the atoms. Rapid spin-lattice relaxation at the abundant nuclei are induced. This increases the relaxing of the dilute nuclei. [46]

It is also important to note that solid-state NMR is a much more expensive test compared to solution NMR spectroscopy. For the purpose of this research, solution NMR is a better experimental technique as it more easily results in quantitative data and require a smaller economical investment.

C.3 Materialise Magics - Computer-Aided Manufacturing

Materialise Magics is the Computer-Aided Manufacturing software used and developed by Materialise NV. This software is made specifically for the additive manufacturing, and can handle all 3D printing technologies, including Selective Laser Sintering. Using Magics, both data and the build can be prepared. This also includes the creation of any additional structures, (automatic) support generation, and nesting of the parts in the build volume.

Nesting refers to the process of positioning the 3D parts in the build volume in order to minimise the wasted space. This reduces wasted material and also increases the productivity of the machine. Support generation is needed in some printing techniques in order to keep the part into its position. Supports are also used to minimise thermal stress since the printed supports can act as a heat sink. Usually this not required for parts printed using the SLS technique.

This software can also be used for analysis and reporting of the printing characteristics. For the research of this thesis, it will be used for the export of geometrical data of several printed batches. This data includes the printed volume and surface area of each part, but also it´s centre location and the dimensions of its bounding box.

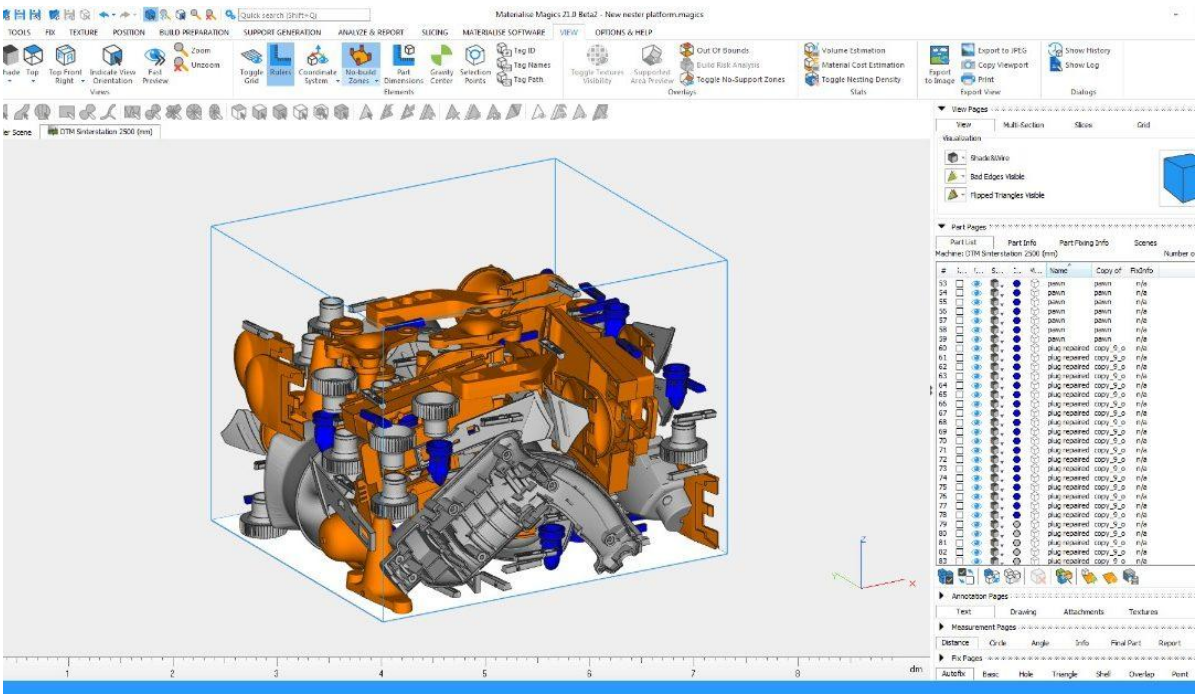

Figure C.4: Example of printing preparation using Materialise Magics

In Figure C.4 [2], an example is shown of several parts that are nested in the build volume using Magics. On the right a list is shown of all parts that are present in the build volume. On the top several menu's are shown, each housing several options for the modification of parts, printing preparation, printing simulation, and data exportation.
In the bottom rigth corner of the figure, an axis system can be seen. This axis system will also be used in this research. The red axis is the x-axis, green axis is the y-axis, and the z-axis is shown in blue.

C.4 Cryogenic Grinder

A cryogenic grinder is a machine used to grind a sample into a fine powder. This machine can be used for all types of materials, ranging from metals, to ceramics. In this research it is used to grind down the polymer sample without raising the temperature too much, since this will result in recrystallisation of the powder. Using this machine, a fine powder will be obtained that has the same degree of crystallinity as the tested sample. The machine used is presented in Figure C.5.

[2] https://www.3d-me.com/materialise-magics

Figure C.5: Fritsch Pulverisette 14 premium line

The Fritsch Pulverisette 14 premium line is a variable speed motor mill. Its design allows for easy cleaning and removing of the grounded powder. Using the funnel on top, both the sample and the liquid nitrogen can be added to the milling chamber. Liquid nitrogen must be added to lower the temperature of the sample during the grinding process. It is important to note that the liquid nitrogen needs to poured into the chamber manually. If too little the liquid nitrogen is added the temperature of the sample will rise vary rapidly due to the high amount of friction experienced by the sample.

The sample is dropped down in to the middle of the machine on top of a rotating disc with cutting knifes on the edge of it. This machine is rotating at a speed between 6 000 and 15 000 rpm, resulting in a peripheral speed between 30 and 69 m/s. The maximum rpm can be altered in the setting of the machine. If the resistance of the sample is too high, the experienced rpm will be lower. Due to the rotation the sample will fly outwards, where it will encounter the aforementioned knifes. If the powder is cut fine enough by these knifes, it will fit through a metal mesh and be deposited into a final chamber. The mesh of this machine can be changed according to the requirements of the powder. The holes in the mesh can range from 0.08 up to 4 mm.

There is no temperature sensor present in the milling chamber, however there is a indicator on the machine, which shows the energy the engine needs to grind the material compared to its maximum output. If a polymer is at a very low temperature it is relatively brittle compared to when it is near melting temperature, since it is very viscous at this point. The machine will have fairly little effort in grinding down a brittle polymer, but it will be unable to cut the sample if it is too viscous. Because of this, the indicator of the motor can be used to as an indication of the sample temperature.

C.5 Scale

The last piece of equipment needed is a scale. This will be used to measure the weight of the (powdered) samples for several purposes. The first purpose that it is used for is the measuring of the powdered material for each sample that is tested using differential scanning calorimetry. Besides that, the scale is also used for measuring the amount of powder that needs to be dissolved for the solution Nuclear Magnetic Resonance spectroscopy. It will also be used to measure the amount of powder that is being tested using solid state NMR spectroscopy. The determination of the porosity of the samples also requires the use of an accurate scale.

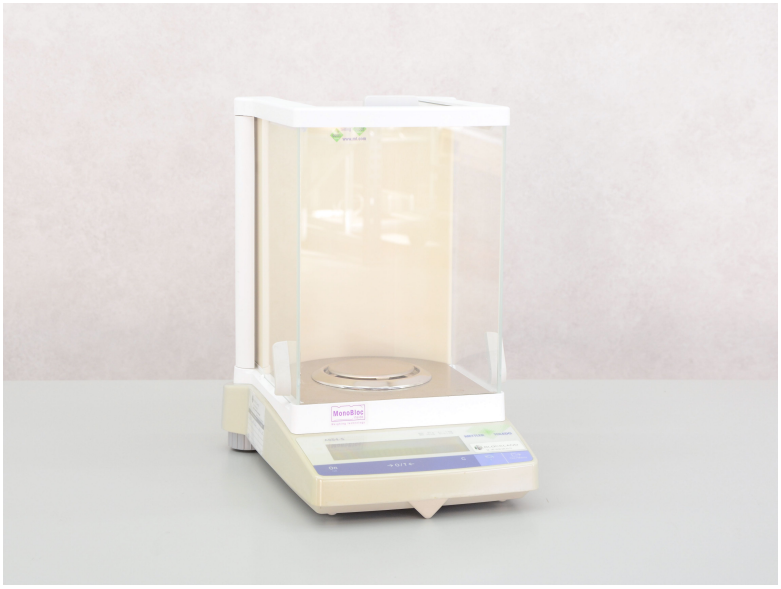

Figure C.6: Mettler Toledo AB54-S Scale

Several scales were used, but the scale that was used for the determination of the porosity is the Mettler Toledo AB54-S and is shown in Figure C.6 [3]. The scale used for the measurements for the DSC tests is a Mettler Toledo XSR 204 and is shown in Figure C.7. It can measure accurately between 0.1 and 51 gram of material. It has a readability of 0.1 mg. Additional technical data can be found in Table C.2 [4].

Table C.2: Technical Data of the Mettler Toledo AB54-S and the XSR 204[30]

Technical Data	**AB54-S**	**XSR 204**
Readability	0.1 *mg*	0.1 *mg*
Max. capacity	51 *g*	220 *g*
Repeatability (sd)	0.1 *mg*	0.07 *mg*
Linearity	0.2 *mg*	0.2 *mg*
(10 ° … 30 °)		
Settling time, typical	3.5 *s*	1.5 *s*
Adjustment weight	built-in	built-in
External dimensions of balance (W/D/H)	245x321x344 *mm*	482x292x195 *mm*
Weighing pan	⌀80*mm*	78*x*73*mm*

[3] https://www.geminibv.nl/labware/mettler-ab54-s-balans/
[4] https://www.mt.com/be/nl/home/products/Laboratory_Weighing_Solutions/Analytical/Excellence/xsr-analytical-balances/XSR204-30355500.html

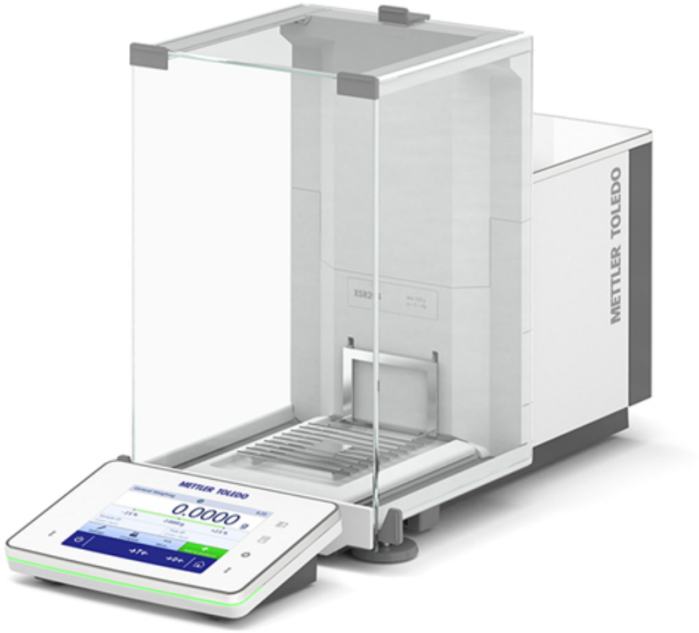

Figure C.7: Mettler Toledo XSR 204